SEMICLASSICAL S-MATRIX THEORY FOR ATOMIC FRAGMENTATION

Jan-Michael ROST

Theoretical Quantum Dynamics, Fakultät für Physik, Universität Freiburg, Hermann-Herder-Str. 3, D-79104 Freiburg, Germany

ELSEVIER

AMSTERDAM – LAUSANNE – NEW YORK – OXFORD – SHANNON – TOKYO

ELSEVIER

Physics Reports 297 (1998) 271–344

PHYSICS REPORTS

Semiclassical S-matrix theory for atomic fragmentation

Jan-Michael Rost

Theoretical Quantum Dynamics, Fakultät für Physik, Universität Freiburg, Hermann-Herder-Str. 3, D-79104 Freiburg, Germany

Received August 1997; editor: J. Eichler

Contents

Abstract

A semiclassical scattering approach is developed which can handle long-range (Coulomb) forces without the knowledge of the asymptotic wave function for multiple charged fragments in the continuum. The classical cross section for potential and inelastic scattering including fragmentation (ionization) is derived from first principles in a form which allows for a simple extension to semiclassical scattering amplitudes as a sum over classical orbits and their associated actions. The object of primary importance is the classical deflection function which can show regular and chaotic behavior. Applications to electron impact ionization of hydrogen and electron–atom scattering in general are discussed in a reduced phase space, motivated by partial fixed points of the respective scattering systems. Special emphasis, also in connection with chaotic scattering, is put on threshold ionization. Finally, motivated by the reflection principle for molecules, a semiclassical hybrid

PII S0370-1573(97)00079-3

approach is introduced for photoabsorption cross sections of atoms where the time-dependent propagator is approximated semiclassically in a short-time limit with the Baker–Hausdorff formula. Applications to one- and two-electron atoms are followed by a presentation of double photoionization of helium, treated in combination with the semiclassical S-matrix for scattering.

PACS: 31.15.–p; 34.20.–b; 34.50.–s

Keywords: Classical cross section; Deflection function; Long-range Coulomb potentials; Asymptotic boundary conditions

1. Introduction

Bohr's model of the atom, sometimes called 'the old quantum theory', is according to our contemporary understanding semiclassical or at least quasiclassical, and in this sense semiclassical methods predate the quantum theory. However, with the failure of the Copenhagen school to describe the bound state of the (non-integrable) helium atom [1], the old quantum theory was forgotten quickly, and quantum mechanics using variational techniques was applied successfully to demonstrate the existence of a stable state for a number of simple systems, e.g. helium [2–4], H_2^+ and so forth. Nevertheless, the semiclassical idea in the form of the WKB approximation has been established as a standard tool and can be found in almost any text book on quantum mechanics. Being essentially a one-dimensional theory it was also applied to scattering problems for the determination of phase shifts [5]. A slight generalization of the WKB approach to higher-dimensional (but integrable) systems was formulated in the EBK quantization. However, for a long time further progress of semiclassical methods was hampered by the lack of computing power (one almost always needs to calculate classical paths numerically) and by the overwhelming success of quantum theory itself.

Only in the late 1960s, Gutzwiller formulated a semiclassical Greens function in terms of periodic orbits, nowadays often referred to as trace formula [6–9]. Almost at the same time a truly three-dimensional formulation of a semiclassical amplitude for potential scattering appeared [10] based on the asymptotic form of the quantum propagator, formulated by Van Vleck already in 1928 [11]. Shortly afterwards a semiclassical S-matrix theory was developed by Miller [12–14] and Marcus [15, 16] and it was applied to inelastic and reactive scattering in molecular physics. The methods which will be described in this report for scattering involving Coulomb forces are very similar to their approach.

In the meantime a purely classical perspective was revived in atomic physics initiated by Percival and coworkers [17, 18] and later on very much connected with the name of Olson who developed the *classical trajectory Monte Carlo* method (CTMC) (see e.g. [19]). This computational technique solves Newton's equation with initial phase space sampled by Monte-Carlo methods. CTMC has been refined over the years and is today one of the standard tools to calculate cross sections. Being a classical approach, it works for many atomic problems much better than one might expect for systems whose domain is quantum mechanics. It is one goal of this report to understand why classical methods are successful for Coulombic scattering problems.

Over the last decade, semiclassical theory has been advanced to a very sophisticated standard and following the great attention classically chaotic dynamics has received, the semiclassical perspective enjoys today a good reputation for offering alternative and important insight into dynamics of microscopic systems. Gutzwiller's original trace formula has been amended by resummation techniques (cycle expansion and equivalent formulations) to make the periodic orbit series convergent. A great success of this effort was the semiclassical calculation of the resonance spectrum of helium [20]. However, periodic orbit techniques have been applied to a variety of problems, among others to the problem of hydrogen in a magnetic field [21], which has become a gauge system for semiclassical theories [22], and to calculate conductance fluctuations and other properties of mesoscopic systems [23]. While the trace formula used to be restricted to classically purely chaotic or regular problems [24], Tanner succeeded recently to quantize intermittency

(i.e. mixed regular and chaotic motion) semiclassically, again exemplified with the almost regular tails of Rydberg series in helium [25]. More recently, the time-dependent semiclassical approach has been very promising, mostly applied (once again!) to molecular problems. A uniformized propagator in combination with a phase-space sampling by Gaussian wavepackets has proven to yield impressive results concerning the accuracy of computed resonance widths and the number of dimensions in phase space which can be handled [26–29]. While the periodic orbit theories emphasize the bound state aspect and the described time-dependent approach relies on the time-correlation function, the direct S-matrix formulation of scattering has hardly been used semiclassically, with the exception of mesoscopic physics and the work related to charged particles presented here.

It is the authors subjective opinion that semiclassical theories, being always approximate, cannot and should not compete quantitatively with quantum mechanical calculations, but, they should provide insight into the dynamics and complement quantum calculations. Hence, it is our goal to demonstrate that the combination of the homogeneous Coulomb potential with semiclassical S-matrix techniques offers a unique understanding of the dynamics of charged particles with many features that are not obvious at all in a full quantum treatment.

The report is organized as follows: In Section 2 we will provide a tutorial on the classical formulation of cross sections and motivate the construction of semiclassical scattering amplitudes which will be derived rigorously from the quantum S-matrix for potential scattering as an example. We also formulate the concept of *partial fixed points*, which will allow us to reduce the number of phase-space dimensions for approximate computations later on. Section 3 is devoted to the unique classical properties of a system of particles interacting with homogeneous potentials in general and with Coulombic forces in particular. In Section 4, we discuss, again mostly in form of a tutorial, the connection of semiclassical phase shifts and the semiclassical S-matrix for potential scattering. While equivalent in quantum mechanics, this identity is typically lost semiclassically, where the representation of a problem plays a key role for the accuracy being achieved. As an application we discuss Rutherford and Mott scattering.

Section 5 finally discusses the application of the semiclassical S-matrix to inelastic electron–atom scattering and ionization with one active target electron. The threshold region (where ionization of an atom becomes energetically possible) is one of the most interesting problems, in particular directly below the threshold, where chaotic scattering occurs. Section 6 extends the semiclassical ideas in the sense of a hybrid approach: While a 'pure' semiclassical theory as in Section 5 involves classical objects only (trajectories and actions) one can keep the wave functions of initial and final states and apply approximations to the propagator only. The reflection principle for molecules is an example and we present akin results for atoms leading to analytic expressions for photoionization cross sections.

We conclude the report with a brief outlook trying to assess the future potential of semiclassical techniques in atomic and molecular problems.

2. Classical and semiclassical cross sections

In this section we will provide the theoretical tools to formulate a cross section classically and semiclassically. In particular, we will discuss the reduction of phase space due to *partial fixed*

points for the calculation of approximate cross sections. These tools can hardly be found in text books where the discussion of scattering in the classical and semiclassical context is mostly restricted to potential or collinear inelastic scattering. On the other hand, the semiclassical approximation to the quantum propagator itself has been described in recent review articles [30–33]. For this reason we will concentrate on the derivation of the *classical cross section*, presented in a way which allows an easy incorporation into a semiclassical expression. We will provide two derivations. The first one is more intuitive and heuristic. It is based on the classical cross section which is transformed into a semiclassical formulation by a standard procedure similar to the correspondence principle itself. The second derivation is more rigorous. It starts from the quantum mechanical T-matrix and arrives at the semiclassical scattering amplitude by evaluating the propagator in the stationary-phase approximation.

2.1. Formulation of the classical cross section

2.1.1. The classical probability density

For the sake of a simple notation we restrict the discussion in the present section to a two-dimensional phase space in Cartesian coordinates. However, the extension to arbitrary dimensions $2N$ is straightforward. Suppose a system[1] is at time t^- in a neighborhood Δx^- of the coordinate x^- and we want to know the probability $P_{\Delta x^-,\Delta x^-}(x^+,x^-,t)$ to find it at time t^+ in Δx^+ at the coordinate x^+. For a conservative system the probability will only depend on the time difference, $t = t^+ - t^-$. Quantum mechanically $P(x^+,x^-,t)$ can be found using the concept of the propagator $U(t)$ which describes the evolution of a state $|x^-\rangle$ in time, $|x^-(t)\rangle = U(t)|x^-\rangle$. The desired probability is constructed from the overlap

$$K(x^+,x^-,t) = \langle x^-|x^-(t)\rangle = \langle x^-|U(t)|x^-\rangle \ . \tag{1}$$

However, as can be seen from the dimensions, $|K(x^+,x^-,t)|^2$ is only a probability *density*, and the probability is

$$P_{\Delta x^+,\Delta x^-}(t) = |K(x^+,x^-,t)|^2 \Delta x^+ \Delta x^- \ . \tag{2}$$

To answer the same question classically we have to find the classical expression $\mathscr{P}(x^+,x^-,t)$ for the probability density $|K(x^+,x^-,t)|^2$. In general, a classical probability density $\mathscr{P}(B^+,A^-,t)$ to find the value B^+ for the observable B at time t^+ and A^- for the observable A at time t^- is given by the phase-space integral

$$\mathscr{P}(B^+,A^-,t) = \frac{1}{\Gamma} \int \mathrm{d}p\, \mathrm{d}q\, \delta(B^+ - B(p,q,t^+))\delta(A^- - A(p,q,t^-)) \,, \tag{3}$$

where Γ is a suitable normalization whose meaning will become obvious shortly. For our question the observable is the position of the system at both times $A = B = X$ and the values are x^- and x^+ at $t = t^-$ and $t = t^+$ respectively. If we choose the initial phase space variables (x^-, p^-) as integration variables (which can be done formally by a canonical transformation) we can fulfill the second δ-function setting $X(t^-) = x^-$ and Eq. (3) simplifies

[1] 'System' stands in our context for a conservative Hamiltonian system which classically obeys Hamilton's equations and quantum mechanically evolves according to the Schrödinger equation.

to

$$\mathscr{P} = \frac{1}{\Gamma}\int \mathrm{d}p^-\,\delta(x^+ - x^-(p^-,t)) = \frac{1}{\Gamma}\sum_{i=1}^{N}\left(\left.\frac{\mathrm{d}x^-}{\mathrm{d}p^-}\right|_{\substack{x^-(p_i^-,t)=x^+\\ p^-=p_i^-}}\right)^{-1} \equiv \frac{1}{\Gamma}\sum_{i=1}^{N}\left|\frac{\mathrm{d}p_i^-}{\mathrm{d}x^+}\right|, \tag{4}$$

where the second equality is a property of the delta function [34, vol. II, appendix 2] which we will write in the following with the short notation of the last fraction. The physical interpretation of the sum is the possible existence of more than one trajectory $X(t)$ which obeys Hamilton's equation while connecting x^- with x^+ in time $t = t^+ - t^-$.

To understand the meaning of the normalization Γ, we ask the question what is the probability to find the system at its position (x^-, p^-) in phase space. Of course, this probability must be one. Formally, we ask now for the probability density with $A^- = x(t^-)$ and the momentum p^- at the *same* time $t^+ = t^-$, i.e. $B^+ = p^-$. It is given according to Eq. (4) by

$$\mathscr{P}(p^-,x^-,0) = \frac{1}{\Gamma}\frac{\mathrm{d}p^-}{\mathrm{d}p^-} = \frac{1}{\Gamma}\,. \tag{5}$$

The corresponding probability (see Eq. (2)) reads

$$1 \equiv P_{\Delta x^-,\Delta p^-}(0) = (1/\Gamma)\Delta x^-\Delta p^- \tag{6}$$

that is $\Gamma = \Delta x^-\Delta p^-$, the phase-space volume the system occupies. Classically, this phase-space volume Γ does not have a canonical value, however, it is convenient to define it as $\Gamma = 2\pi\hbar$ which can be obtained semiclassically and quantum mechanically in the following way: Repeating our question what is the probability to find $|x^-\rangle$ at time $t^+ = t^-$ with momentum $|p^-\rangle$ we realize that for $t = t^+ - t^- = 0$ there is nothing to propagate and $U(0) = 1$. It follows from Eq. (1) that the quantum probability density is

$$|K(p^-,x^-,0)|^2 = |\langle p^-|x^-\rangle|^2 = |\mathrm{e}^{\mathrm{i}p^-x^-/\hbar}/\sqrt{2\pi\hbar}|^2 = 1/2\pi\hbar\,. \tag{7}$$

Comparison with the classical result (Eq. (5)) shows that the quantum and the classical probability density agree if $\Gamma = 2\pi\hbar$. In many derivations or statements of the classical probability density this normalizing phase-space volume Γ is taken from quantum mechanics, leading to the puzzling notion that a classical quantity contains an $\hbar$-dependence. Therefore, it should be emphasized that this is purely a convenient way to obtain an agreement of the classical and quantum probability densities in the extreme case of no propagation ($t = 0$).

2.1.2. *Classical observables*

We can also ask for the probability density to find the observable A at time t^+ for a system being at x^+ if it was at x^- for t^-. Formally, this is a transition probability (density) which would be described quantum mechanically by $|\langle x^+|A(t)|x^-\rangle|^2$. Classically, it is the sum of $A(x^-, p_j^+, t)$ for all trajectories j which connect x^+ with x^- in time t weighted with the respective probability density to do so

$$\mathscr{A}(x^+,x^-,t) = \frac{1}{\Gamma}\sum_j A(x^+, p_j^+, t)\left|\frac{\mathrm{d}p_j^-}{\mathrm{d}x^+}\right|\,. \tag{8}$$

2.1.3. The classical cross section

A cross section can be formulated with the transition probability density, which contains the essential dynamical information. However, since a cross section is defined as a transition for $t \to \infty$ any transition probability $P(t)$ would become infinite since in this time limit infinitely many scattering events lead to the specified transition [35, Ch. 15]. Hence, the cross section is defined, quantum mechanically as well as classically, as

$$\Delta\sigma = \lim_{t^+\to\infty} \frac{1}{\Phi_v} \frac{\mathrm{d}}{\mathrm{d}t^-} P_{\Delta q^+ \Delta q^-}(t^+ - t^-)\,, \tag{9}$$

where the rate $\mathrm{d}P/\mathrm{d}t^-$ is normalized to the incident flux $\Phi_v = v/\Delta \boldsymbol{x}^-$ of particles with velocity v in the volume $\Delta \boldsymbol{x}^-$ [35, Ch. 15] and $\boldsymbol{q}^+, \boldsymbol{q}^-$ are the initial and final state observables, respectively. In the following, we will derive on the basis of Eq. (9) the classical cross section for the following processes:

1. potential scattering,
2. fragmentation: $A + (BC)_{n^-} \to A + B + C$,
3. excitation: $A + (BC)_{n^-} \to A + (BC)_{n^+}$,
4. rearrangement: $A + (BC)_{n^-} \to C + (AB)_{n^+}$,

where $(BC)_n$ refers to the nth excited state of particles B and C. We will begin with potential scattering where one has not to deal with complicated initial and final states whose classical description requires additional considerations.

Potential scattering: In potential scattering a (pseudo-)particle is scattered elastically from an obstacle (represented by a potential). The particle gets only deflected while maintaining its speed. The observable is the scattering angle $\Omega^- \equiv (\theta^+, \phi^+)$ measured relatively to the initial momentum vector, usually chosen to be $\boldsymbol{p}^- = (0, 0, p^-)$ in Cartesian coordinates. According to Eq. (9) we have for the cross section

$$\Delta\sigma = \lim_{t\to\infty} \frac{\Delta\Omega^+ \Delta \boldsymbol{p}^-}{\Phi_v \Gamma^3} \frac{\mathrm{d}}{\mathrm{d}t^-} \int \mathrm{d}^3x\, \mathrm{d}^3p\, \delta(\boldsymbol{p} - \boldsymbol{p}^-)\delta(\Omega - \Omega^+) \tag{10}$$

which simplifies immediately using Eq. (6) for Γ and the explicit form of Φ_v (see below Eq. (9)) to

$$\Delta\sigma = \lim_{t\to\infty} \frac{\Delta\Omega^+}{v} \frac{\mathrm{d}}{\mathrm{d}t^-} \int \mathrm{d}^3x^-\, \delta(\Omega - \Omega^-)\,. \tag{11}$$

To carry out the time derivative in Eq. (11) we have to locate the explicit time dependence in the initial variables. While the coordinates x^- and y^- serve as impact parameters the trajectories propagate asymptotically along the z-axis with $z^-(t^-) = vt^- + z_0^- \equiv p^-/mt^- + z_0^-$. Hence, we can replace $\mathrm{d}z^- = v\mathrm{d}t^-$ and get

$$\Delta\sigma = \lim_{t\to\infty} \Delta\Omega^+ \int \mathrm{d}x^-\, \mathrm{d}y^-\, \delta(\Omega - \Omega^+) \tag{12}$$

which reduces to

$$\frac{\Delta\sigma}{\Delta\Omega^+} = \lim_{t\to\infty} \sum_i \frac{\partial(x_i^-, y_i^-)}{\partial(\cos\theta^+, \phi^+)}\,, \tag{13}$$

where

$$\partial(x_1^-,\ldots,x_n^-)/\partial(q_1^+,\ldots,q_n^+) \tag{14}$$

is a symbolic notation for the Jacobi determinant $|\det \mathscr{A}|$ of the $n \times n$ matrix $\mathscr{A}$ with elements $A_{ij} = \partial x_i^-/\partial x_j^+$. Under cylindrical symmetry the Jacobi determinant reduces to the derivative of the deflection function, $|b\mathrm{d}b(\theta)/\mathrm{d}\theta|$ with impact parameter b, and in this form Eq. (13) is easily recognized as the classical cross section [36, Ch. 3.10]. The sum in Eq. (13) indicates again that in general more than one trajectory has the correct boundary conditions in order to contribute to the cross section. An additional consequence is an infinite cross section (*rainbow scattering*) at impact parameters for which $\theta(b)$ has an extremum. Other singularities in the cross section result from *orbiting* trajectories and from *glories*. These effects are described extensively in the literature, e.g. [30; 36, Ch. 3.10; 37, Ch. 5].

Fragmentation: In scattering experiments fragmentation typically occurs when a projectile has enough energy to ionize an atom (or in chemistry, dissociate a molecule). After the collision there exist at least three fragments A, B, C. Before the collision we have two fragments where one fragment contains two particles bound to each other, formally $A+(BC)_{n^-} \to A+B+C$. Apart from the higher dimensionality of the problem there is an additional complication: The bound motion of (BC) in the initial state must be described classically. This can be done as long as the motion takes place on a torus, that is, as long as it has conserved action variables $\boldsymbol{I}_0^-$. For molecules the situation is approximately given by normal mode motion [32]. For an atomic bound state one valence electron in the central field approximation fulfills this condition as well, with fixed (energy-dependent) action and angular momentum.

The observables for the most detailed differential cross section are now the angles of the fragments in suitable (Jacobi) coordinates Ω_1 and Ω_2 and the kinetic energy associated with one Jacobi vector, E_1. Via conservation of the total energy E, the energy of the motion along the other Jacobi vector is fixed by the initial state, characterized by an action vector $\boldsymbol{I}^-$ for the bound subsystem and by the momentum $\boldsymbol{p}^-$ for the projectile as already known from potential scattering. The cross section reads

$$\Delta\sigma = \lim_{t\to\infty} \frac{\Delta\Omega_1^+\Delta\Omega_2^+\Delta E_1^+}{(2\pi)^3} \int \mathrm{d}x\,\mathrm{d}y\,\mathrm{d}^3\eta\,\mathrm{d}^3 I\,\delta(\Omega_1-\Omega_1^+)\delta(\Omega_2-\Omega_2^+)\delta(E_1-E_1^+)\delta(\boldsymbol{I}-\boldsymbol{I}^-)\,, \tag{15}$$

where the components of $\boldsymbol{\eta}^-$ with normalization $(2\pi)^3$ are the angular variables conjugated to the actions $\boldsymbol{I}^-$. As from Eq. (12) to Eq. (13) the cross section reduces to

$$\frac{\mathrm{d}^5\sigma}{\mathrm{d}\Omega_1\,\mathrm{d}\Omega_2\,\mathrm{d}E_1} = \frac{1}{(2\pi)^3}\sum_i \frac{\partial(x_i^-, y_i^-, \boldsymbol{\eta}_i^-)}{\partial(\cos\theta_1, \phi_1, \cos\theta_2, \phi_2, E_1)}\,, \tag{16}$$

where we have moved to a differential notation instead of the differences in Eq. (13). Also, from now on we drop for simplicity the '+' sign for the final state variables.

Excitation and rearrangement: Since we have already introduced the classical description of a bound state excitation and rearrangement can also be described. Instead of the angles and energy (Ω_1, E_1) in the coordinate one, we have now an action vector $\boldsymbol{I}_1$ describing the bound state in the final channel. For rearrangement the roles simply are exchanged in the final channel $(1 \leftrightarrow 2)$. For completeness we give the final results for the cross sections:

Excitation, $A + (BC)_{n^-} \rightarrow A + (BC)_n$:

$$\frac{\mathrm{d}^5\sigma}{\mathrm{d}\boldsymbol{I}_1\,\mathrm{d}\Omega_2} = \frac{1}{(2\pi)^3}\sum_i \frac{\hat{\sigma}(x_i^-, y_i^-, \boldsymbol{\eta}_i^-)}{\hat{\sigma}(\boldsymbol{I}_1, \cos\theta_2, \phi_2)}\,, \tag{17}$$

Rearrangement, $A + (BC)_{n^-} \rightarrow C + (AB)_n$:

$$\frac{\mathrm{d}^5\sigma}{\mathrm{d}\boldsymbol{I}_2\,\mathrm{d}\Omega_1} = \frac{1}{(2\pi)^3}\sum_i \frac{\hat{\sigma}(x_i^-, y_i^-, \boldsymbol{\eta}_i^-)}{\hat{\sigma}(\boldsymbol{I}_2, \cos\theta_1, \phi_1)}\,. \tag{18}$$

We have only derived cross sections for three particles. However, an extension to more particles does not involve any new elements and can be easily inferred from the three-particle cross sections. Some care is needed if the separation of the fragments, as they appear in the scattering events, is described in different Jacobi coordinates before and after the collision.

2.2. *Reduction of phase space for non-periodic motion*

A full (semi-)classical study of only three particles demands already control over 12 phase-space dimensions which is even with today's computer power quite problematic. Moreover, for the purpose of understanding the basic mechanisms and phenomena, it seems to be more desirable to split the description of a system into partitions whose effective phase space is reduced to a manageable volume. This does not necessarily imply the construction of a model which is unrealistic under experimental conditions. If one is only interested in rather global quantities such as integrated (total) or singly differential cross sections, the analysis of the classical problem with respect to partial fixed points can help to effectively reduce the phase space which has to be taken into account.

2.2.1. *Invariant manifolds*

Fixed points, important to characterize bounded motion in phase space [38], do not necessarily occur for unbounded motion, which is typical for scattering. Nevertheless, some coordinates may exist which are periodic, i.e.

$$p_i(t_n) = p_0\,, \quad q_i(t_n) = q_0\,, \tag{19}$$

where $t_n = nT$ is a multiple of the basic period T. More frequently, one will encounter the situation that a coordinate keeps a specific value for *all* times, i.e.,

$$p_i(t) = 0\,, \quad q_i(t) = q_0\,, \tag{20}$$

which is a special case of Eq. (19). A pair of phase space variables with this property we will call a *partial fixed point*, partial since only the value of a specific pair (q_i, p_i) is periodic (or fixed). The dynamics of trajectories whose initial conditions are on the *invariant manifold* defined by the phase space variables orthogonal to (q_i, p_i) remains on this manifold. Hence, the effective dynamics is reduced to a phase space whose dimensionality has decreased by two for a (simple) partial fixed point.

Classical transition probabilities and invariant manifolds: The existence of an invariant manifold due to a partial fixed point leads to block-diagonal form of the Jacobi matrix whose determinant, which decides transition probabilities classically (see Eqs. (8) and (14)), factorizes. Assume e.g. that

we have an eight-dimensional phase space $(p_1,\ldots,p_4,q_1,\ldots,q_4)$ where $(q_1 = q_1^*, p_1^* = 0)$ represent a partial fixed point. A change of $(p_2, p_3, p_4, q_2, q_3, q_4)$ will not influence the fixed point values. Consequently, the partial derivatives $\partial p_1^*/\partial q_j = 0$ $(j = 2,3,4)$ and the determinant of the Jacobi matrix factorizes,

$$\left|\frac{\partial(p_1^-,\ldots,p_4^-)}{\partial(q_1^+,\ldots,q_4^+)}\right| = \left|\frac{\partial(p_1^-)}{\partial(q_1^+)}\right| \left|\frac{\partial(p_2^-,p_3^-,p_4^-)}{\partial(q_2^+,q_3^+,q_4^+)}\right| . \tag{21}$$

The first determinant approximates the contribution to the propagator in the fixed point variables and the second determinant involves the coordinates orthogonal to the partial fixed point.

Stability analysis of partial fixed points: The time evolution of small deviations $\delta\gamma = (\delta p_1,\ldots,\delta p_n, \delta q_1,\ldots,\delta q_n)$ from a fixed point can be determined from the linearization of the Hamilton flow γ about the fixed point [39],

$$\dot{\mathbf{M}} = \mathscr{A}\mathbf{M}, \tag{22}$$

where $\mathbf{M}(t)$ is the stability matrix with elements $M_{ij} = \partial\gamma_i(t)/\partial\gamma_j(0)$. The dynamical matrix $\mathscr{A}(t) = \mathbf{\Gamma}_n\mathscr{H}(t)$ is composed of the Hamilton matrix $\mathscr{H} = \partial^2 H/\partial\gamma\partial\gamma$ and an auxiliary matrix

$$\mathbf{\Gamma}_n = \begin{pmatrix} 0 & -\mathbf{1}_n \\ \mathbf{1}_n & 0 \end{pmatrix} . \tag{23}$$

From $\det(\mathbf{M} - \mathbf{\Lambda}) = 0$ one obtains the Liapunov exponents of the partial fixed point,

$$\lambda_k(t) = \frac{1}{t}\ln \Lambda_k(t) \equiv \lim_{N\to\infty}\frac{1}{N}\sum_{j=0}^{N-1} a_k(jt/N) . \tag{24}$$

Thereby, an eigenvector of the dynamical matrix (which is a linear combination of the $\delta\gamma_j$) changes in a small time interval $\Delta t = t/N$ according to

$$\delta u_k(\Delta t) = \delta u_k^- \, \mathrm{e}^{a_k \Delta t} , \tag{25}$$

where $\delta u_k^- = \delta u_k(0)$ and $\lambda_k \approx a_k$ within Δt. However, as Eq. (24) shows, the Liapunov exponent is in general a time average over the eigenvalues a_k taken at successive time steps $t_j = jt/N$. The partial fixed point is stable if the λ_k are purely imaginary and unstable if they are real. Because of Eq. (24) this property follows directly from the corresponding property of the eigenvalues $a_k(t)$ of the dynamical matrix.

A partial fixed point as defined above decouples from the other phase-space variables (see Eq. (21)). Consequently, the stability matrix $\mathbf{M}$ can be written in block diagonal form with the determinant taking a product form $\det(\mathbf{M} - \mathbf{\Lambda}) = \det(\mathbf{M}^* - \mathbf{\Lambda})\det(\mathbf{M}' - \mathbf{\Lambda})$, where M^* is the stability matrix of the fixed point variables and M' is the stability matrix for the rest of the phase space. We will discuss an example in the next section.

Dynamics on invariant manifolds can be used to approximate observables if the motion linearized about the coordinates of the partial fixed point is stable. Imagine that a stable partial fixed point has been found in the domain of a variable over which is integrated for the desired observable. A reasonable approximation would be to assume that the true result is proportional to the value at the fixed point since the dynamics outside the stable fixed point will not lead to qualitatively different results (but tend to those of the partial fixed point).

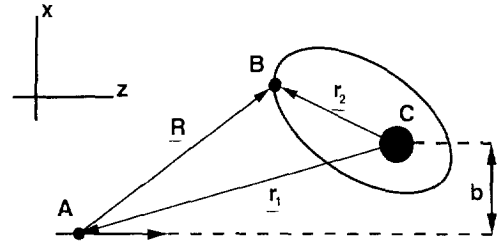

Fig. 1. The initial conditions in a typical scattering experiment. The y-axis is perpendicular to the paper plane, b represents the impact parameter.

The situation is very different for an unstable partial fixed point. Since the system is asymptotically open (in the sense that all trajectories reach infinity in coordinate space for infinite time) an initial value slightly away from an unstable partial fixed point may lead to a qualitatively different result compared to the one at the fixed point. Of course, this phenomenon is reminiscent of the stability properties of true fixed points.

2.2.2. *Planar three-body scattering*

We illustrate the concept of partial fixed points in connection with a typical scattering process $A+(BC)$ where the forces are two-body forces only. We use independent particle coordinates $\boldsymbol{r}_1 \equiv \boldsymbol{r}_{AC}$ and $\boldsymbol{r}_2 \equiv \boldsymbol{r}_{BC}$ in which the Hamiltonian can be represented as

$$H = \frac{\boldsymbol{p}_1^2}{2m_{AC}} + \frac{\boldsymbol{p}_2^2}{2m_{BC}} + \frac{\boldsymbol{p}_1\boldsymbol{p}_2}{m_C} + V_1(r_1) + V_2(r_2) + V(R) \tag{26}$$

with the reduced masses $m_{\alpha,\beta} = m_\alpha m_\beta/(m_\alpha + m_\beta)$ and $\boldsymbol{R} = \boldsymbol{r}_2 - \boldsymbol{r}_1$; see also Fig. 1. The typical initial conditions for a scattering event contain a trajectory for the projectile A and the bound system (BC) which can lie in the same plane, i.e. $p_{y,i} = y_i = 0$. These initial conditions define in a natural way a *partial fixed point* γ^*. However, we have to see if this partial fixed point is stable. Firstly, we calculate small deviations from $\gamma^* = (p_{y,1}, p_{y,2}, y_1, y_2) = (0,0,0,0)$ directly from the equations of motion:

$$\delta\dot{p}_{y,i} = -\delta\left(\frac{\partial H}{\partial y_i}\right) = -\sum_j \frac{\partial^2 H}{\partial y_i \partial \gamma_j}\delta\gamma_j\,,$$

$$\delta\dot{y}_i = \delta\left(\frac{\partial H}{\partial p_{y,i}}\right) = \sum_j \frac{\partial^2 H}{\partial p_{y,i}\partial\gamma_j}\delta\gamma_j\,. \tag{27}$$

Eq. (27) can be compactly written in the form of Eq. (22). Since the stability properties of the partial fixed point follow from the eigenvalues of the dynamical matrix (see Eq. (24)) we need the Hamilton matrix $\mathscr{H}^*$ about the partial fixed point $\gamma^* \equiv (p_{y,1}, p_{y,2}, y_1, y_2) = 0$ for our example Eq. (26):

$$\mathscr{H}^*|_{\gamma=\gamma^*} \equiv \frac{\partial^2 H^*}{\partial\gamma\partial\gamma} = \begin{pmatrix} t_1 & t & 0 & 0 \\ t & t_2 & 0 & 0 \\ 0 & 0 & v_1 & -v \\ 0 & 0 & -v & v_2 \end{pmatrix}, \tag{28}$$

where

$$t_1 = 1/m_{AC}\,, \qquad t_2 = 1/m_{BC}\,, \qquad t = 1/m_C\,,$$

$$v = \frac{\partial V}{\partial R}\frac{1}{R} \qquad v_i = \frac{\partial V_i}{\partial r_i}\frac{1}{r_i} - v \equiv w_i + v\,, \quad i = 1,2\,. \tag{29}$$

Note that the Hamilton matrix about the partial fixed point contains only first derivatives of the potential, i.e. forces. This is in contrast to a stability matrix at a generic phase space point where second derivatives of the potential appear. These terms disappear at a partial fixed point since they occur multiplied by the components of the phase space point which are zero at the partial fixed point. The eigenvalues of $\mathbf{A}^*$ are determined as usual by the characteristic polynomial equation

$$\lambda^4 + \lambda^2\left(\frac{w_1}{m_{AC}} + \frac{w_2}{m_{BC}} + \frac{v}{m_{AB}}\right) + \frac{m_A + m_B + m_C}{m_A m_B m_C}(w_1 w_2 + (w_1 + w_2)v) = 0\,. \tag{30}$$

Purely imaginary eigenvalues for a stable partial fixed point constitute a rather restrictive condition since it must hold for any value of every phase space variable orthogonal to the partial fixed point. It can be shown that a sufficient and necessary condition for imaginary roots of Eq. (30) is

$$w_1 w_2 + (w_1 + w_2)v > 0. \tag{31}$$

A physical realization of condition, Eq. (31), is the *gravitational three-body problem*. The attractive forces stabilize the plane in which the three bodies move initially.

However, in the microscopic world we are interested in the dynamics of charged particles where the typical situation is that two particles (A and B) repel each other while they are attracted by C, with $w_i > 0$ and $v < 0$. Then, a configuration with (almost) stable motion in the plane consists of two heavy and one light particle, e.g. $m_A \approx m_B \gg m_C$. In this case we get approximately linear stability ($\lambda^2 = 0$) in one direction and oscillatory behavior in the other direction since Eq. (30) reduces to

$$\lambda^2(\lambda^2 + (1/m_C)(w_1 + w_2)) = 0\,. \tag{32}$$

This behavior results for any combination of two heavy and one light particle.

The planar dynamics of electron–atom and positron–atom scattering is generally unstable. We discuss electron–atom (ion) scattering first. With the potentials $V_i = -Z/r_i$ and $V = 1/R$ the inequality, Eq. (31), can be written as

$$\sin\alpha^3 + \cos\alpha^3 - Z(1 - \sin(2\alpha)\cos\theta)^{3/2} < 0\,, \tag{33}$$

where $\tan\alpha = r_1/r_2$ and $\cos\theta = \boldsymbol{r}_1\boldsymbol{r}_2/(r_1 r_2)$. In Fig. 2 the regions of stability are shown for electron–hydrogen scattering ($Z = 1$). The same diagram (part a) holds also for positron–hydrogen scattering. One sees that the repulsion between the two electrons creates instability with respect to motion in the plane. The stability develops differently for the electron and the positron projectile if the charge Z of

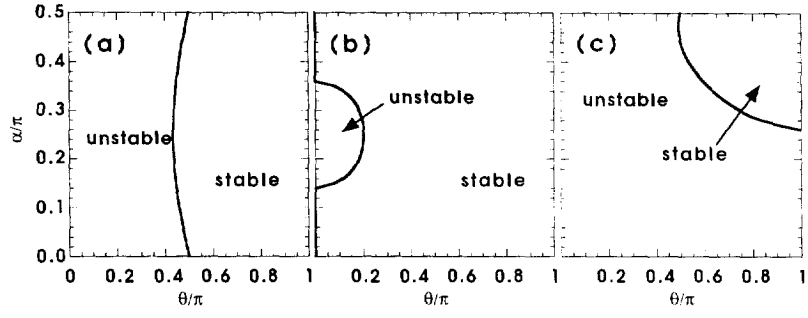

Fig. 2. Maps for the stability of planar motion for three charged particles, the coordinates are explained in the text. Part (a) represents the electron–hydrogen and the positron–hydrogen system, part (b) is for $e^- - O^{7-}$ and part (c) for $e^- - O^{7+}$.

the target ion is raised. Fig. 2b demonstrates that higher Z stabilizes the electron–ion system while it destabilizes the positron–ion scattering system (Fig. 2c). In summary, the stability analysis shows that the partial fixed points which define planar scattering are unstable for electron/positron–atom scattering. Hence, planar scattering is not a good approximation for these cases.

However, if we find another fixed point in a stable region of Fig. 2 we may use the corresponding, even lower dimensional phase space, as a good approximation. In Fig. 2a and Fig. 2b the line $\theta = \pi$ lies in the stable region. It corresponds to a collinear configuration where the particle in the middle screens the charges of like sign of the two outer particles. In the next section we will prove that $\sin\theta = 0$ defines partial fixed points and will examine their stability. Our starting point is the planar Hamiltonian which still has the form of Eq. (24). For convenience, we define $\theta = \theta_1 - \theta_2$ explicitly as a dynamical variable with conjugate momentum p_θ. The counterpart is the angle $\vartheta = \theta_1 + \theta_2$ whose conjugate momentum is the total angular momentum, $p_\vartheta = L$. For simplicity, we will demonstrate the derivation of the fixed point for two light and one heavy particle with the Hamiltonian

$$\frac{p_1^2}{2} + \frac{p_2^2}{2} + \left(\frac{1}{r_1^2} + \frac{1}{r_2^2}\right)\frac{p_\theta^2 + L^2}{2} + \left(\frac{1}{r_1^2} - \frac{1}{r_2^2}\right) p_\theta L + V_1 + V_2 + V\,. \tag{34}$$

2.2.3. *Collinear three-body scattering*

As already mentioned, the Hamiltonian Eq. (34) has partial fixed points defined by $\theta^* = 0$ or $\theta^* = \pi$ and $p_\theta^* = L^* = 0$. The structure of the stability matrix for deviations $(\delta p_\theta, \delta L, \delta\theta, \delta\vartheta)$ from the fixed point is similar to Eq. (28) where now

$$\begin{aligned} v_1 &= \frac{\partial V}{\partial R}\frac{r_1 r_2}{R^2}\cos\theta\,, \qquad v_2 = v = 0\,, \\ t_1 = t_2 &= \frac{1}{r_1^2} + \frac{1}{r_2^2}\,, \qquad t = \frac{1}{r_1^2} - \frac{1}{r_2^2}\,. \end{aligned} \tag{35}$$

This leads to the characteristic polynomial $P(\lambda) = \lambda^2(\lambda^2 + t_1 v_1)$. Hence, the fixed point at $\theta^* = \pi$ is stable and the fixed point at $\theta^* = 0$ is unstable or vice versa depending on the sign of $\partial V/\partial R$. The roots $\lambda^2 = 0$ indicate that the total angular momentum L is a cyclic variable (constant of motion). We will analyze the collinear motion ($\theta = \pi$) in the context of electron impact ionization in Section 5.

Depending on the observable of interest, additional fixed points may reduce the effective phase space further. Obviously, for the calculation of cross sections differential in the angles θ_i, the phase space cannot be reduced beyond the planar dynamics. For cross sections, only differential in the energy of the fragments, collinear collision dynamics may be used. Note, however, that the partial fixed-point analysis reveals properties under the most general circumstances. It does not preclude the possibility of integrable motion under special dynamical conditions. Such an example is provided by the so-called planetary two-electron configurations [40]. They have both electrons on the same side, which corresponds to a globally unstable configuration. Nevertheless, the planetary modes represent integrable motion. This is possible according to our stability map (Fig. 2) as long as the integrable motion restricts the range of the angles α, θ to the stable regions.

2.3. Projectors onto fragments in reduced phase space

If we reduce the effort to calculate cross sections to collinear phase space we lose any angular information and, moreover, the ability to calculate absolute cross sections. What is left, is the energy sharing of the fragments. Formally, we may write on the collinear manifold:

$$\frac{\mathrm{d}^5\sigma}{\mathrm{d}\Omega_1\mathrm{d}\Omega_2\mathrm{d}\varepsilon} = \frac{\mathrm{d}^4\sigma^*}{\mathrm{d}\Omega_1\Omega_2}\frac{\mathrm{d}P}{\mathrm{d}\varepsilon}\,, \tag{36}$$

where

$$\frac{\mathrm{d}^4\sigma^*}{\mathrm{d}\Omega_1\Omega_2} = \frac{\partial(y_1^*, y_2^*, \theta^*, \vartheta)}{\partial(\cos\theta_1, \varphi_1, \cos\theta_2, \varphi_2)} \tag{37}$$

is the cross section at the partial fixed point and $\mathrm{d}P/\mathrm{d}\varepsilon$ describes the energy sharing of the fragments. However, this energy sharing determines if two or three fragments are created after the collision. If particle A is free after the collision and its energy $\varepsilon > E$ then the system (BC) has necessarily negative energy and is bound. Hence, we can define the three-particle formation probability as

$$\sigma_3^*(E) = \int \mathrm{d}\Omega_1\mathrm{d}\Omega_2 \frac{\mathrm{d}^4\sigma^*}{\mathrm{d}\Omega_1\Omega_2}\int_0^E \mathrm{d}\varepsilon\frac{\mathrm{d}P}{\mathrm{d}\varepsilon} = \sigma^* P_3(E)\,. \tag{38}$$

Moreover, we may assume the total probability to be normalized:

$$1 = P(E) = \int_{-\infty}^{+\infty} \mathrm{d}\varepsilon\frac{\mathrm{d}P}{\mathrm{d}\varepsilon} = P_2(E) + P_3(E)\,. \tag{39}$$

The probabilities P_3 and $P_2 = 1 - P_3$ represent projectors onto two-body and three-body fragment spaces on the collinear phase-space manifold. With these projectors we can define a parameter-free ratio between two-body and three-body fragmentation with the respective cross sections σ_2 and σ_3. Since the fixed point contains the dominant contribution to the dynamics, we may write

$$\sigma_3/\sigma_2 \approx P_3/(1 - P_3)\,. \tag{40}$$

We can even calculate *absolute* three-body fragmentation cross sections with the help of these projectors if a total cross section σ_{tot} for the scattering process is available. The latter is normally

much easier to calculate and a useful formulation of σ_3 reads

$$\sigma_3 \approx \sigma_{\text{tot}} P_3 / P_{\text{tot}} \,. \tag{41}$$

In Section 6 we will apply the idea of projectors onto fragment spaces on reduced phase-space manifolds to double photoionization of helium.

Finally, we remark that for a system interacting solely through Coulomb forces, a rather peculiar global fixed point exists. This fixed point is the singular point where all particles are together. It will be analyzed in Section 3 and in Section 5 we show that its stability characterizes the ionization cross section of an atom at threshold $E = 0$ [41].

So far, we have worked within the framework of classical mechanics. However, all results carry over to the semiclassical expressions which are constructed with classical information only.

2.4. Phenomenological derivation of the semiclassical cross section

2.4.1. The semiclassical propagator

As a rule of thumb, the semiclassical approximation to the quantum mechanical propagator in a standard Cartesian representation, $\langle x|U(t)|x^-\rangle$, can be obtained from the classical probability density, Eq. (4), by

$$U_{\text{SCL}}(\boldsymbol{x}, \boldsymbol{x}^-, t) = \sum_j \sqrt{\mathscr{P}_j(\boldsymbol{x}, \boldsymbol{x}^-, t)}\, e^{i\Phi_j/\hbar - i\nu_j \pi/2} \,, \tag{42}$$

where Φ_j is the action and $\nu_j = \sum_i \text{sign}(\lambda_i)$, the number of sign changes of the eigenvalues λ_i of the Jacobi determinant $\mathscr{P}_j$ along the trajectory j. Although Eq. (42) contains only classical information it represents a complex amplitude with the possibility of interference. A rigorous derivation of Eq. (42) proceeds from the Feynman path integral representation of the propagator $U(t)$ leading in stationary-phase approximation to the semiclassical limit where only the paths with the least action Φ (the classical paths) contribute.

2.4.2. Semiclassical transition matrix elements and observables

In principle, Eq. (42) is also applicable to observables and transition elements. There are at least two ways to do this. The first possibility is to approximate the initial and final states semiclassically (classically) as well. This version is closest to the classical case, with the only difference that any classical action of a bound state motion is now quantized as prescribed in the EBK quantization. Hence, we can substitute the action vectors $\boldsymbol{I}$ by the quantum number vectors $\boldsymbol{n}$. This allows us to use the initial-state phase-space variables $\boldsymbol{n}^-$ and $\boldsymbol{\eta}^-$ for phase-space integration and leads to the formulation

$$\langle \boldsymbol{n}|A(t)|\boldsymbol{n}^-\rangle_{\text{SCL}} = \frac{1}{(2\pi)^{N/2}} \sum_j \left| \frac{d\boldsymbol{n}}{d\boldsymbol{\eta}_j^-} \right|^{-1/2} A(\boldsymbol{n}, \boldsymbol{\eta}_j^-, t) e^{i\Phi_j/\hbar - i\nu_j \pi/2} \,. \tag{43}$$

The semiclassical expression, Eq. (43), preserves the classical structure to a large extent. It is most suitable for the purpose of interpretation and intuitive understanding of processes and has the great advantage of being very simple if the sum contains only a few classical paths.

On the other hand, if very many paths contribute an alternative semiclassical formulation gains attractivity where the initial and final states $|i\rangle$ and $|f\rangle$ remain quantum mechanical,

$$\langle f|A(t)|i\rangle_{\mathrm{SCL}} = \int \mathrm{d}\boldsymbol{x}\,\mathrm{d}\boldsymbol{x}^{-}\,\langle f|\boldsymbol{x}\rangle\,\langle \boldsymbol{x}|A(t)|\boldsymbol{x}^{-}\rangle_{\mathrm{SCL}}\,\langle \boldsymbol{x}^{-}|i\rangle$$
$$= \int \mathrm{d}\boldsymbol{x}\,\mathrm{d}\boldsymbol{x}^{-}\psi_f^{*}(\boldsymbol{x})\psi_i(\boldsymbol{x}^{-})A(\boldsymbol{x},\boldsymbol{x}^{-},t)_{\mathrm{SCL}}\,. \tag{44}$$

Here, $A(\boldsymbol{x},\boldsymbol{x}^{-},t)_{\mathrm{SCL}}$ is the semiclassical probability density to find the observable A at $\boldsymbol{x}$ and time t,

$$A(\boldsymbol{x},\boldsymbol{x}^{-},t)_{\mathrm{SCL}} = \frac{1}{\Gamma^{3/2}}\sum_j \left|\frac{\mathrm{d}\boldsymbol{x}_j}{\mathrm{d}\boldsymbol{p}^{-}}\right|^{-1/2} A(\boldsymbol{x},\boldsymbol{p}_j,t)\mathrm{e}^{\mathrm{i}\Phi_j/\hbar - \mathrm{i}\nu_j\pi/2}\,. \tag{45}$$

As it stands this formulation is still a boundary value problem which requires root search to simultaneously satisfy the boundaries $\boldsymbol{x}$ and $\boldsymbol{x}^{-}$. However, as first shown by Miller [42], it is easy to transform the problem to an initial-state formulation which avoids the time-consuming root search procedure, using the canonical transformation from final coordinate $\boldsymbol{x}$ to initial momentum $\boldsymbol{p}^{-}$, $|\mathrm{d}\boldsymbol{p}^{-}/\mathrm{d}\boldsymbol{x}|$. The semiclassical transition amplitude takes the form

$$\langle f|A(t)|i\rangle_{\mathrm{SCL}} = \frac{1}{\Gamma^{3/2}}\sum_j \int \mathrm{d}\boldsymbol{p}^{-}\,\mathrm{d}\boldsymbol{x}^{-}\psi_f^{*}(\boldsymbol{x})\psi_i(\boldsymbol{x}^{-})\left|\frac{\mathrm{d}\boldsymbol{x}_j}{\mathrm{d}\boldsymbol{p}^{-}}\right|^{1/2} A(\boldsymbol{x},\boldsymbol{p})\mathrm{e}^{\mathrm{i}\Phi_j/\hbar - \mathrm{i}\nu_j\pi/2}\,, \tag{46}$$

where

$$\boldsymbol{x} = \boldsymbol{x}(\boldsymbol{p}_j^{-},\boldsymbol{x}^{-}), \qquad \boldsymbol{p} = \boldsymbol{p}(\boldsymbol{p}_j^{-},\boldsymbol{x}^{-})\,.$$

This initial value representation in connection with Monte-Carlo integration of Eq. (46) has been used recently to successfully generate semiclassical spectra including resonance widths [26–29].

2.4.3. *Semiclassical cross sections*

Using Eqs. (42) and (43) we can immediately translate the classical cross sections from Eqs. (13), (16) and (18) into semiclassical cross sections. For potential scattering we get

$$\frac{\mathrm{d}^2\sigma}{\mathrm{d}\Omega} = \lim_{t\to\infty}\left|\sum_j \left|\frac{\partial(x_j^{-},y_j^{-})}{\partial(\cos\theta,\phi)}\right|^{1/2} \mathrm{e}^{\mathrm{i}\Phi_j/\hbar - \mathrm{i}\nu_j\pi/2}\right|^2. \tag{47}$$

Note that the action Φ_j in Eq. (47) and in all semiclassical cross sections is special in two respects. First, it is an action *difference* between the action from a trajectory propagated under the full Hamiltonian H and under the asymptotic ('free') Hamiltonian H_0. This is a consequence of the definition of the S-matrix as [44, Ch. 8d]

$$S = \lim_{t\to\infty}\mathrm{e}^{\mathrm{i}H_0 t}\mathrm{e}^{-\mathrm{i}2Ht}e^{\mathrm{i}H_0 t} \equiv \lim_{t\to\infty} U_0^{\dagger}(t)U(2t)U_0^{\dagger}(t)\,. \tag{48}$$

Second, since the scattering amplitude is defined from S−matrix elements in momentum space, the action is expressed in generalized *momentum* coordinates,

$$\Phi_j = \Delta\Phi_j(\boldsymbol{p},\boldsymbol{p}^{-},E) = \int_{p^{-}}^{p}\boldsymbol{q}_j(H_0)\,\mathrm{d}\boldsymbol{p}' - \int_{p^{-}}^{p}\boldsymbol{q}_j(H)\,\mathrm{d}\boldsymbol{p}'\,, \tag{49}$$

where $\boldsymbol{q}(H)$ and $\boldsymbol{q}(H_0)$ stand for a trajectory under H and H_0, respectively. Fragmentation into three particles described by the fivefold differential cross section reads

$$\frac{\mathrm{d}^5\sigma}{\mathrm{d}\Omega_1\,\mathrm{d}\Omega_2\,\mathrm{d}E_1} = \lim_{t\to\infty}\frac{1}{(2\pi)^3}\left|\sum_j \left|\frac{\partial(x_j^-, y_j^-, \eta_j^-)}{\partial(\cos\theta_1, \phi_1, \cos\theta_2, \phi_2, E_1)}\right|^{1/2} \mathrm{e}^{\mathrm{i}\Phi_j/\hbar - \mathrm{i}\nu_j\pi/2}\right|^2 . \tag{50}$$

Excitation and rearrangement are expressed similarly whereby the classical action is replaced by the corresponding quantum number function n taken at the discrete, quantized values as described later on in Eq. (71). Generally, the semiclassical cross sections as described above differ from the classical ones through (a) the quantized values of the action vectors $\boldsymbol{I}$, (b) through the *complex* contribution of each path j to the scattering amplitude due to the phase factor, and (c), if necessary, through the symmetrization for indistinguishable particles. The determination of the action Φ_j for each path needs some care if the final and initial state are defined in different sets of Jacobi coordinates; for details see Refs. [31, 43].

2.5. *The semiclassical cross section derived from the quantum S-matrix*

To derive the expressions for the semiclassical cross sections from the quantum cross sections, one could start again from the time-dependent formulation of Eq. (9) which is also quantum mechanically valid. However, we will provide here a derivation which takes as a starting point the more familiar time-independent formulation with the T-matrix directly related to the scattering amplitude. The construction will be exemplified with potential scattering.

To make contact with the semiclassical approximation of the propagator, we need the fundamental quantum relation [44, Ch. 8]

$$\langle \boldsymbol{p}|S-1|\boldsymbol{p}^-\rangle = -2\pi i\hbar\,\delta(E-E^-)T(\boldsymbol{p},\boldsymbol{p}^-)\,. \tag{51}$$

For potential scattering the scattering amplitude is expressed through the T-matrix as [44, Ch. 3]

$$f(\theta) = m(2\pi i\hbar)^2 T(\boldsymbol{p},\boldsymbol{p}^-) \tag{52}$$

with $\theta = \arccos[\boldsymbol{p}\boldsymbol{p}^-/(pp^-)]$ and the reduced mass m. The construction of a semiclassical scattering amplitude from Eqs. (51) and (52) consists of two steps [45]. Firstly, the usual semiclassical approximation to the propagator, in this case the S-matrix, must be constructed. This has been done many times before in the literature and we only refer to the result (Eq. (42)). The second step is less well known but easier to perform. Since semiclassically we have the S-matrix we need to 'invert' the energy conserving δ-function in Eq. (51) to obtain the T-matrix. Energy conservation means invariance of the system against translation in time [46, Ch. II]. In terms of trajectories which represent the system and which are the backbone of the semiclassical propagator translational invariance in time means invariance of the propagator against *spatial* translation *along* the trajectories. This fact has already been used in the formulation of the classical cross section with Eqs. (11) and (12).

The δ-function in Eq. (51) may be written as a limit in time [34], [II, App. 2],

$$\delta(E-E^-)=\frac{m}{p}\delta(p-p^-)=\frac{m}{p}\lim_{t\to\infty}\left(\frac{t}{2\pi i\hbar m}\right)^{1/2}e^{i(p-p^-)^2t/2m\hbar}. \tag{53}$$

Then the quantum scattering amplitude in terms of the S-matrix expressed as the time limit of propagators (Eq. (48)) reads

$$f(\boldsymbol{p},\boldsymbol{p}^-)=\frac{p}{m}\lim_{t\to\infty}\left(\frac{(2\pi i\hbar m)^3}{t}\right)^{1/2}\left\langle \boldsymbol{p}|U_0^\dagger(t)U(2t)U_0^\dagger(t)-1|\boldsymbol{p}^-\right\rangle, \tag{54}$$

where the time variable t stands here for the final time $t\to\infty$ and also for the negative initial time, $t=-t^-$. Using the semiclassical expression, Eq. (42), for the propagator in momentum representation we may write

$$f(\boldsymbol{p},\boldsymbol{p}^-)=\lim_{t\to\infty}{\sum_j}'\frac{p}{\sqrt{tm}}\left|\frac{\partial x^-}{\partial \boldsymbol{p}}\right|^{1/2}e^{i\Phi_j(\boldsymbol{p},\boldsymbol{p}^-,2t)/\hbar-i\nu_j\pi/2}, \tag{55}$$

with the action difference as in Eq. (49),

$$\Phi_j(\boldsymbol{p},\boldsymbol{p}^-,E)=\lim_{t\to\infty}\Delta\phi_j(\boldsymbol{p},\boldsymbol{p}^-,2t). \tag{56}$$

The primed sum in Eq. (55) indicates that non-scattered trajectories have to be omitted from the sum. As a next step we can eliminate the explicit time dependencies in Eq. (55) using the asymptotic property of free classical motion outside the potential for large times,

$$\lim_{t\to\infty}\boldsymbol{p}(t)=\boldsymbol{p}_\infty=m\boldsymbol{x}(t)/t. \tag{57}$$

Applying Eq. (57) to both, the factor p outside as well as to $\boldsymbol{p}$ in the determinant of Eq. (55), yields

$$f(\boldsymbol{p},\boldsymbol{p}^-)=\lim_{t\to\infty}{\sum_j}'r\left|\frac{\partial \boldsymbol{x}^-}{\partial \boldsymbol{x}}\right|^{1/2}e^{i\Phi_j(\boldsymbol{p},\boldsymbol{p}^-,t-t^-)/\hbar-i\nu_j\pi/2}. \tag{58}$$

The scattering amplitude in form of Eq. (58) has been derived by Pechukas in a different way, by construction of a semiclassical wave function [10]. To obtain the familiar form of the scattering cross section, we must choose the appropriate coordinates. We assume that the particle is initially at a point with Cartesian coordinates $\boldsymbol{x}^-=(x^-,y^-,z^-)$, where $z^-\ll 0$ and $\boldsymbol{p}^-=(0,0,p^-)$. The final point of the trajectories is described in spherical coordinates $\boldsymbol{r}=(r\sin\Theta\cos\varphi,\ r\sin\Theta\sin\varphi,\ r\cos\Theta)$ with $\boldsymbol{p}=p\hat{r}$, with (Θ,φ) being the scattering angles. Note that the formulation does not rely on a spherically symmetric potential. Then,

$$\left|\frac{\partial \boldsymbol{x}}{\partial \boldsymbol{x}^-}\right|=\left|\frac{\partial \boldsymbol{x}}{\partial \boldsymbol{r}}\right|\left|\frac{\partial \boldsymbol{r}}{\partial \boldsymbol{x}^-}\right|, \tag{59}$$

where $|\partial \boldsymbol{x}/\partial \boldsymbol{r}|^{-1} = r^2 \sin\Theta$ is the determinant of the Jacobian for the transformation between Cartesian and spherical coordinates and

$$\frac{\partial \boldsymbol{r}}{\partial \boldsymbol{x}^-} = \begin{pmatrix} \frac{\partial r}{\partial x^-} & \frac{\partial r}{\partial y^-} & \frac{\partial r}{\partial z^-} \\ \frac{\partial \Theta}{\partial x^-} & \frac{\partial \Theta}{\partial y^-} & \frac{\partial \Theta}{\partial z^-} \\ \frac{\partial \varphi}{\partial x^-} & \frac{\partial \varphi}{\partial y^-} & \frac{\partial \varphi}{\partial z^-} \end{pmatrix} . \tag{60}$$

Now, we have to use the invariance against translation in time induced by the energy conservation. For a given trajectory this means that shifting time is equivalent to shifting the starting point about some increment *along* the trajectory. In other words, a shift dz^- of the starting point *along* the trajectory will not affect the scattering angle and will only cause an irrelevant shift dr *along* the trajectory at the final point. Hence, $\partial r/\partial z^- \approx 1$ while $\partial\Theta/\partial z^- \approx \partial\varphi/\partial z^- \approx 0$ and we arrive at

$$\lim_{t\to\infty} |\partial \boldsymbol{x}/\partial \boldsymbol{x}^-|^{-1} = (1/r^2)\,\mathrm{d}\sigma/\mathrm{d}\Omega\,, \tag{61}$$

where $\mathrm{d}\Omega = \sin\Theta\,\mathrm{d}\Theta\,\mathrm{d}\phi$. This step parallels the transition from Eqs. (11)–(13) in the derivation of the classical crossection. Combining Eqs. (58) and (61) we see that the contribution of an individual trajectory to the semiclassical scattering amplitude is indeed of the form $(\mathrm{d}\sigma/\mathrm{d}\Omega)^{1/2}\mathrm{e}^{\mathrm{i}[\Phi/\hbar - \nu\pi/2]}$ as phenomenologically derived in Eq. (47). Moreover, Eq. (58) is also valid for Coulomb potentials, despite their long tail, since no asymptotic wave function or some equivalent is necessary to determine the scattering amplitude.

In general, many classical paths can contribute to a differential cross section. If there is one pair of trajectories among them with the same starting and ending points in momentum and time and with a difference of action less than $\hbar$, the semiclassical description fails. Examples are the classical rainbow and glory effects [5].

3. Classical and semiclassical properties of scaling systems

3.1. Homogeneous potentials, hyperspherical coordinates and the virial theorem

Homogeneous potentials. In classical as well as in quantum mechanics a homogeneous interaction has profound consequences for the dynamics of a system. The Coulomb potential, through which nuclei and electrons in atoms and molecules interact, is homogeneous of degree $k = -1$ since it fulfills the general scaling relation

$$V(x_1, x_2, \ldots) \equiv \lambda^{-k} V(\lambda x_1, \lambda x_2, \ldots)\,. \tag{62}$$

Hyperspherical coordinates. There is a set of coordinates which is very helpful in dealing with homogeneous potentials namely *hyperspherical coordinates*[2] in which the potential of Eq. (62) takes the simple form

$$V(x_1, x_2, \ldots) \equiv V(\mathscr{R}, \boldsymbol{\Omega}) = C(\boldsymbol{\Omega})\mathscr{R}^k \,. \tag{63}$$

With the $\boldsymbol{r}_i = (x_i, y_i, z_i)$ being a set of mass weighted Jacobi coordinates, the hyperradius $\mathscr{R} = \sqrt{\sum_i r_i^2}$ measures the radius of the $3N-$dimensional sphere in which the N particles can be found. The other variables in configuration space consist of a set of hyperangles $\boldsymbol{\Omega} = (\Omega_1, \Omega_2, \ldots, \alpha_1, \alpha_2, \ldots)$, where the Ω_i express the position of $\boldsymbol{r}_i$ in the three-dimensional space while the angles α_i specify the relative lengths of the vectors $\boldsymbol{r}_i$, e.g. $\alpha_1 = \arctan(r_1/r_2)$. The canonical conjugated momenta are a generalized angular momentum $\boldsymbol{\Lambda}(\boldsymbol{\Omega})$ and the hyperradial momentum $\mathscr{P} = \mathrm{d}\mathscr{R}/\mathrm{d}t$. We have used these coordinates already dealing with the stability of partial fixed points in three-body systems in Section 2.2.2.

The virial theorem. Probably, the best-known consequence of a homogeneous interaction is linked to the virial theorem, which states (classically and quantum mechanically) that

$$\langle \text{kinetic energy} \rangle_{\text{av}} = -\frac{1}{2} \left\langle \sum_j q_j F_j \right\rangle_{\text{av}} \,. \tag{64}$$

Classically, the average is taken over time and quantum mechanically over the wave function of a stationary state. The F_j are the components of external and internal forces on the coordinates q_i of the system which may consist of many particles. The classical as well as the quantum mechanical proof of Eq. (64) is remarkably simple and can be found in Ref. [49].

The r.h.s. of Eq. (64) is proportional to the force in the direction of the hyperradius of the system and hence we may rewrite Eq. (64) as

$$\left\langle \frac{\mathscr{P}^2}{2} + \frac{\boldsymbol{\Lambda}^2}{2\mathscr{R}^2} \right\rangle_{\text{av}} = -\frac{1}{2} \langle \mathscr{R} F_{\mathscr{R}} \rangle_{\text{av}} \,. \tag{65}$$

If we insert now the radial force $F_{\mathscr{R}} = -kC(\boldsymbol{\Omega})\mathscr{R}^{k-1}$ resulting from a homogeneous potential like Eq. (63) we obtain the virial theorem for scaling systems,

$$\langle \text{kinetic energy} \rangle_{\text{av}} = \tfrac{1}{2}k \langle \text{potential energy} \rangle_{\text{av}} \,. \tag{66}$$

For $k = 2$ (quadratic potential) this is the familiar result that, on average, potential and kinetic energy are equal and half the total energy for an oscillator.

In the following we will investigate the classical scaling properties for Coulomb systems in more detail and we will discuss classical and semiclassical implications which are less well known than the virial theorem.

[2] The construction of hyperspherical coordinates for N particles is described in Ref. [47], a more abstract derivation of the Laplace operator on a N-dimensional sphere and its eigenfunctions can be found in Ref. [48].

3.2. Classical scaling and semiclassical eigenvalues

Suppose we have a Hamiltonian of the form

$$E \equiv H = \sum_j \frac{p_j^2}{2} + V(x_1, x_2, \ldots)$$
$$= \frac{\mathscr{P}^2}{2} + \frac{\Lambda^2}{2\mathscr{R}^2} + C(\Omega)\mathscr{R}^k \,, \tag{67}$$

where the potential is homogeneous of degree k as in Eq. (62). Then it is possible to construct a scaled, energy-independent, Hamiltonian through the transformation

$$H = \tilde{H}E/E_0 \,, \quad p = \tilde{p}\sqrt{E/E_0} \,, \quad x = \tilde{x}(E/E_0)^{1/k} \,, \tag{68}$$

where E_0 is an arbitrary constant energy to keep the units of unscaled and scaled variables identical. Quantities with the dimension of an action (like angular momentum) and the action itself scale then as

$$\Phi = \tilde{\Phi}(E/E_0)^{(2+k)/2k} \tag{69}$$

and for the time we get with $t = \mathrm{d}\Phi/\mathrm{d}E$ the scaling

$$t = \tilde{t}(E/E_0)^{(2-k)/2k} \,. \tag{70}$$

The scaled Hamiltonian has the constant value $\tilde{H} = E_0$. We also note that hyperspherical coordinates scale like the ordinary Cartesian coordinates, i.e. $\mathscr{R}$ like a length, $\mathscr{P}$ like a momentum and Λ like an angular momentum. All angles Ω are of course not affected by the scaling.

As it is well known energy levels of one-dimensional systems are semiclassically obtained by quantizing the action [39, Ch. 7.3]

$$\Phi(E_n) = \tilde{\Phi}(E/E_0)^{(1/2)+1/k} = 2\pi\hbar(n + \tfrac{1}{2}) \,. \tag{71}$$

In higher-dimensional systems it is possible to quantize single stable (and even slightly unstable) periodic orbits [40, 20]. The quantization condition, Eq. (71), must be slightly generalized in this case with $n + \frac{1}{2}$ replaced by $n - \mu$, where μ contains information about the dynamics of the system in all directions in phase space which are perpendicular to the local direction of the periodic orbit. The wave functions which correspond to the quantized energies are said to be scarred along those orbits [50].

For a scaling system the semiclassical quantization implies the existence of a *series* of states based on one periodic orbit whose action together with the scaling relation determines the spacing of the quantized energies according to Eq. (71),

$$E_n = E_0 \left(\frac{\tilde{\Phi}}{2\pi\hbar(n-\mu)} \right)^{-2k/(2+k)} \,. \tag{72}$$

Prominent examples are periodic orbits in a Coulomb system which lead with $k = -1$ in Eq. (62) to the existence of Rydberg series built on these orbits with

$$E_n = -E_0 \left(\frac{\tilde{\Phi}/(2\pi\hbar)}{n - \mu} \right)^2 . \tag{73}$$

In this case we would interpret $\tilde{\Phi}/(2\pi\hbar)$ as an effective charge and μ as a quantum defect and E_0 is conveniently chosen to be the Rydberg constant.

For one-dimensional systems with homogeneous potentials the fundamental action $\tilde{\Phi}(\tilde{E} = E_0)$ can often be calculated easily and the semiclassical energies from Eq. (72) are quite accurate for all but the lowest levels. The same is true in higher-dimensional systems for the shorter periodic orbits.

Also noteworthy in the context of quantizing scaling systems is another quasiclassical method, *dimensional scaling* [51]. This method is most suitable to approximate ground states since it retains the commutator to all orders in $\hbar$ [52]. However, dimensional scaling has also been applied successfully to describe resonances [53].

3.3. The hyperradius as a function of time in a scaling system

We now come to the consequences of classical scaling. Under certain conditions one can determine – without explicit calculation of the trajectories – the kind and number of extrema of the hyperradius $\mathscr{R}(t)$ of single classical trajectories in scaling systems. For this purpose we note that at an extremum of $\mathscr{R}$ we have $\dot{\mathscr{R}} = 0 = \mathscr{P}$ and therefore from energy conservation

$$E = \Lambda^2/2\mathscr{R}^2 + C(\Omega)\mathscr{R}^k . \tag{74}$$

The kind of extremum is determined by the second derivative of $\mathscr{R}$ which can be expressed through Hamilton's equations as

$$\dot{\mathscr{P}} = -\frac{\partial H}{\partial \mathscr{R}} = \frac{\Lambda^2}{\mathscr{R}^3} - kC\mathscr{R}^{k-1} . \tag{75}$$

We do not know the sign of $C(\Omega)$; however, we may use Eq. (74) to rewrite Eq. (75) as

$$\dot{\mathscr{P}} = \frac{k+2}{2}\frac{\Lambda^2}{\mathscr{R}^3} - \frac{Ek}{\mathscr{R}} . \tag{76}$$

Now, $\dot{\mathscr{P}}$ is positive, i.e. all extrema of $\mathscr{R}$ are minima in the following three cases:

$$k > 0 \text{ and } E < 0 \tag{77a}$$

$$k = 0 \tag{77b}$$

$$0 > k \geq -2 \text{ and } E > 0 . \tag{77c}$$

Similarly, all extrema of $\mathscr{R}$ are maxima under the condition

$$k \leq -2 \quad \text{and} \quad E < 0 . \tag{78}$$

If these conditions apply, we can draw the following conclusion: Since a trajectory is continuous in time it can have at most *one* minimum (or maximum in the case of Eq. (78)) if all of its extrema must be minima (maxima).

Here we will discuss only the cases which are interesting for scattering situations. Since the asymptotic conditions imply an infinite hyperradius the only possibility is a single minimum. Moreover, the potential must vanish for $\mathscr{R} \to \infty$ for a well-defined scattering problem. This leaves the trivial case (Eq. (77b)) of constant potential and the interesting case (Eq. (77c)) which contains most importantly the Coulomb interaction, $k = -1$. Hence, *for positive total energies E the hyperradius $\mathscr{R}(t)$ of each trajectory in a Coulombic multi-particle system has a single minimum.* As we will see later this property of a Coulomb system is related to the absence of resonances for positive energies in Coulomb systems in a similar way as this is the case quantum mechanically as shown by Simon [54]. Briefly, the classical signature of a resonance is a time delay in the trajectories which is indicated by multiple extrema in the hyperradius compared to the direct trajectories with a single turning point in $\mathscr{R}$. For positive energies in a Coulomb system we have proven that only 'direct' trajectories with a single turning point exist. We also note in passing that the simplest application of these scaling properties is Rutherford scattering. In this case the hyperradius is the ordinary radial coordinate, the distance between the two charged particles, and $C(\Omega) = Z_1 Z_2$ is just the product charge which does not depend on the angle. We will discuss potential scattering between two particles in more detail in Section 4.

Finally, it is clear that no fixed points can exist for Coulombic systems at positive energies due to the single minimum in the hyperradius. However, partial fixed points as introduced in Section 2.2.1 do not require periodic motion and they exist in a scattering system involving Coulombic forces.

3.4. The all-particle collision manifold in Coulomb systems

In this section we will derive the all-particle collision manifold for a system of three charged particles, more specifically for the two-electron atom. However, the results can be easily generalized to an arbitrary number of charged particles with arbitrary masses.

3.4.1. Regularization of the all-particle coalescence

For the two-electron atom, we have already reduced the full phase space to the collinear collision manifold due to partial fixed points in Sections 2.2.2 and 2.2.3. Can we find a global fixed point by completing the successive construction of partial fixed points for the variables α and $\mathscr{R}$ on the collinear collision manifold? It is obvious that the standard construction of $\mathscr{R} = \mathscr{R}_0$ and $\mathscr{P} = 0$ will not work in this case since this is the condition for the minimum in $\mathscr{R}$ which characterizes individually each trajectory but not globally a partial fixed point. Hence we have to look for the other possibility, $\mathscr{P} = \mathscr{P}_0$ and $\mathscr{R} = 0$. However, this is not a straightforward task since $\mathscr{R} = 0$ is a singular point for Coulombic potentials. Moreover, we have to secure the boundary condition $\mathscr{R} \geq 0$ which can be done by defining a new variable $\mathscr{R} = u^2$ with conjugate momentum $p_u = 2u\mathscr{P}$. The singular behavior of the equations of motion at $u = 0$ can be regularized by forming a new Hamiltonian $H - E$ of value zero. It can be multiplied by a function $f(p_i, q_i)$ which may depend on any phase-space variables

$$h = (H - E)f \equiv 0\,. \tag{79}$$

The construction leads to

$$\frac{\mathrm{d}p_i}{\mathrm{d}t_f} = -\frac{\partial h}{\partial q_i} = -\frac{\partial H}{\partial q_i} f = \frac{\mathrm{d}p_i}{\mathrm{d}t} f \tag{80}$$

and represents a canonical transformation (i.e. the form of Hamilton's equations is preserved) if $\mathrm{d}t = f\mathrm{d}t_f$. Hence, f introduces a new time scale which may explicitly depend on the actual phase-space variables. This regularization is used in celestial mechanics [55] as well as in the formalism of path integrals for singular potentials [56]. For the Coulomb problem we define $f = f(u) = u^2$ with $\mathrm{d}t = u^2\mathrm{d}t_u$ which has the reasonable effect that for constant time intervals Δt_u the real time intervals Δt become smaller when the singularity is approached. Putting the regularization and the point transformation $\mathscr{R} = u^2$ together, we arrive at the new Hamiltonian for the collinear two-electron problem

$$h = \frac{p_u^2}{8} + \frac{p_\alpha^2}{2u^2} + C(\alpha) - Eu^2 \equiv 0\,, \tag{81}$$

where

$$C(\alpha) = -\frac{Z}{\sin\alpha} - \frac{Z}{\cos\alpha} + \frac{1}{\sin\alpha + \cos\alpha}\,. \tag{82}$$

The Hamiltonian in Eq. (81) is similar to that of an inverted two-dimensional oscillator and was used for the first time by Eckhardt [41] to determine the stability properties of the triple collision manifold. To find possible partial fixed points we need the equations of motion:

$$\mathrm{d}p_u/\mathrm{d}t_u = (p_\alpha^2/u^3) + 2Eu\,, \qquad \mathrm{d}p_\alpha/\mathrm{d}t_u = -\mathrm{d}C/\mathrm{d}\alpha\,,$$

$$\mathrm{d}u/\mathrm{d}t_u = \tfrac{1}{4}p_u\,, \qquad \mathrm{d}\alpha/\mathrm{d}t_u = p_\alpha/u^2\,.$$

For $u = 0$ the differential equations of Eq. (83) may still become singular. Hence, we need another transformation of the time to $\mathrm{d}\tau = u\mathrm{d}t_u$ and a non-canonical transformation $P_\alpha = p_\alpha/u$. Denoting the time derivative $\mathrm{d}/\mathrm{d}\tau$ by a dot we have finally

$$\begin{aligned} &\dot{p}_u = P_\alpha^2 + 2Eu^2\,, \qquad \dot{P}_\alpha = -(\mathrm{d}C/\mathrm{d}\alpha) - P_\alpha p_u/4\,,\\ &\dot{u} = \tfrac{1}{4}p_u u\,, \qquad \dot{\alpha} = P_\alpha\,. \end{aligned} \tag{84}$$

3.4.2. Stability analysis of the global fixed point

For Eq. (84) $u^* = P_\alpha^* = \mathrm{d}C/\mathrm{d}\alpha = 0$ defines a couple of partial fixed points with $\mathrm{d}C/\mathrm{d}\alpha = 0$ at $\alpha^* = \pi/4$. Inserting these values into the Hamiltonian Eq. (81) we get $p_u^* = \pm(-8C(\alpha^*))^{1/2}$. Hence, $(u^* = 0, p_u^*)$ indeed constitutes a partial fixed point in the sense of Section 2.2.1 with the peculiar property that the fixed point is at the singularity $u = 0$ which defines the coalescence of all three particles.

The stability of the fixed point is now easily determined by constructing the stability matrix from Eq. (84) with $\delta\dot{\gamma} = \mathbf{M}\delta\gamma$ (see Section 2.2.1). The characteristic polynomial for the eigenvalues reads

$$\lambda\left(\frac{p_u^*}{4} - \lambda\right)\left(\lambda^2 + \frac{p_u^*}{4}\lambda + \frac{\mathrm{d}^2C^*}{\mathrm{d}\alpha^2}\right) = 0 \tag{85}$$

and has the roots

$$\lambda_{1/2} = \frac{p_u^*}{4}\left(-\frac{1}{2} \pm \sqrt{\frac{1}{4} + \frac{2}{C^*}\frac{\mathrm{d}^2 C^*}{\mathrm{d}\alpha^2}}\right),$$
$$\lambda_3 = 0\,, \qquad \lambda_4 = \tfrac{1}{4} p_u^* \tag{86}$$

with $C^* = C(\alpha^*)$. The eigenvalues λ_i show that the dynamics on the triple collision manifold is no longer symplectic which is formally a consequence of the last (non-canonical) transformation of the variables. The time evolution of the eigenvectors $\delta\gamma_i(\tau) = \cos\xi_i \delta\alpha + \sin\xi_i \delta P_\alpha$ with $\tan\xi_i = \lambda_i$ reads as in Eq. (27). In Section 5.2.1 we will need the stability matrix element $(\delta P_\alpha/\delta\alpha^-)^{-1}$. In terms of the eigenvectors $\delta\gamma_i^-$ we have

$$\delta P_\alpha = \frac{\cos\xi_2\, \mathrm{e}^{\lambda_1\tau}\delta\gamma_1^- - \cos\xi_1 \mathrm{e}^{\lambda_2\tau}\delta\gamma_2^-}{\sin\xi_1\cos\xi_2 - \sin\xi_2\cos\xi_1}\,, \tag{87}$$

which implies

$$\delta P_\alpha/\delta\alpha^- = (\mathrm{e}^{\lambda_1\tau} - \mathrm{e}^{\lambda_2\tau})/(\lambda_1 - \lambda_2)\,. \tag{88}$$

Using $\delta u(\tau) = \exp(p_u^*/4\tau)\delta u^-$ we may replace τ in Eq. (88) by δu which measures the distance from the triple collision manifold since $u^* = 0$:

$$\delta P_\alpha/\delta\alpha^- = (\delta u/\delta u^-)^{4\lambda_1/p_u^*} - (\delta u/\delta u^-)^{4\lambda_2/p_u^*}/(\lambda_1 - \lambda_2)\,. \tag{89}$$

To summarize, through successive construction of partial fixed points we have determined a global fixed point (in all phase space variables) which is generic for Coulombic many particle systems and which corresponds to the coalescence of all particles. For two electron atoms it is characterized by the variables total angular momentum $L^* = 0$, hyperradius $\mathscr{R} = 0$, the angles $\theta^* = \pi$, $\alpha^* = \pi/4$, the momenta $P_\theta^* = P_\alpha^* = 0$, and finally, the radial momentum $p_u^* = \pm(-8C(\alpha^*))^{1/2}$. We will see in Section 5.2.1 that this fixed point directly determines the cross section for complete fragmentation at $E = 0$.

4. Semiclassical potential scattering

In this section we will start to apply the semiclassical scattering description to Coulomb problems. Since the Coulomb potential is spherically symmetric an additional simplification arises if the scattering amplitude or S-matrix is expanded into partial waves. Although not very suitable for the Coulomb problem, the formulation of potential scattering in terms of semiclassical phase shifts nevertheless has been the method of choice for a long time. The reason is easy to understand: Based in one or the other way on the WKB-approximation, traditional semiclassical methods have been essentially one-dimensional. Since scattering from a spherically symmetric potential can be reduced to a problem in the radial coordinate by expanding the scattering amplitude into partial waves, an early application of semiclassical methods to scattering problems was the semiclassical formulation of phase shifts. The approximation is in general useful for a sufficiently small de Broglie wavelength $\lambda = h/p$ of the incident particle compared with the range a of the potential.

Using all constants of motion for a diagonal representation of the S-matrix we can write [44, p. 181]

$$\langle E,\ell,m|S|E^-,\ell^-,m^-\rangle = s_l(E)\delta(E-E^-)\delta_{ll^-}\delta_{mm^-}\,. \tag{90}$$

Since the S-matrix is unitary it can be written as a phase

$$s_l(E) = \mathrm{e}^{i2\delta_l}\,, \tag{91}$$

where δ_l is called the phase shift. The scattering amplitude is proportional to matrix elements of the S-matrix in momentum representation. For each partial wave with angular momentum l the angles have been already integrated over and only the radial part of Eq. (49) is left. It is not affected by the integration of the S-matrix over the angles to be performed for the representation Eq. (90) in l, l^-. We can conclude that the semiclassical phase shift is given by the radial action difference in momentum space,

$$2\delta_l^{\mathrm{SCL}} \equiv \Delta\Phi_L/\hbar = \frac{2}{\hbar}\int_0^{p_\infty} r_0(p_0)\,\mathrm{d}p_0 - \frac{2}{\hbar}\int_0^{p_\infty} r(p)\,\mathrm{d}p\,, \tag{92}$$

where

$$p^2(r) = p_\infty^2 - 2mV - L^2/r^2\,, \tag{93}$$

$$p_0^2(r) = p_\infty^2 - L^2/r_0^2\,. \tag{94}$$

The limits of the integral are defined through the asymptotic momentum $p_\infty = \sqrt{2mE}$ and the momentum $p = 0$ at the turning points $r = r_m$ (with potential V) and $r_0 = b = L/p_\infty$ (with $V = 0$) for a trajectory with impact parameter b. In this formulation the correct phase shift $\delta_L = 0$ for free motion is automatically obtained. The semiclassical phase Φ_L for free motion is easily calculated from the first term in $\Delta\Phi_L$,

$$\int_0^{p_\infty} r(p_0)\,\mathrm{d}p_0 = L\int_0^{p_\infty}(p_\infty^2 - p_0^2)^{-1/2}\,\mathrm{d}p_0 = L\pi/2\,. \tag{95}$$

However, what remains unclear is the relation of the quantum number l to the classical angular momentum L. Should the radial problem be taken from quantum mechanics implying that $L/\hbar = \sqrt{l(l+1)}$ or should we consequently apply semiclassical quantization rules implying that $L/\hbar = l + \frac{1}{2}$?

In answering this question as it was done in the literature, we briefly review the traditional derivation of the semiclassical phase shifts in spatial representation. Before we begin, the partial wave expansion should be quoted for completeness. It reads for the scattering amplitude [44, Ch. 6]

$$f(\theta) = \frac{\hbar}{p_\infty}\sum_{l=0}^{\infty} g_l P_l(\cos\theta)\,, \tag{96}$$

where

$$g_l = (l+\tfrac{1}{2})(\mathrm{e}^{\mathrm{i}2\delta_l} - 1) \tag{97}$$

with the scattering angle θ.

4.1. Scattering amplitude from semiclassical phase shifts

Clearly, the phase shifts must follow from solving the radial problem for each partial wave l,

$$\left(-\frac{\mathrm{d}^2}{\mathrm{d}r^2}+\frac{2mV(r)}{\hbar^2}+\frac{L(l)^2}{\hbar^2 r^2}-\frac{p_\infty^2}{\hbar^2}\right)\psi_l(r)=0\,, \tag{98}$$

with the functional dependence $L^2(l)/\hbar^2 = l(l+1)$. The phase shift is defined in terms of the asymptotic solution to Eq. (98):

$$\psi_l(r\to\infty)\to\sin\left(\int_{r_m}^{\infty} p\frac{\mathrm{d}r}{\hbar}+\frac{\pi}{4}\right)\,. \tag{99}$$

The asymptotic WKB-wave function reads

$$\psi_l^{\mathrm{WKB}}(r\to\infty)\to\sin(p_\infty r/\hbar-l\pi/2+\delta_l)\,. \tag{100}$$

Comparing Eq. (99) with Eq. (100) we see that

$$\begin{aligned}\delta_l^{\mathrm{WKB}} &= \int_{r_m}^{\infty} p\frac{\mathrm{d}r}{\hbar}+\frac{(l+\frac{1}{2})\pi}{2}-\frac{p_\infty r}{\hbar}\\ &= \int_0^{p_\infty} r\frac{\mathrm{d}p}{\hbar}+\frac{(l+\frac{1}{2})\pi}{2}\,.\end{aligned} \tag{101}$$

Using Eq. (95) in Eq. (101) the WKB phase shift for free motion becomes $\delta_l = (-L(l)/\hbar+l+\frac{1}{2})\pi/2$ which does not reduce to the correct value zero if the quantum mechanical value $L^2/\hbar^2 = l(l+1)$ is used in $p(r)$. Also, the behavior of the radial wave function near the origin $r=0$ is not predicted correctly by the naive WKB approach. Already in 1926, Kramers [57] noticed that these deficiencies could be eliminated when $l(l+1)$ was replaced by $(l+\frac{1}{2})^2$. The substitution of the angular momentum $\sqrt{l(l+1)}\to l+\frac{1}{2}$ is called Langer modification after Langer who obtained this substitution from an analysis of the problem with a transformation of the radial coordinate into a Cartesian coordinate $r=\mathrm{e}^x$ [58].

This history provides a lesson about the delicate details of semiclassical approximations and recalls the fact that standard correspondences between quantum and semiclassical objects should only be formulated in Cartesian coordinates. Essentially, the Langer modification results indeed from the mapping of the radial coordinate $r\in[0,\infty[$ into the Cartesian coordinate $x\in]-\infty,\infty[$ and from the application of the quantization condition and the connecting formulae in this set of coordinates. Transforming back to radial coordinates finally yields the modification of the angular momentum. A recent application of this transformation can be found in Ref. [59]. Even more recently, Friedrich and coworkers have proposed a new correction which works better than the Langer modification [60]. The same problem of formulating semiclassical quantities in non-Cartesian coordinates emerges in the context of path integrals. The path integral, asymptotic in $\hbar$, involves e.g. in spherical coordinates a curvature correction which amounts exactly to the Langer modification [24, Ch. 13.5].

Incidentally, one could have started from the beginning by treating all degrees semiclassically. Quantizing the angular action (the angular momentum) in the usual way leads immediately to $L^2/\hbar^2 = (l+\frac{1}{2})^2$ and the regularization of the radial problem is no longer necessary. The reason for the difficulty in the WKB phase shift defined from Eq. (101) lies in the fact that essentially two phases

are subtracted from each other where the one for free motion, $(l+\frac{1}{2})\pi/2$, is taken from exact quantum mechanics while the other one, $L\pi/(2\hbar)$, comes from a semiclassical approximation. If both phases are calculated on the same footing as in the formulation of the phase shift with the action difference of Eq. (92) this problem does not occur. The observation leads to a generally valid notion in the context of semiclassical techniques: Results are more reliable if the semiclassical approximation is applied consistently to all relevant quantities.

The 'collisional' action [67, 37] of Eq. (92) defines not only the semiclassical phase shift but also determines through partial derivatives important classical quantities for scattering such as the deflection function Θ and the collision time delay τ, i.e. the time delay between a free trajectory and a trajectory in the presence of the potential,

$$\Theta(E,L) = \partial\Delta\Phi_L/\partial L|_E\,, \qquad \tau(E,L) = \partial\Delta\Phi_L/\partial E|_L\,. \tag{102}$$

The relations are analogous to the entropy in statistical mechanics where here (L,Θ) and (E,τ) define pairs of conjugate variables with the total action differential given by

$$\mathrm{d}\Delta\Phi(E,L) = \Theta(E,L)\mathrm{d}L + \tau(E,L)\mathrm{d}E\,. \tag{103}$$

Similarly, changing the independent variable in $\Delta\Phi$ requires a Legendre transformation, e.g.

$$\Delta\Phi(E,\Theta) = \Delta\Phi(E,L) - L\Theta\,. \tag{104}$$

The construction of a semiclassical scattering amplitude using the partial wave sum, Eq. (96), and the semiclassical phase shifts, Eq. (92), requires three steps of approximations as first noticed by Ford and Wheeler [5]. In the first step the sum over l is replaced by an integral over L. However, doing this in a naive way can lead to serious errors because the summands in Eq. (96) are highly oscillatory. The best transformation to convert a sum into an integral semiclassically is the *Poisson summation formula*

$$\sum_{l=0}^{\infty} g_l = \frac{1}{\hbar}\sum_{\mu=-\infty}^{\infty} \mathrm{e}^{-\mathrm{i}\mu\pi}\int_0^{\infty}\mathrm{d}L\, g[l(L)]\mathrm{e}^{\mathrm{i}2\pi\mu L/\hbar}\,, \tag{105}$$

where the index μ indicates in our context how many times a path has circled the origin (i.e. the scattering center). The naive sum is recovered for paths without multiple revolutions, $\mu = 0$.

The second step approximates the summands in Eq. (96) by their large L limit. This includes the phase shift δ_l which is taken from Eq. (92) and the approximate form for the Legendre polynomials

$$P_{l(L)}(\cos\theta) \approx \left(\frac{2\hbar}{L\pi\sin(\theta)}\right)^{1/2}\cos\left(\frac{L\theta}{\hbar} - \frac{\pi}{4}\right) \tag{106}$$

which is valid everywhere but close to 0 or π. For these limits other formulae can be used, see [30, Ch. 6]. Using Eqs. (92), (105) and (106) the scattering amplitude, Eq. (96), takes the form

$$f(\theta) \approx -\frac{\mathrm{i}}{p_\infty}(2\pi\hbar\sin\theta)^{-1/2}\sum_{\mu=-\infty}^{\infty}\mathrm{e}^{-\mathrm{i}\mu\pi}(\mathrm{e}^{-\mathrm{i}\pi/4}I_\mu^+ + \mathrm{e}^{\mathrm{i}\pi/4}I_\mu^-)\,, \tag{107}$$

where

$$I_\mu^{\pm} = \int_0^{\infty}\mathrm{d}L L^{1/2}\mathrm{e}^{\mathrm{i}[\Delta\Phi_L + L(\pm\theta+2\mu\pi)]/\hbar}\,. \tag{108}$$

In a third level of approximation the integrals of Eq. (108) are evaluated (for small $\hbar$) in stationary-phase approximation: Only those values $L(\theta)$ contribute for which the exponent in Eq. (108) is stationary,

$$\Delta\Phi_L/\mathrm{d}L = \mp\theta - 2\mu\pi\,. \tag{109}$$

Recalling Eq. (102) we realize that the deflection angle

$$\Theta = \mp\theta - 2\mu\pi \tag{110}$$

and that through the stationary-phase approximation only *classical paths* are selected from the integrals of Eq. (108) for the resulting semiclassical scattering amplitude

$$f(\theta) = \sum_j \delta_j \left(\frac{L_j(\theta)}{p_\infty^2 \sin\theta |\mathrm{d}\Theta/\mathrm{d}L_j|} \right)^{1/2} \mathrm{e}^{\mathrm{i}\Phi_j/\hbar}\,. \tag{111}$$

Here, $\Phi_j = \Delta\Phi_j(\Theta) = \Delta\Phi_j(L) - L\Theta$ is the collisional action in the variable Θ (Eq. (104)).

In the present context, once again, we are more interested in cases where a small number of trajectories contribute to an observable. Hence, the direct description through the semiclassical scattering amplitude in terms of classical trajectories is more appropriate. This approach has been formulated in an intriguing paper by Pechukas [10].

4.2. Coulomb scattering

4.2.1. Deflection function and Rutherford cross section

We know (see text below Eq. (14)) that the classical deflection function is the relevant object for potential scattering in a spherically symmetric potential. It formulates the deflection angle Θ as a function of the impact parameter, $\Theta(b)$, or as a function of the angular momentum $\Theta(L)$. For a standard scattering situation $\boldsymbol{p}^- = (0, 0, p^-)$ and hence $L = bp^-$. For attractive potentials the deflection angle Θ may not be identical to the scattering angle θ since a trajectory may circle the scattering center some times before it recedes from it. For a central potential the deflection function can be directly calculated with Eqs. (92), (95) and (102),

$$\Theta(b) = \pi - 2b \int_{r_0}^{\infty} \frac{\mathrm{d}r}{r^2} \left(1 - 2mV(r)/p_\infty^2 - b^2/r^2\right)^{-1/2}\,, \tag{112}$$

where r_0 denotes the largest turning point, i.e. where the square root becomes zero. For the Coulomb potential $V(r) = Z_1Z_2/r$ with charges Z_1 and Z_2 of the two particles the integral Eq. (112) can be solved analytically to give $\Theta(b) = 2\arctan[Z_1Z_2/(2Eb)]$. Since $\Theta(b)$ is *monotonic* it can easily be inverted to obtain $b(\Theta)$ and subsequently $\mathrm{d}b/\mathrm{d}\Theta$ which leads with Eq. (13) to the classical Rutherford cross section

$$\frac{\mathrm{d}\sigma^{\mathrm{CL}}}{\mathrm{d}\theta} = \left(\frac{Z_1Z_2}{4E}\right)^2 \frac{1}{\sin(\theta/2)^4}\,. \tag{113}$$

Due to the monotony of the deflection function, Eq. (112), there is a unique relation between θ and b, i.e. only a single trajectory contributes to the differential cross section. This implies also that the semiclassical cross section is identical to the classical cross section since a single contribution

does not lead to interferences in Eq. (47). Moreover, as it is well known, the classical Rutherford cross section is even quantum mechanically exact and the same cross section is also obtained in first Born approximation [44, Ch. 14]. Hence, despite the difficulties one encounters in the presence of the Coulomb potential (defining modified phase shifts, etc.) the deflection function leads without any complications to the (even quantum mechanically correct) answer.

Clearly, the Coulomb potential is a very special potential due to the high symmetry of the involved dynamics which can be represented quantum mechanically by the O(4) group for negative energies [61]. It has been shown by Gutzwiller [6] and by Percival and coworkers in a series of papers [62–65] that – if all these symmetries are used – the Coulomb problem can be completely described semiclassically, essentially through the construction of a semiclassical Greens function which remains quantum mechanically correct. However, it is possible to obtain semiclassical scattering amplitudes which provide the quantum mechanically correct answer without these refined mathematical tools. This is interesting when quantum interferences occur as they do for potential scattering of identical, charged particles (e.g. α–α scattering) also known as non-relativistic Mott scattering. The direct approach with the deflection function leads in this case once again to the quantum mechanically correct answer [45] which will be briefly sketched.

4.2.2. Semiclassical Mott scattering

Non-relativistic Mott scattering is defined as the elastic collision between two identical particles. Since the particles are not distinguishable quantum mechanical interferences occur between the 'direct' and the 'exchange' amplitude.[3] Using the relative momentum $\boldsymbol{p} = \boldsymbol{p}_1 - \boldsymbol{p}_2$ the exchange of the particles corresponds to $\boldsymbol{p} \to -\boldsymbol{p}$ and the cross section reads

$$\mathrm{d}\sigma/\mathrm{d}\Omega = \tfrac{1}{2}|f(\boldsymbol{p},\boldsymbol{p}^-) \pm f(\boldsymbol{p},-\boldsymbol{p}^-)|^2 , \tag{114}$$

where the sum of the scattering amplitudes from Eq. (58) refers to bosons and the difference to fermions and $\boldsymbol{p}$ denotes the final momentum while $\boldsymbol{p}^-$ stands for the initial momentum. In addition to Eq. (113) we now need the action difference Eq. (56) which is given by [24, p. 182]

$$\Delta\Phi(\boldsymbol{p},\boldsymbol{p}^-,E) = -\frac{Z_1 Z_2 m}{p_\infty} \ln \frac{\sqrt{1+\Delta}+1}{\sqrt{1+\Delta}-1}, \qquad \Delta = \frac{(p^2 - p_\infty^2)((p^-)^2 - p_\infty^2)}{p_\infty^2 |\boldsymbol{p} - \boldsymbol{p}^-|^2} , \tag{115}$$

Eq. (115) gives the action for any two momenta $\boldsymbol{p},\boldsymbol{p}^-$ which are connected by a classical trajectory of energy E. However, according to Eqs. (56), (57) we need the action only in the asymptotic regime outside the range of the potential, where $p, p^- \to p_\infty$. Hence, for all nonzero scattering angles ($\boldsymbol{p} \neq \boldsymbol{p}^-$), it is clear that $\Delta \ll 1$ and

$$\lim_{p,p^- \to p_\infty} \Delta\Phi(\boldsymbol{p},\boldsymbol{p}^-,E) = 2\left(\sigma_0 - \frac{Z_1 Z_2 m}{p_\infty} \ln[\sin \Theta/2]\right) , \tag{116}$$

with

$$\sigma_0 = \frac{Z_1 Z_2 m}{2 p_\infty} \ln\left[\frac{(p^2 - p_\infty^2)((p^-)^2 - p_\infty^2)}{p_\infty^4}\right] . \tag{117}$$

[3] The interference effect was first predicted by Mott and experimentally seen by Chadwick [66], see also Taylor [44].

The constant $\sigma_0 = \hbar\delta_0$ is the semiclassical phase shift for angular momentum $L = 0$ and does not depend on the scattering angle $\theta = \arccos[\boldsymbol{p}\cdot\boldsymbol{p}^-/(pp^-)]$. Putting together all the pieces the semiclassical Mott scattering cross section, Eq. (114), reads

$$\frac{d\sigma}{d\Omega} = \left(\frac{Z_1Z_2}{4E}\right)^2 \left[\frac{1}{\sin^4\theta/2} + \frac{1}{\cos^4\theta/2} \pm \frac{2\cos[Z_1Z_2m/p_\infty \ln(\cot\theta/2)]}{\sin^2\theta/2\cos^2\theta/2}\right] \tag{118}$$

and is identical to the exact quantum cross section [44]. Apart from the symmetrization, only one trajectory contributes per final scattering angle, i.e., there is only one classical 'root' to the double-ended boundary condition $p_{\text{initial}} = p$, $p_{\text{final}} = p^-$. This means that caustic singularities are not a problem, since caustics result from the 'rainbow' effect of two (or more) roots coalescing.

We complete our discussion of the simplest possible process which leads to a final state of two charged particles in the continuum with a remark on the semiclassical cross section of this process calculated with the semiclassical phase shifts of Eq. (92). Due to the fact that there is only one classical path for each scattering angle θ which is uniquely related to some angular momentum L or impact parameter $b = L/p_\infty$, the scattering amplitude, Eq. (111), contains only one term (apart from symmetrization). However, there is no contradiction to the rule of thumb that semiclassical (or classical) approximations are useful in the limit of large quantum numbers or in a situation where many partial waves contribute. In fact, Coulomb scattering always involves *all* partial waves l since the potential has infinite range. (A well known consequence is the divergence of the integrated cross section). Hence, for any differential cross section one is always in the limit of large quantum numbers.

5. Inelastic scattering

In this section we will deal with three-body Coulomb systems. For simplicity, we restrict the discussion to two-electron atoms, described by the Hamiltonian

$$H = \frac{\boldsymbol{p}_1^2}{2} + \frac{\boldsymbol{p}_2^2}{2} - \frac{Z}{r_1} - \frac{Z}{r_2} + \frac{1}{|\boldsymbol{r}_1 - \boldsymbol{r}_2|}, \tag{119}$$

where Z is the nuclear charge and the $\boldsymbol{r}_i$ are the electron–nucleus vectors. Many aspects of the following discussion apply in slightly modified form to particles with arbitrary masses. In these cases the coordinates must be replaced by a set of respective Jacobi coordinates (see Eq. (24)).

Belonging to the class of simple but not analytically solvable problems, three charged particles have been in the center of attention since the very beginning of quantum mechanics. Early attempts to quantize the helium atom [11] and the H_2^+ ion [68] in a similar way as Bohr–Sommerfeld succeeded to do with the hydrogen atom failed. This certainly was one reason why the old 'quantum theory', which is essentially the precursor of today's semiclassical theory, was neglected from the late 1920s on when the quantum theory itself was born. Moreover, it turned out to be relatively easy to describe the ground state of helium quantum mechanically, and most importantly to prove theoretically that this state is stable [2–4].

Nowadays we know, mostly through work from the group of the late Dieter Wintgen [69], that it is possible to quantize helium semiclassically. The semiclassical mechanics of the classical orbits

from the early days of atomic physics, e.g. the Langmuir orbit, has been worked out as well [70]. Nevertheless, bound states and in particular the ground state still present a challenge to the semiclassical approach, because the underlying classical dynamics has only a set of orbits of measure zero (periodic orbits) which do not lead to autoionization in some finite time. We will come to this point in the context of double photoionization of helium in Section 6.

In the present section we will study inelastic scattering, namely ionization in its simplest form, electron–hydrogen scattering. As already noted in the previous section, semiclassical scattering approximations have been studied for a long time, however, mostly for potential scattering. A semiclassical treatment of inelastic scattering first became popular in physical chemistry, where Miller [12–14], Marcus [15, 16] and others studied reactive scattering. The reason that molecular scattering problems were treated fully semiclassically before this was done with electron scattering lies probably in the standard argument for the semiclassical limit: Atoms and molecules reach shorter de Broglie wavelengths than electrons and seem to be more suitable for semiclassical mechanics. Moreover, the singularity, particularly of the attractive Coulomb force, indicated complications.

It is a primary goal of this article to demonstrate that there is no reason to fear these obstacles. The singularity causes only technical problems and even has advantages: Loosely speaking, it pushes the possible source of caustics, a nasty limitation for the application of semiclassical theory, 'out to infinity' where it is of (almost) no harm. We will explain this later in more detail. The applicability of semiclassical methods can be assessed in a rough way by a refined version of the short wavelength condition. The relative change of the wave number $k(x)$ must be small within a local wavelength $\lambda(x) = 2\pi/k$ [71],

$$Q(x) \equiv \lambda \mathrm{d} \ln k(x)/\mathrm{d}x \ll 1 \,. \tag{120}$$

For high energies (i.e. when the kinetic energy dominates) this condition is trivially fulfilled. However, for the Coulomb potential the condition leads even near the singularity only to a square root divergence, since $Q(r \to 0) \propto r^{-1/2}$. Moreover, as already mentioned, the Coulomb singularity helps to avoid caustics in the semiclassical approximation which are related to potentials of finite depth. Other advantages of the Coulomb potential in connection with (semi-)classics are the scaling properties which have been discussed in some detail in Section 3. Focusing on scattering, the severe conceptual and technical problems of quantum scattering with the long range Coulomb force do not appear in a semiclassical scattering theory which is based on the S-matrix and not on the T-matrix whose mathematical justification for several charged particles is questionable [72]. Of course, the problems which arise from the logarithmic phase shift are also encountered in form of a logarithmically diverging classical action which appeared already in the last section for semiclassical Mott scattering. In molecular dynamics programs and with the so-called CTMC method [73] it has become possible to calculate classically integrated or low-dimensional differential observables (cross sections) in large phase spaces. Semiclassical calculations have not reached this level yet, one has to find individual trajectories in order to identify coherent contributions to the propagator (see the discussion in Section 2). Nevertheless, the progress is promising [26–29] and has been, once again, mostly achieved with molecular systems. Here, we are rather interested to work out the special properties of Coulomb systems with respect to semiclassical mechanics than to perform and analyze large-scale semiclassical calculations.

5.1. Classical collinear electron–atom scattering

5.1.1. Integral cross sections

Over the years many approximations have been proposed to reduce the dimensionality of the scattering problem. A prominent example is the so-called *s-wave model* where the interaction of the electrons is restricted to the line $r_1 = r_2$ [74, 75]. For a semiclassical approach, the natural reduction is a collinear phase space which has been defined and motivated in Section 2.2.3 by means of partial fixed points. The collinear configuration with the electrons on opposite sides of the nucleus is stable and therefore a suitable approximation for angular integrated cross sections [76, 77].

We may ask if there are other fixed points which would reduce the phase space even further for the energy-integrated probability of excitation and ionization. As already mentioned, there is indeed a partial fixed point at $r_1 = r_2$, $p_1 = -p_2$ (see the discussion of the triple collision manifold, Section 3.4); however this fixed point cannot be used to reduce the phase space for two reasons. First of all it is (globally) unstable; second, it is not contained in the initial conditions for colliding an electron with an atom (here we have $r_1 \gg r_2$), and related to this observation, the fixed point describes (for $E > 0$) an ionizing trajectory but no excitation. This partial fixed point has been used by Kazansky and Ostrovsky [78, 79] in a series of papers to calculate the angle-resolved differential cross section of double photoionization of helium with equal energy sharing of the electrons. Clearly, in this case the partial fixed point corresponds formally to the manifold of final observables. However, we will see in Section 6 that in a quasi-classical model of the double-photoionization process equal energy sharing is only reached asymptotically by certain trajectories which all start close to the nucleus with asymmetric initial conditions. Hence, they are *not* contained in the fixed-point manifold $r_1 = r_2$.

Coming back to the collinear scattering case we will proceed by constructing the approximate cross section. For simplicity, we restrict ourselves to an initial bound state of $l=0$ expressed through its radial action angle variables (I^-, η^-). Initial variables which are fixed (stars indicate partial fixed points) are now the action I^-, the interelectronic angle θ^*, the impact parameter (or equivalently the total angular momentum) b^*, the two out of plane Cartesian coordinates y_i^* with respective momenta $p_{y,i}^* = 0$ and the momentum of the projectile p^-. As demonstrated in Section 2.2.1 the consequence of partial fixed points is a factorization of the Jacobi determinant, Eq. (16), which describes the classical cross section. Variables within the collinear manifold do not depend on fixed point variables. Hence, $\partial\eta/\partial y_i^* = \partial\eta/\partial\theta^* = \partial\eta/\partial b^* = 0$ and the cross section takes the form

$$\mathrm{d}\sigma/\mathrm{d}\varepsilon(E) = \mathscr{P}(\varepsilon, E)\sigma^* , \tag{121}$$

with σ^* as in Eq. (38) and

$$\mathscr{P}(\varepsilon, E) \equiv \frac{\mathrm{d}P}{\mathrm{d}\varepsilon} = \frac{1}{2\pi}\frac{\partial\eta}{\partial\varepsilon} , \tag{122}$$

the probability to find an electron with energy ε on the fixed point manifold after the collision. This probability is normalized with respect to the collinear phase space: All particles that started in the collinear phase space remain there and the summation of all the possibilities in the collinear phase space must be unity. Of course, this result can be found directly if the scattering is formulated on the collinear manifold.

To summarize, if an experimental situation can be found where the fixed-point conditions apply, it is sufficient to calculate the reaction probability $\mathscr{P}(\varepsilon, E)$ on the collinear manifold for an approximate (not absolute) cross section.

The collinear reaction probability: As noted above, we can formulate the reaction probability $P(E, \varepsilon)$ of Eq. (122) directly as a rate in close analogy to Eq. (9). The relevant observables are initially the action I^- of the radial bound motion of the target electron or, equivalently, the energy of the bound motion. This determines the momentum of the projectile electron at a given total energy E. Hence, we choose as initial variables the conjugate pairs (I^-, η^-) for the bound electron and (r^-, p^-) for the projectile. The flux is in one dimension given by $\Phi_v = v/\Delta r^-$. The only observable after the collision is the energy sharing between the electrons. We fix the energy of one electron ε^+. The reaction probability now reads

$$\mathscr{P}(\varepsilon^+, E) \equiv \frac{\Delta P(E)}{\Delta \varepsilon^-} = \lim_{t\to\infty} \frac{\Delta p^-}{\Phi_v \Gamma^2} \frac{\mathrm{d}}{\mathrm{d}t} \int \mathrm{d}p\, \mathrm{d}r\, \mathrm{d}I\, \mathrm{d}\eta\, \delta(I - I^-)\delta(p - p^-)\delta(\varepsilon - \varepsilon^+)\,. \tag{123}$$

Using the initial-phase-space variables for integration with the normalization $\Gamma^2 = 2\pi \Delta p^- \Delta r^-$ for one bound and one free particle, we may simplify Eq. (123) similar to Eq. (11) and get (suppressing the '+' sign for final-state variables)

$$\mathscr{P}(\varepsilon, E) = \frac{1}{2\pi} \sum_j \frac{\mathrm{d}\eta_j^-}{\mathrm{d}\varepsilon}\,. \tag{124}$$

Alternatively, we may perform the time derivative in Eq. (123) with the asymptotic angle $\eta^-(t^-) = \omega t^- + \eta_0$ of the bound motion instead of the position of the projectile $r^-(t)$ as in Eq. (12). In this case we get

$$\mathscr{P}(\varepsilon, E) = \frac{1}{R} \sum_j \frac{\mathrm{d}r_j^-}{\mathrm{d}\varepsilon}\,. \tag{125}$$

The normalization $R = 2\pi v/\omega$, which is independent of the properties of a particular reaction trajectory j, has a simple meaning [76]. It has the dimension of a length which measures the distance the projectile travels during one period $T = 2\pi/\omega$ of the target electron. The reaction probability, Eq. (124), is a slightly generalized version of Miller's classical S-matrix for collinear reactive scattering [31] where the present formulation includes the possibility of fragmentation into three particles in the continuum. The dynamically relevant quantity in Eq. (125) is the deflection function $\varepsilon(r^-)$.

5.1.2. *The collinear orbits and the regularization of the equations of motion*

The restriction to the collinear configuration space has the advantage that it is possible to visualize the trajectories in ordinary graphs. The collinear $e^- + H(1s)$ scattering can lead classically to three different processes which are distinguished by the possible energy sharing of the electrons. Assume that electron 2 is bound initially, i.e. $\varepsilon_2^- < 0$, and that the total energy of the system is $E > 0$. The collision can lead to

1. *Excitation*: $\varepsilon_1 > E$,
2. *Fragmentation*: $\varepsilon_1 > 0$, $\varepsilon_2 > 0$,
3. *Exchange*: $\varepsilon_2 > E$.

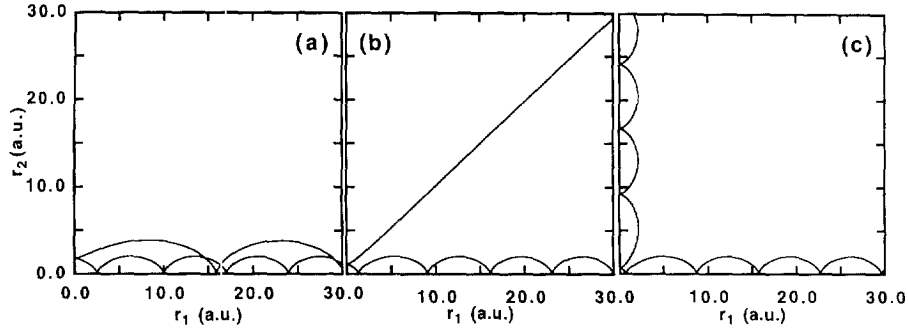

Fig. 3. Trajectories in collinear electron–hydrogen collision at a total energy of $E = 0.1$ a.u. The nucleus is located at the origin: (a) excitation, (b) fragmentation, (c) exchange.

The respective ranges for the energies ε_i are additionally limited by energy conservation. For $|t| \to \infty$ we have $\varepsilon_1 + \varepsilon_2 = E$. Typical trajectories are shown in Fig. 3. The nucleus is located at the origin and $r_i = 0$ corresponds to a collision between the nucleus and electron i. These collisions lead to an abrupt change of the radial electron momentum p_i from $-\infty$ to $+\infty$ since there is no angular momentum barrier. For a numerical calculation of the trajectories as shown in Fig. 3 singularities appear when an electron bounces back from the nucleus ($r_1 = 0$ or $r_2 = 0$). The regularization of these singularities proceeds similarly as in Section 3.4.

Regularization of the equations of motion. The relevant Hamiltonian for collinear two-electron motion is

$$\frac{p_1^2}{2} + \frac{p_2^2}{2} - \frac{Z}{r_1} - \frac{Z}{r_2} + \frac{1}{r_1 + r_2} . \tag{126}$$

The regularization is performed similarly as in Section 3.4.1 for $\mathscr{R} = 0$. To regularize the Coulomb singularities $r_i = 0$, we introduce a point transformation to oscillator-like coordinates where $r_i = Q_i^2$. The conjugated momenta turn out to be $p_i = P_i/(2Q_i)$. The new momenta P_i remain finite at $r_i = 0$. The regularization is completed with a change of the time variable such that the singularity is passed in small time steps with respect to real time, $\mathrm{d}\tau = r_1 r_2/(r_1 + r_2)\mathrm{d}t$. To keep the form of Hamilton's equations invariant under the transformation of the time variable, we must work with a Hamiltonian of value zero which can be multiplied by the necessary time differentials, $\mathscr{H} = (H - E)\mathrm{d}t/\mathrm{d}\tau \equiv 0$. For this form of $\mathscr{H}$ we get

$$\frac{\mathrm{d}x}{\mathrm{d}\tau} = \frac{\mathrm{d}x}{\mathrm{d}t}\frac{\mathrm{d}t}{\mathrm{d}\tau} = \frac{\partial H}{\partial p}\frac{\mathrm{d}t}{\mathrm{d}\tau} = \frac{\partial \mathscr{H}}{\partial p} . \tag{127}$$

The singularity free, collinear Hamiltonian reads finally

$$\mathscr{H} = \frac{P_1^2 Q_2^2 + P_2^2 Q_1^2}{8(Q_1^2 + Q_2^2)} - Z + \frac{Q_1^2 Q_2^2}{(Q_1^2 + Q_2^2)^2} - E\frac{Q_1^2 Q_2^2}{Q_1^2 + Q_2^2} . \tag{128}$$

5.1.3. The deflection function

The classical deflection function is determined numerically with the Hamiltonian Eq. (126). The initial conditions for a trajectory are selected with the bound electron starting at the outer turning

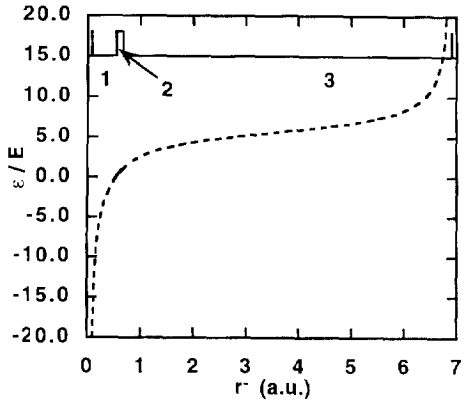

Fig. 4. Classical deflection function for the final energy ε of the projectile electron as a function of its initial position 1000 au$+r^-$ at a total energy of $E = 0.1$ a.u.. The intervals indicate the range of initial conditions leading to excitation (1), fragmentation (2), and exchange (3).

point which is given by $p_2^- = 0$ while r_2^- is determined by the energy ε_2^-. Hence, electron 2 has the same initial conditions in phase space for all trajectories. The projectile electron has the momentum $p_1^- < 0$ which is fixed by the energy conservation $\varepsilon_2^- + \frac{1}{2}(p_1^-)^2 = E$. However, the position $r_1^- = r_0 + r_j^-$ is different for each trajectory where r_0 is some large distance (we have chosen 1000 a.u.) and $r_j^- \leq R$ with R from Eq. (125).

The deflection function is shown in Fig. 4. Since the energy of the projectile electron has been recorded, *excitation* corresponds to $\varepsilon/E > 1$, *fragmentation* occurs for $0 < \varepsilon/E < 1$ and the rest of initial conditions r^- leads to *exchange* with $\varepsilon < 0$. The deflection function of Fig. 4 is monotonic. This has two consequences which are both very welcome for a semiclassical analysis. First, there is only a *single* trajectory which contributes to a final energy ε. Second, since the deflection function is even strictly monotonic, its derivative is never zero and no caustics exist which complicate the semiclassical treatment. The situation is very similar to the case of Rutherford scattering: The deflection function there is monotonic, only a single trajectory gives the differential cross section, and in both cases each trajectory has a single minimum in its (hyper-)radius. However, the collinear three-body system is much more complicated because the analogue to the angular momentum of the Rutherford scattering, the momentum p_α conjugated to the hyperangle $\arctan(r_1/r_2)$ (see Section 3), is not a constant of motion.

Is this surprisingly simple result for collinear scattering realized in an experimental situation? We have to look for conditions where it is sufficient that the $L = 0$ partial cross section is available.

5.1.4. *A note on zero angular momentum collisions*

For dominant S-wave scattering one would immediately think of threshold collision where only the S-wave survives for $E \to 0$ [44, Ch. 11]. However, this result holds only for short-range potentials. It turns out that in the Coulomb case the threshold region is also described well by the S-wave only. However, this has a very different reason which can be seen from the scaling properties. We know that the total angular momentum L is conserved by the Hamiltonian Eq. (119). Hence, we

may write this Hamiltonian in energy-scaled hyperspherical coordinates (see Section 3.1) as

$$\tilde{H}_{\tilde{L}} = \frac{\tilde{P}^2}{2} + \frac{\tilde{\Lambda}^2(\tilde{L},\Omega)}{2\tilde{R}^2} + \frac{C(\boldsymbol{\Omega})}{\tilde{R}} . \tag{129}$$

Recalling the scaling of angular momentum, Eq. (69), we see that for any fixed L we have with $E \to 0$ that $\tilde{L} = L(E/E_0)^{1/2} \to 0$. This means that the scaled Hamiltonian for any partial wave $\tilde{L}$ goes over into the Hamiltonian for $L = \tilde{L} = 0$ in the limit $E \to 0$. In contrast to the short range potential not only the S-wave contributes at threshold but all partial waves L contribute (with a priori unknown weight) like the S-wave. Hence, we can hope that the S-wave from collinear collisions gives a realistic picture of the integrated fragmentation cross section and the energy sharing near threshold.

5.2. *Ionization of hydrogen by electron impact near threshold*

We come to a fundamental process in atomic physics, electron–hydrogen scattering. Despite its simplicity, it was only a few years ago that this collision could be treated in a full numerical calculation which reproduced for the first time the integrated ionization cross section on an absolute scale from about 10 to 500 eV excess energy [80]. The range from threshold to 10 eV could not be computed due to the highly oscillatory behavior of the used basis functions [80]. Recent attempts to get closer to threshold with the so-called *hyperspherical diabatic bisector method* [81] have been successful down to about 1 eV where the same difficulties prohibited to compute the cross section down to threshold. Hence, this oscillatory behavior seems to be generic for the limit $E \to 0$. It can be directly seen in a path-integral representation for the S-matrix,

$$\langle x^+|S(E)|x^-\rangle = \int \mathscr{D}[x] e^{i\Phi[x]/\hbar} , \tag{130}$$

where Φ is the Lagrangian action along any path $x(t)$. From Section 3 we know that the action scales with energy as $\Phi = \tilde{\Phi}/\sqrt{E}$. Hence, for $E \to 0$ (just like for $\hbar \to 0$) the integrand in Eq. (130) will oscillate rapidly.

On the other hand, the situation seems to be very suitable for a semiclassical approach for the same reason. Moreover, it is exactly the problem which can be described according to our previous considerations on the collinear manifold.

Indeed, in 1953 Wannier [82] was the first to predict an anomalous power law $\sigma \propto E^{1.127}$ for the ionization cross section close to threshold. Without the tools of modern nonlinear dynamics, he derived this result by calculating the phase-space flow which reaches the region of three free particles. In the next section we will show that this power law comes from the instability of a global fixed point on the triple collision manifold (TCM) as discussed in Section 3.4. However, since a global fixed point for positive energies is only possible in the limit $E \to 0$ the power law is – even within the limitations of classical mechanics – strictly valid only at threshold $E = 0$.

There have been attempts to calculate the ionization cross section close to threshold classically by CTMC methods [83]. However, this is a difficult task since the accuracy of the CTMC methods lives from statistical significance which is difficult to obtain for the ionization cross section which goes to zero for $E \to 0$. Although the numerical classical data were not accurate enough to compare them with the experiment they have confirmed qualitatively Wannier's analysis. Over the years a lot of

work has been invested into a 'translation' of Wannier's classical approach to quantum mechanics. The result was a WKB approach where the wavefunction was expanded about the classical TCM and lead to the same and a few additional results as Wannier's classical consideration [84–90, 41]. Still, a comparison with experiment (beyond the asymptotic behavior near $E = 0$ where the experimental values are uncertain) was not possible.

Moreover, it still was not completely accepted that Wannier's perspective on threshold ionization was correct to begin with [91–93]. An alternative formulation by Temkin [94–96] based on his quantum mechanical dipole theory drew a very different picture of the mechanism for threshold ionization. Its quantitative predictions could not be discriminated against Wannier's result by comparison with the experiment. Last not least there had been so much work over the years in the name of Wannier's 'threshold scenario' that it is difficult to say precisely what this jargon means. As of today Wannier's threshold law is generally agreed upon. This is due to some convincing results over the last few years, beginning with a (semi-)classical calculation [76] in very good agreement with the corresponding experimental cross section [97]. Later, Feagin achieved similar agreement with a fourth-order Wannier threshold theory [98]. Further insight into the threshold behavior has been gained recently by Macek and coworkers [99–102] with the *hidden crossing theory*, a semiclassical formulation of quantum transitions in the complex plane of adiabatic potential curves, originally formulated by Solovev for heavy ion collisions[4] [104, 105].

An interesting example for the confusion which reigned for a long time the threshold problem was emphasized by Richter and Wintgen [106] and concerns the so called *Wannier orbit*. This trajectory on the potential ridge, emerging from the TCM keeping all partial fixed points but the radial one in $\mathscr{R}$ (i.e. collinear electrons with $\boldsymbol{r}_1 = -\boldsymbol{r}_2$) was believed to be the leading path to ionization. However, as Richter and Wintgen note correctly, this trajectory does not occur among scattering paths since it is exponentially unstable [106]. Indeed, Wannier never wrote that this trajectory lead to ionization, quite on the contrary, he wrote in his remarkable paper from 1953 [82] that the trajectories will be in general asymmetric with respect to the two electrons and will only reach asymptotically for large times (i.e. far away from the nucleus) the ridge with $\boldsymbol{r}_1 \approx -\boldsymbol{r}_2$.

With the concept of partial fixed points as introduced in Section 2 and applied to the electron-atom system at the beginning of this section it is almost obvious where this misunderstanding came from. The ridge contains an *unstable* partial fixed point $\tan\alpha^* = r_1/r_2 = 1$ as we have seen. Therefore, it cannot be used to approximate collision dynamics for finite energies E. Rather, one must treat the unstable degree of freedom explicitly on the collinear manifold as described in the beginning of this section. For the behavior of the cross section at threshold, however, the properties of the TCM may be used to arrive at an analytical result.

5.2.1. *Analytical cross section for threshold ionization from the instability of the triple collision manifold*

Intuitively, one would expect that at very low energies $E \approx 0$ the collision is already decided far away from the scattering center (nucleus). This is indeed the case, however, it is difficult to deal with quantities when their values approach infinity. Therefore, we switch to scaled coordinates where

[4] This theory focuses on *series* of avoided crossings as a function of a real adiabatic parameter. The curves cross at complex values of the adiabatic parameter and the locus of all the crossings form a path in the complex plane. Isolated avoided crossings have been treated in the complex plane as well, see e.g. Ref. [103] and references therein.

a scaled finite distance $\tilde{r}_0$ leads through $r = \tilde{r}_0 E_0/E$ to an infinite unscaled distance r for $E \to 0$ according to Eq. (68).

The initial state: The target electron is bound before the collision with some upper limit r_0 for its distance to the nucleus, more precisely $r_2 = \mathscr{R}^- \sin\alpha \leq r_0$. At the partial fixed point $\alpha^* = \pi/4$ we have in scaled coordinates

$$\tilde{\mathscr{R}}^- \leq r_0 E/E_0 \sin\alpha^* \tag{131}$$

which means that $\tilde{\mathscr{R}} \to 0$ for $E \to 0$. Hence, the initial bound state of the target projects the system onto the triple collision manifold for $E \to 0$. On the other hand, a finite E is proportional to the distance $\delta\tilde{\mathscr{R}}$ from the TCM and for the regularized radial variable $u = \sqrt{\mathscr{R}}$ we may write

$$\delta\tilde{u}^- = \sqrt{E/E_0}\, u_0 \tag{132}$$

with u_0 finite.

The final state: An ionizing event is characterized by both electrons reaching infinite distance from the nucleus after the collision. This is possible at the partial fixed point α^* for $\mathscr{R} \to \infty$ with a finite arbitrary scaled $\tilde{\mathscr{R}}_0$ which can be achieved by an arbitrarily small but finite distance from the TCM ($u^* = 0$),

$$\delta\tilde{u} = \tilde{u}_0 - u^* = \tilde{u}_0 \,. \tag{133}$$

The ionization probability: We have seen that the ionization process close to $E \to 0$ can be represented in scaled coordinates as the variation about the TCM. To get a quantitative expression for the ionization probability we must evaluate $P(\varepsilon, E)$ from Eq. (125) on the TCM. Using the appropriate variables on the TCM we can rewrite

$$\mathscr{P}(\varepsilon, E) = \frac{1}{R}\left|\frac{\mathrm{d}r^-}{\mathrm{d}\alpha^-}\frac{\mathrm{d}\alpha^-}{\mathrm{d}P_z}\frac{\mathrm{d}P_z}{\mathrm{d}\varepsilon}\right| \,. \tag{134}$$

The first and third derivative in Eq. (134) only represent coordinate transformations, which can be easily calculated,

$$\left|\mathrm{d}r^-/\mathrm{d}\alpha^-\right|_{\mathrm{TCM}} = (u^-)^2/\sqrt{2} \qquad \left|\mathrm{d}P_z/\mathrm{d}\varepsilon\right|_{\mathrm{TCM}} = u^2\, 4/p_u^* \,. \tag{135}$$

The second derivative in Eq. (134) represents the important stability matrix element which has been calculated already in Section 3.4.2 (Eq. (89)). However, with the help of Eqs. (132), (133) we can convert the distance δu from the TCM into a dependence on the energy E, and in the limit $E \to 0$ we get the simple form

$$\left(\frac{\delta P_z}{\delta\alpha^-}\right)^{-1} = \frac{(\tilde{u}_0/u_0)^\zeta}{\lambda_1 - \lambda_2}\left(\frac{E}{E_0}\right)^\zeta \tag{136}$$

with $\zeta = 2\lambda_1/p_u^*$ where λ_1 is the eigenvalue from Eq. (86). The exponent ζ is identical to the well-known Wannier coefficient and takes the value $\zeta = 1.127$ for electron–hydrogen scattering. Since the scale E_0 of the energy E is not known in the present approximation, it is not possible to calculate the absolute value of the ionization probability. Hence, it is also not worthwhile to explicitly write down all the constants which emerge from the derivatives of Eq. (135) and we

leave it to the reader to convince himself that these constants remain finite in the limit $E \to 0$. The final result from Eqs. (134)–(136) for the ionization probability can be written in the form

$$\mathscr{P}^{+}(\varepsilon, E \to 0) = \frac{a_0}{E}\left(\frac{E}{E_0}\right)^{\zeta} \tag{137}$$

which can be trivially integrated for the total ionization cross section

$$\sigma_3(E \to 0) = \sigma_3^{*}\,(E/E_0)^{\zeta} \tag{138}$$

with the constants σ_3^{*} and E_0 remaining undetermined in the analytical derivation of the threshold ionization cross section from the triple collision manifold. However, we can determine E_0 within a semiclassical S-matrix calculation as will be shown in the following.

5.2.2. The classical ionization cross section

For the ionization probability on the collinear collision manifold we have to sum over all initial conditions which lead to ionization, i.e. to a final energy $0 \le \varepsilon \le E$ for one electron. Since the deflection function $\varepsilon(r^{-})$ (Fig. 4) is monotonic the summation is over a continuous interval. With Eqs. (121), (122) and (125) we obtain

$$P(E) = \frac{1}{R}\int_0^E \mathrm{d}\varepsilon \frac{\mathrm{d}r^{-}}{\mathrm{d}\varepsilon} = \frac{\Delta r^{-}}{R}. \tag{139}$$

Although the deflection function is monotonic with only one trajectory leading to a final electron energy ε the classical result nevertheless is not the same as the semiclassical result. The situation is similar to Mott scattering (Section 4.2.2), we have to take into account that the electrons are indistinguishable.

5.2.3. The semiclassical ionization cross section

The Pauli principle requires the scattering amplitude to be symmetrized (the total wave function for fermions must be antisymmetric). For this reason we have contributions from *two* trajectories. One leads to the desired final energy ε of the, let us say, projectile electron, the other one leads to $E - \varepsilon$ (with the target electron of energy ε). Semiclassically, this might lead to an interference due to an action difference between the two paths, similarly as in the case of Mott scattering (Section 4.2.2). According to Eqs. (16), (121) and (122) we can write the S-matrix element for a collision where the projectile electron goes from energy ε^{-} to ε:

$$\begin{aligned} {}^{1}S^{\mathrm{e}} &: \frac{\mathrm{d}\sigma^{s}}{\mathrm{d}\varepsilon} \equiv P^{-}_{\varepsilon,\varepsilon^{-}}(E) = |S_{\varepsilon,\varepsilon^{-}}(E) + S_{E-\varepsilon,\varepsilon^{-}}(E)|^2\,, \\ {}^{3}S^{\mathrm{e}} &: \frac{\mathrm{d}\sigma^{t}}{\mathrm{d}\varepsilon} \equiv P^{-}_{\varepsilon,\varepsilon^{-}}(E) = |S_{\varepsilon,\varepsilon^{-}}(E) - S_{E-\varepsilon,\varepsilon^{-}}(E)|^2\,, \end{aligned} \tag{140}$$

with the S-matrix element

$$S_{\varepsilon,\varepsilon^{-}}(E) = \sqrt{\mathscr{P}(\varepsilon,E)}\,\mathrm{e}^{\mathrm{i}(\Delta\Phi(\varepsilon,\varepsilon^{-},E)-\nu\pi/2)}\,. \tag{141}$$

The total wave function, which must be antisymmetric for fermions, factorizes in a spin-dependent part and a spatial part in the LS-coupling scheme. Hence, the symmetric '+' scattering amplitude

goes with an antisymmetric spin wave function, i.e. for two electrons in a spin singlet state, $^1S^e$, and vice versa.

Although surprising it is not difficult to see that the action along the two paths is the same. We start from the initial state consisting of a bound (Kepler) orbit with fixed energy and eccentricity zero (no angular momentum) and a free projectile with momentum p_1^-. We want to prove that the action for an orbit that goes from this initial state to a final continuum state with momenta p_1, p_2 is the same as for an orbit which starts with the same initial state but ends at a final state with *exchanged* electrons, p_2, p_1. The action differential $d\Phi = r_1 dp_1 + r_2 dp_2$ itself is symmetric under electron exchange. We have to prove that

$$\int_{p_1^-,p_2^-}^{p_1,p_2} d\Phi = \int_{p_1^-,p_2^-}^{p_2,p_1} d\Phi , \tag{142}$$

where p_2^- denotes the initial momentum on the Kepler ellipse. Interchanging the indices $1 \leftrightarrow 2$ on the r.h.s of Eq. (142) reveals that Eq. (142) is valid if $p_1^- = p_2^-$. Since p_1^- is fixed by the projectile energy we must be able to choose the initial momentum on the Kepler ellipse $p_2^- = p_1^-$. This choice is indeed always possible for two reasons. First, in principle, all momenta $p_2^- \in]-\infty, \infty[$ are available along a Kepler ellipse. Second, we are free to choose the starting point on the Kepler ellipse. Although the initial phase η^- is determined by the final momenta p_i (see Eq. (122)) for fixed initial position r^- of the projectile we may still shift the entire system in the asymptotic region ($t^- \to -\infty$) by some increment Δt^- without changing the action integral Eq. (142). This follows from the construction of the collisional action, Eq. (95), according to the conditions of a collision. Recalling that asymptotically we have $r^- = p_1^- / m t^-$ and $\eta^- = \omega t^-$ we can always find a Δt^- with $p_2^-(\Delta t^-) = p_1^-$. Hence, the action of the direct and the exchanged path are indeed identical. Nevertheless, the semiclassical result does still not reduce to the classical one, although it might be expressed by knowing the classical differential cross section (probability) only.

Energy sharing between the electrons. For further analyzing the symmetry properties of the scattering amplitude under electron exchange, it is convenient to introduce a scaled energy variable $x = \varepsilon/E - \frac{1}{2}$ with the electron exchange given by inversion, $x \to -x$. Keeping in mind that only one trajectory contributes to $S_{x,x^-}(E)$ the symmetrized probabilities, Eq. (140), are now simply given by

$$P^{\pm}_{x,x^-}(E) = \tfrac{1}{2}\left(\sqrt{\mathscr{P}(x,x^-)} \pm \sqrt{\mathscr{P}(-x,x^-)}\right)^2 . \tag{143}$$

Normalized to $P^+_{0x^-}$ they are shown in Fig. 5 for energies spanning three orders of magnitude from $E = 10^{-3}$ to 1 a.u. In the singlet configuration there is at threshold a preference of about 5% for equal energy sharing. This threshold energy sharing was also obtained by Read [108] and Gailitis [109] in classical trajectory calculations without a physical initial state. The semiclassical S-matrix result with a well-defined initial state, together with these previous results, confirm that certain properties of threshold ionization are independent of the initial state as already predicted by Wannier [82]. However, only in the limit $E \to 0$ the energy distribution is universal with a 5% preference for equal energy sharing. As described in Ref. [76] this preference decreases towards a "transition region" around 3 eV excess energy where the energy distribution is flat within 1%. For higher energies a preferred unequal energy sharing is approached (with a fast projectile electron and a slow target electron). In the $^3S^e$ symmetry there is no transition since equal energy sharing is not allowed. Hence, the shape of the cross section changes only slightly for different excess energies (Fig. 6). The ratio of triplet to singlet probability is reflected by P^-_x / P^+_0 which demonstrates that the

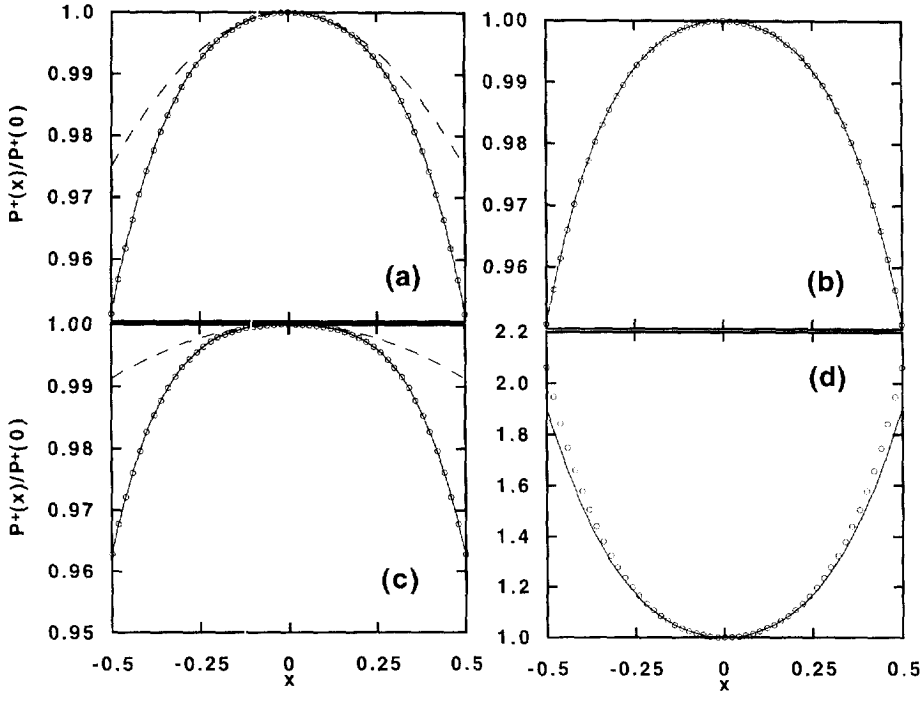

Fig. 5. The energy-sharing probability $P^+(x)$ normalized to the value at $x = 0$ for various excess energies, $E = 10^{-3}$ a.u. in (a), $E = 10^{-2}$ a.u. in (b), $E = 10^{-1}$ a.u. in (c) and $E = 1$ a.u. in (d). The exact values are denoted with circles, the solid line and the dashed line correspond to approximations, see text.

triplet probability is orders of magnitudes smaller relative to the singlet probability for small excess energies. At $E = 1$ a.u. both probabilities have the same order of magnitude (compare Fig. 5d with Fig. 6d). The behavior can be understood analytically from a perturbation expansion about the triple collision manifold.

Analytical interpretation of the differential scattering cross section. The unsymmetrized scattering amplitude $\mathscr{P}(x)$ can be represented as a sum of two functions $P_g(x)$ and $P_u(x)$ which are symmetric and antisymmetric under electron exchange. These two functions scale differently with the total energy,

$$P_g(x,x^-,E) \propto E^{\zeta}, \qquad P_u(x,x^-,E) \propto E^{2\zeta}, \tag{144}$$

where $\zeta = 1.127$ is the Wannier exponent. The reason for the scaling can be found from an analysis of the triple collision manifold (TCM) which is responsible for the ionization dynamics in the limit $E \to 0$ [41]. Essentially, each contact of a trajectory with the TCM leads to a factor E^{ζ} in the probability for this trajectory. For trajectories contributing to P_g one contact is sufficient while for the antisymmetric probabilities two contacts with the TCM are necessary. This explains the scaling Eq. (144) which is demonstrated in Fig. 7 for an energy range spanning the same three orders of magnitude, 10^{-3} a.u. $\leq E \leq 1$ a.u. as in the previous figures. While the total energy dependence follows Eq. (144) very well, the dependence of $P_g(x)$ and $P_u(x)$ on x changes appreciably from 10^{-3} to 1 a.u. excess energy.

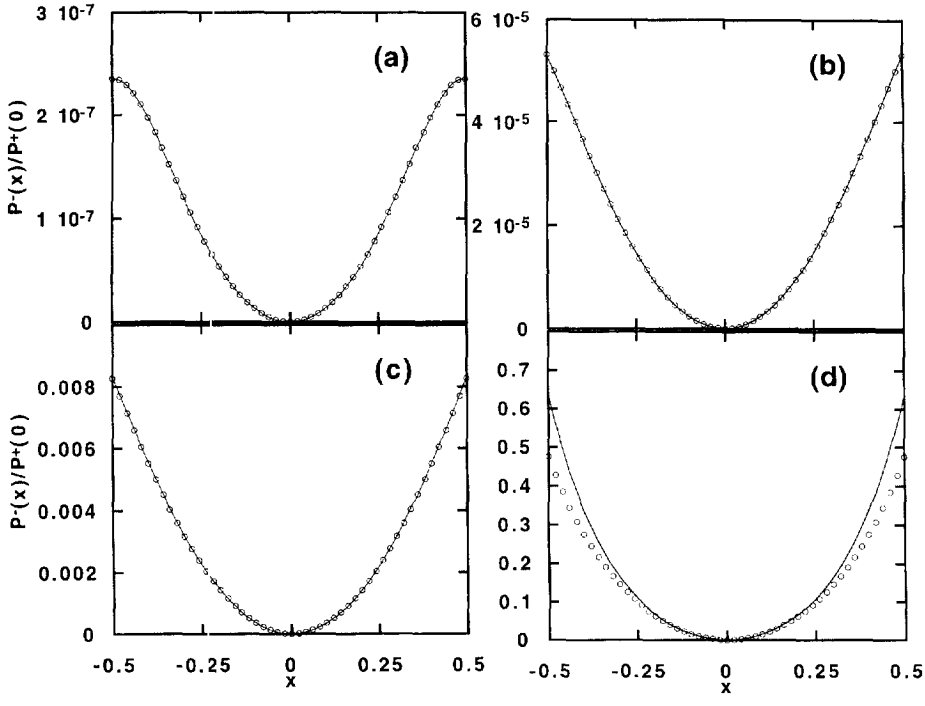

Fig. 6. Same as Fig. 5, but for the $P^{-}(x)$ probability, normalized to $P^{+}(0)$.

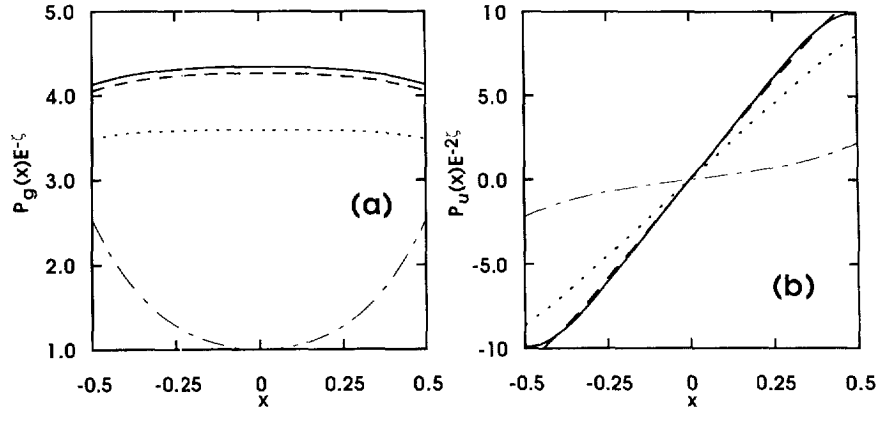

Fig. 7. The classical probabilities, (a) $P_g(x)$, and (b) $P_u(x)$ as defined in the text and scaled according to their behavior with the total energy for $E = 10^{-3}$ a.u. (solid), $E = 10^{-2}$ a.u. (dashed), $E = 10^{-1}$ a.u. (dotted) and $E = 1$ a.u. (dashed–dotted).

As an immediate consequence of Eq. (144) we can expand the mixed term in the singlet and triplet probabilities $P^{\pm}$ from Eq. (143) according to

$$P^{+}(x,x^{-},E) \approx P_g(x) - P_u(x)^2/4P_g(x) \propto E^{\zeta},$$
$$P^{-}(x,x^{-},E) \approx P_u(x)^2/2P_g(x) \propto E^{3\zeta}. \tag{145}$$

The approximation Eq. (145), shown in Figs. 5 and 6 with solid lines, is excellent for small excess energies and even for $E = 1$ a.u. still reasonable. From Eq. (145) follows that $P^+/P^- \approx E^{-2\zeta}$ which is for $E = 1/10$ a.u. still a factor of 100.

With regard to the question of semiclassical corrections to the classical result close to threshold, our analysis shows that even the triplet cross section is classical in the sense that no $\hbar$ dependence occurs. Due to the symmetry of the action $S(x)$ under electron exchange, classical probabilities in the form of Eq. (143) are sufficient to describe the symmetrized cross sections. The result might prove interesting for the justification of purely classical trajectory methods such as the CTMC. With the classical probabilities obtained by these methods symmetrized cross sections could be constructed according to Eq. (143).

Most Wannier-like threshold approaches use a quadratic approximation about the Wannier saddle ($x = 0, \theta_{12} = 180^\circ$). In this context it is interesting to note that the energy-sharing distribution $P^\pm(x)$ can only be represented by a function quadratic in x in a very limited region around $x = 0$ (see dashed lines in Fig. 5a and Fig. 5c). The necessity to go beyond the quadratic approximation has also been emphasized recently by Kazansky and Ostrovsky [79] and Feagin [98] in his *fourth-order Wannier threshold theory*. Another necessary extension of the Wannier theory towards reliable differential observables like the energy sharing probability is a realistic description of the initial state. Without invoking the Wannier picture the semiclassical S-matrix approach satisfies both criteria. Hence, the transition from the threshold behavior manifested in preferred equal energy sharing to the preference for unequal energy sharing characteristic for higher excess energies could be demonstrated here and awaits experimental confirmation.

The total cross section. It is formally obtained for a given symmetry by integration of Eq. (143),

$$P^\pm(E) = \int_{-1/2}^{1/2} P^\pm_{x,x^-}(E)\,\mathrm{d}x\,. \tag{146}$$

As expected from the energy scaling Eq. (144) the singlet cross section for $E \to 0$ follows the Wannier power law $P^+(E) \propto E^{1.127}$ (dashed line in Fig. 8) and the triplet cross section behaves as $P^-(E) \propto E^{3.381}$. More interestingly, the symmetrized cross section $P^+(E)$ lies very close to the purely classical total cross section, Eq. (139). This follows from Eq. (145) since

$$P^-(E) \approx \int_{-1/2}^{1/2} P_g(x)\,\mathrm{d}x = \int_{-1/2}^{1/2} (P(x) + P(-x))\,\mathrm{d}x = 2P_{\mathrm{cl}}(E)\,. \tag{147}$$

Thus, the Pauli principle has mainly the effect of doubling the classical cross section for ^1S symmetry as can be expected for perfect constructive interference. Based on the underlying classical trajectories we can interpret the ^3S cross section with the semiclassical S-matrix as a destructive interference effect between the two classical paths whose contribution to the scattering amplitude must be summed coherently. For an experiment with unpolarized electrons, triplet and singlet cross sections must be averaged over. Translated to our context '+' and '−' states are equally often realized (by partial waves of different angular momentum, spin and parity). Hence, according to Eq. (147) $P(E \to 0) = \frac{1}{2}(P^+ + P^-) \to P_{\mathrm{cl}}$ since P^- is negligible in the limit $E \to 0$.

In the "classical" electron impact ionization experiment of McGowan and Clarke [97] the total cross section has been measured from 0 to 8 eV excess energy. It is shown together with the present result of semiclassical S-matrix theory in Fig. 8. Only the overall normalization was matched

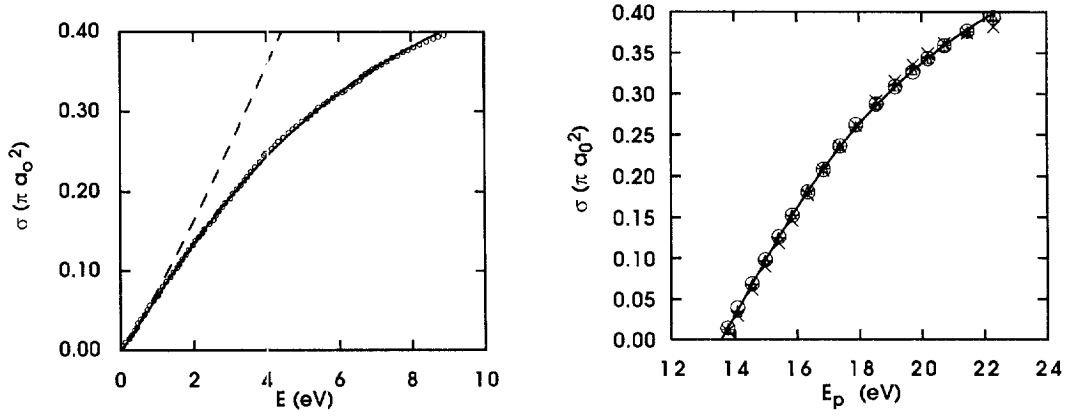

Fig. 8. The total ionization cross section for electron impact on H(1s). The experimental data points are taken from Ref. [97]. The calculated cross section (solid) has been normalized to the experimental data at 5.84 eV. The dashed line is the Wannier cross section $\sigma(E) = \sigma_0(E/E_0)^{1.127}$.

Fig. 9. Total ionization cross section as in Fig. 8. Some experimental points (open circles) are shown together with the normalized semiclassical theory (solid line) and several fits: Eq. (148) (+), Eq. (149) (×), Eq. (150) (△).

at some arbitrary energy (5.84 eV). The good agreement of the theoretical curve with the experimental data justifies a posteriori our approximations, first of all the semiclassical approach, and within this approach the restriction to the $L = 0$ contribution and to the partial fixed point at $\theta_{12} = 180°$. Still, the theoretical curve must be normalized to the data at one point since under the present approximations it is not possible to predict an absolute cross section. However, our inclusion of the initial state determines the energy scale which is in most threshold theories another fit parameter.

Form of the cross section. Since the total cross section is smooth, almost any correction term to the asymptotic power law together with the two fit parameters E_0, σ_0 for the energy axes and the absolute magnitude of the cross section will reproduce the experimental curve. This is demonstrated in Fig. 9 for the three analytical forms of the cross section

$$\sigma = \sigma_0 x^{1.127}(1 + ax)\,, \tag{148}$$

$$\sigma = \sigma_0 x^{1.127}(1 - a\sqrt{x})\,, \tag{149}$$

$$\sigma = \sigma_0 x^{1.127}/(1 + ax)^{2.127}\,, \tag{150}$$

where $x = E/E_0$. As can be seen from Fig. 9 all fits are close to the experimental cross section, only the 'normal' Taylor expansion, Eq. (148), is a bit more off than the other two fits. This insensitivity certainly shows that the total cross section is not a suitable observable to prove the quality of threshold theories which include two fitting parameters (essentially the scale of the two axes, σ_0 and E_0). On the other hand, one could suspect this insensitivity to imply the existence of a universal shape function for ionization cross sections where only the two scale factors σ_0 and E_0 depend on the specific collision system.

Table 1
Examples of Wannier exponents for various collisional systems with the same potential, but different masses for projectile (m_P) and target (m_T)

	m_P	m_T	ζ
e^-–M_∞	1	∞	1.127
e^-–H	1	1836	1.127
e^+–M_∞	1	∞	2.651
e^+–H	1	1836	2.650
p^-–M_∞	1836	∞	1.160
p^-–H	1836	1836	1.199
p^+–M_∞	1836	∞	98.675
p^+–H	1836	1836	69.74

5.3. *Universal parameterization for the ionization cross section of atoms*

Beginning with Thomson in 1912 [110] there have been many attempts over the years to parameterize cross sections semi-empirically. Probably, the best-known example is the Lotz formula which describes ionization of atoms by *electron* impact with the emphasis on the high-energy end [112–114]. An overview of other parameterizations is given in Ref. [115], recent results on electron impact can be found in Ref. [116]. All these formulae try to parameterize the cross section with the ionization potential I and a number of fitting parameters. In many cases it is even possible to include electrons from different shells. However, in none of these formulae the low-energy power-law behavior has been built in.

5.3.1. *The universal shape function for direct fragmentation*

A typical ionization cross section resulting from direct ionization is a rather structureless curve with one maximum characterized by (σ_M, E_M). The asymptotic behavior for $E \to 0$ has been discussed in detail. It is given by the classical power law E^ζ where ζ depends again on the collision system (see Table 1). For high energies, the classical behavior has been known since Thomson to be E^{-1}, while quantum mechanics introduces a logarithmic correction with the cross section falling off as $\ln E/E$ for very high energies. For a simple form of the cross section from threshold to energies beyond the maximum we assume the classical behavior in both limits of E. We may combine the two limits in a natural way by writing the ionization cross section as the product

$$\sigma(E) \propto \frac{1}{E+E_0}\left(\frac{E}{E+E_0}\right)^\zeta, \tag{151}$$

where E is the excess energy of the system measured from the ionization threshold. The first factor $(E+E_0)^{-1}$ in Eq. (151) reproduces the classical high-energy limit with $\sigma(E \gg 1) \propto E^{-1}$. The second factor, while approaching unity for large E, reduces to the classical power-law behavior $(E/E_0)^\zeta$ near the ionization threshold $E = 0$. The constant $E_0 = E_M/\zeta$ is fixed by the maximum of the cross section, $\sigma_M = \sigma(E_M)$. In order to give a shape function which can be easily applied to experimental situations we use dimensionless variables $y = \sigma/\sigma_M$ and $x = E/E_M$ where σ_M and E_M can be determined either

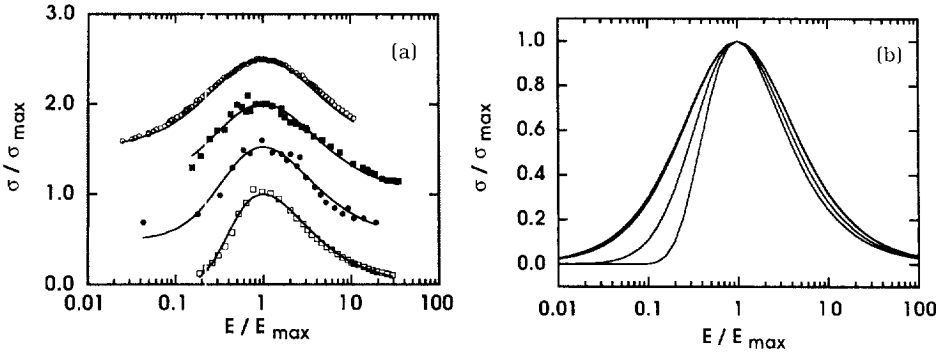

Fig. 10. Part (a) shows experimental cross sections for the ionization of hydrogen by various projectiles plotted in scaled coordinates $y = \sigma/\sigma_M$ versus E/E_M. The solid line is the shape function Eq. (152), no fit parameters are needed. Proton impact [118] is indicated by open squares and positron impact ($y + 0.5$, Ref. [119]) by filled circles. Antiproton impact with helium as a target is shown with filled squares ($y + 1$, Ref. [120]), and electron impact with open circles ($y + 1.5$, Ref. [126]). Part (b) shows theoretical shape functions, Eq. (152), for the systems of part (a).

from theory or experiment. (The latter case amounts to fitting the cross section with two parameters, σ_M and E_M.) Then, Eq. (151) reads

$$y \equiv \frac{\sigma(x)}{\sigma_M} = \frac{f_\zeta(x)}{f_\zeta(1)} \tag{152}$$

where

$$f_\zeta(x) = \frac{1}{x + \zeta^{-1}} \left(\frac{x}{x + \zeta^{-1}} \right)^\zeta . \tag{153}$$

The normalization of Eq. (152) with $f(1)$ guarantees that $y = 1$ at the position $x = 1$ of the maximum of the cross section. Hence, the *shape* of the ionization cross section, Eq. (152), is *parameter free*. It compares favorably with the experiment as can be seen in Fig. 10 where the experimental cross sections are plotted in the reduced units x and y together with the ζ-dependent shape-function Eq. (152). The respective exponent ζ determines the width of the peak in the ionization cross sections. This width becomes smaller for increasing ζ as can be seen in Fig. 10b where only the theoretical shape functions are plotted for the same collisional systems as in Fig. 10a.

Compared to all existing parameterizations of cross sections, Eqs. (151) and (152) include the threshold behavior. This results in a unified view of collisions involving very different projectiles: The same analytical form of the shape function describes electron–atom, positron–atom, proton–atom and antiproton–atom ionization [117]. All these ionization processes (in Fig. 10 with hydrogen or helium as the target atom) are equally well reproduced by the respective shape function. The lower energies are problematic for antiparticle impact (filled symbols in Fig. 10a) since direct fragmentation must be experimentally discriminated against positronium or anti-hydrogen formation.

The representation of the low-energy tail of the ionization cross section for electron ($\zeta = 1.127$) and positron ($\zeta = 2.65$) impact is mostly accepted [121] and well established (see Ref. [77] and references therein) and the possibility to parameterize the cross sections for these processes with

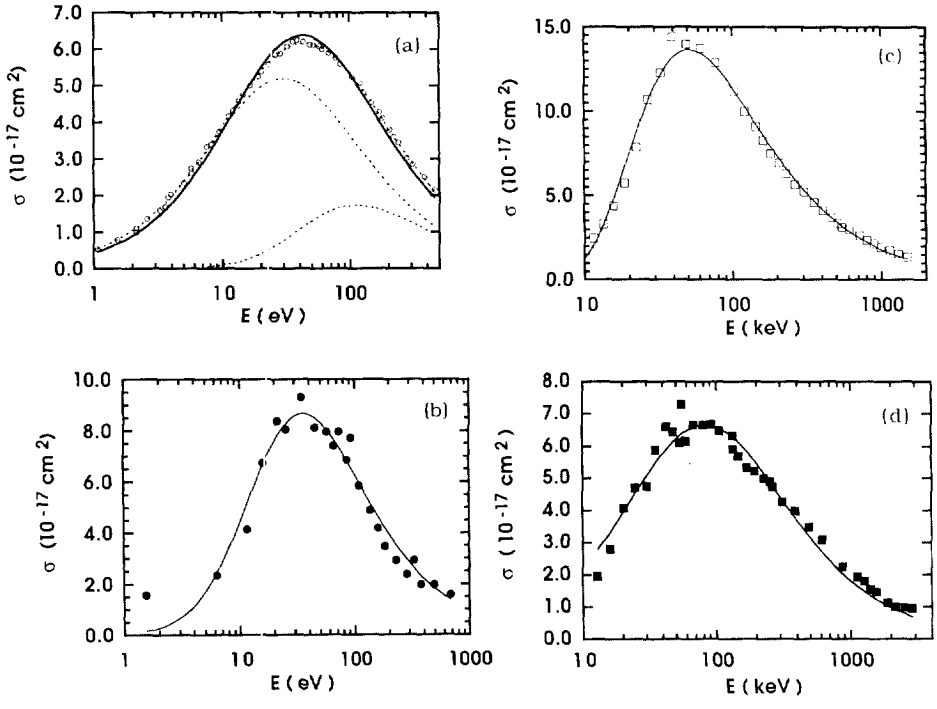

Fig. 11. Ionization of hydrogen by electrons (a), positrons (b) and protons (c). Part (d) shows ionization of helium by antiprotons. Symbols and experimental data are the same as in Fig. 10. The solid line is the respective cross section Eq. (151) with E_M and σ_M fitted to the experimental data, for the dashed lines see text.

Eq. (151) is certainly less surprising than for heavy particle impact which is therefore the crucial test for the universality of the proposed parameterization.

From proton impact one knows that ionization at threshold is highly suppressed and one would probably not expect any relevance of the threshold power law with $\zeta \approx 70$ in this case. However, as Fig. 11c shows, this is not true. Rather, the large exponent ζ reflects the suppression of threshold ionization and is apparently needed to reproduce the shape of the ionization cross section. Maybe even more interestingly, "threshold ionization" is not suppressed for heavy anti-particle impact ($\zeta = 1.20$ for antiprotons on hydrogen). Indeed, in scaled coordinates, the shape for electron-impact ionization and antiproton-impact ionization is almost the same (Fig. 10b).

To apply Eq. (152) one needs to know the exponent ζ which is defined through

$$\zeta = -\frac{1}{4} + \sqrt{\frac{1}{16} + \frac{C''(\gamma_0)}{2C(\gamma_0)}}, \tag{154}$$

where $C'' = \mathrm{d}^2C/\mathrm{d}\gamma^2$ with

$$C(\gamma) = \frac{Q_{13}}{\sin(\gamma_1 + \gamma)} + \frac{Q_{23}}{\sin(\gamma_2 - \gamma)} + \frac{Q_{12}}{\cos(\gamma)} \tag{155}$$

for $-\gamma_1 < \gamma < \gamma_2$. The angles are

$$\gamma_i = \arcsin[\sqrt{m_{12}m_{i3}}/m_i]$$

with the reduced masses $m_{ij} = m_i m_j/(m_i + m_j)$ between particles i and j. Finally,

$$Q_{ij} = Z_i Z_j \sqrt{m_{ij}/M}$$

with $M = \sum_{i=1}^{3} m_i$ being the total mass and the particles labeled with $Z_1 Z_2 > 0$ holding for the respective charges Z_i. The function $C(\gamma)$ in Eq. (155) is the effective, coordinate-dependent three-particle Coulomb charge on the collinear manifold, using mass-scaled coordinates. In the two-electron case, $C(\gamma)$ reduces to Eq. (82); however, γ is different from the angle α used in Eq. (82). The angle γ_0 is defined through $C'(\gamma_0) = 0$ and must be obtained numerically unless the particles 1 and 2 are identical in which case $\gamma_0 = 0$. However, small differences in γ have little influence on the shape function and for practical purposes it will be sufficient to use the limit of infinite mass for the target as provided in Table 1.

Electron impact: A closer inspection of Fig. 11a reveals that the shape function Eq. (152) overshoots the actual cross section near the maximum slightly. This is not observed in the other three cases. Electron-impact ionization differs from the other three collisional systems through the indistinguishable target and projectile electrons. The Pauli principle imposes an additional symmetry which leads to two partial cross sections. According to Eq. (145) they behave as E^{ζ} and $E^{3\zeta}$ close to threshold. On the other hand, for high energies, symmetrization is unimportant since projectile and target electron differ very much in energy. In this situation we may extend the shape function to the form

$$f_{\mathrm{sym}}(x) = f_{\zeta}(x) + \rho f_{3\zeta}(\rho x)\,, \tag{156}$$

where $\rho = E_{\mathrm{M}}^{(\zeta)}/E_{\mathrm{M}}^{(3\zeta)}$, now a true fitting parameter, is the ratio of the maximum positions of the contributions f_{ζ} and $f_{3\zeta}$. The relative weight of f_{ζ} and $f_{3\zeta}$ in Eq. (156) is fixed by the requirement that both components contribute equally in the asymptotic range for large E where the ionized target and the projectile electron are virtually distinguishable through their large difference in velocity. Note, that for Eq. (156) $x \equiv E/E_{\mathrm{M}}^{(\zeta)} = 1$ is not the position of the maximum of the cross section anymore. Fig. 11a shows the two contributions f_{ζ} and $f_{3\zeta}$ separately, the sum – also dashed but hardly visible – fits the experimental cross section very well. It can be seen that $f_{3\zeta}$ is indeed strongly suppressed as compared to f_{ζ} close to threshold $E = 0$ and correspondingly reaches its maximum at a higher energy, $E_{\mathrm{M}}^{(3\zeta)} > E_{\mathrm{M}}^{(\zeta)}$.

Heavy ion impact: For heavy ion collisions (i.e. projectiles with masses of the order of $10^3 m_{\mathrm{e}}$ and charges $Z \geq 1$), $\zeta \approx \sqrt{\mu}$ [122], where μ is the reduced mass of projectile and target in atomic units, i.e. $\zeta \approx 10^2$ (see Table 1). Eq. (153) may be simplified in this case by taking the limit $\zeta \to \infty$. Then we have

$$\lim_{\zeta \to \infty} f\zeta(x) = (1/x)\mathrm{e}^{-1/x}\,. \tag{157}$$

Indeed, the shape according to Eq. (157) (dashed) is indistinguishable from the shape of Eq. (153) (solid) with the 'correct' $\zeta = 69.7$ in Fig. 11c. This implies e.g. that all cross sections for different charge states of the heavy projectile A^{N+} will be represented by one scaled curve as in Fig. 10b

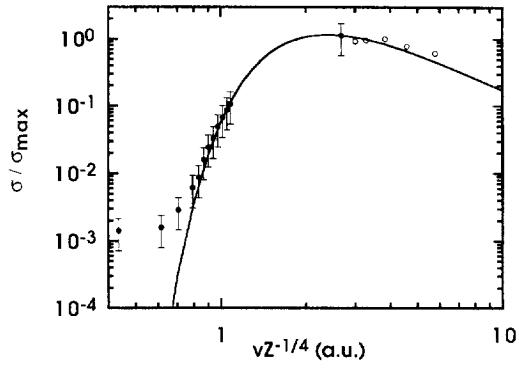

Fig. 12. Ionization of helium by slow oxygen ions (O^{8+}), the data with error bars are from Ref. [123], the open circles from an earlier experiment [124]. The solid line is formula, Eq. (152), where v_{max} and σ_{max} have been fitted.

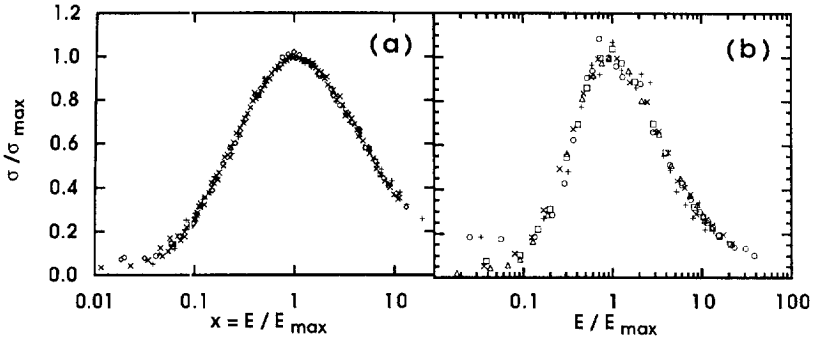

Fig. 13. Electron impact (a) and positron impact (b) ionization cross sections of atoms. The axes have been scaled to the respective maximum values σ_M and E_M. The data in (a) represent the hydrogen target (○) as in Fig. 10, and from Ref. [125] helium (+), nitrogen (×), carbon (□), and oxygen (△). The data in (b) are for the hydrogen target (+) as in Fig. 10, and from Ref. [127] for helium (△), argon (○), H_2 (□) and for neon (×).

with the scaling properties only dependent on the position and value of the maximum of the cross section. We present one example for the application of Eq. (157) in the context of extremly slow heavy ion collisions for which recently direct ionization has been measured for the first time [123]. In Fig. 12 we show a comparison of the experiment for $O^{8+} + He \rightarrow O^{8+} + He^- + e^-$.

Quite generally, the function, Eq. (153), implies identical shapes for the ionization cross section involving different targets but the same projectile. This is demonstrated in Fig. 13 for electron-impact and for positron-impact ionization. The poor agreement among the positron cross sections close to the fragmentation threshold can be attributed to the difficult subtraction of the background in the experiment, i.e. positronium formation which also produces a positive ion.

It would certainly be desirable to link the (experimental) position of the maximum E_M to the ionization potential I which is in most cases theoretically known. From the high-energy limit of the classical Thomson formula, one can derive a connection between σ_M and E_M [111] which would reduce the priori unknown quantities for the prediction of an absolute cross section to one parameter. Unfortunately, this classical relation does not reflect the experimental situation very well and a theoretical foundation of the empirical values (σ_M, E_M) is still lacking.

5.3.2. *Universal near-threshold ionization cross section*

In the case of electron–atom collisions near threshold, a relation between the energy scale E_M and the ionization potential has been established, once again, empirically. In Ref. [77] it was found that the ionization cross sections σ_A for various target electrons could be expressed through the hydrogenic cross section σ_H using the scaling relation

$$\sigma_A(E) = \beta_A \sigma_H(\rho_A E)\,. \tag{158}$$

Fig. 14 shows ionization cross sections of valence shell electrons for He(1s), Na(3s) and, as already discussed, H(1s). In addition, three innershell ionization cross sections are shown, namely Ne(1s), Ar(1s) and Xe(2p). The solid lines correspond to Eq. (158) with suitable scaling parameters β_A and ρ_A. As can be seen the agreement is generally good despite the great variation of the ionization potential from around 5 eV for Na to nearly 5 keV for Xe. On a logarithmic scale $\ln \rho_A$ is a linear function of $\ln \rho(I_A)$ with a slope of $-\frac{3}{4}$ (Fig. 15a). Hence, we may approximate

$$\rho(I) = \left(\frac{13.6\,\text{eV}}{I}\right)^{3/4}\,. \tag{159}$$

With Eq. (158), only the absolute scale of the individual cross sections σ_A remains undetermined. To demonstrate the validity of Eq. (159) we show in Fig. 15b all experimental cross sections from Fig. 14, scaled to the hydrogenic cross section according to Eq. (159).

This result indicates that the cross section for any threshold ionization behaves like the hydrogenic cross section characterized with the Wannier exponent ζ. Particularly for inner shell ionization this deserves some explanation. The electron pair leaving the atom from an inner shell region must penetrate the entire atomic electron cloud [88]. Slow electrons might be even passed by the Auger electron following the decay of the inner shell hole. Subsequently, the slow ionized electron will see a core whose charge has increased by one and it is conceivable that a significant fraction of the slow electrons will not escape but fall back into the nucleus. These hindered ionization events should change the ionization characteristics compared to a structureless target. Why do such processes not alter the energy dependence of the cross section? The energy-sharing function (Fig. 5) provides an explanation. This function is relatively smooth (from threshold to 8 eV excess energy in hydrogen the maximum difference between the probability for an electron with energy $\varepsilon \approx 0$ and $\varepsilon \approx E/2$ is not more than 8% (compare with Fig. 5c of Ref. [76]). In a crude approximation we could assume that the energy sharing is constant. In this case, the eventually missing tail of slow electrons in the energy-sharing distribution of the ionization yield of inner shell electrons will mainly affect the absolute value of the signal (which is represented by β_A in Eq. (158)) but not the functional energy dependence of the total ionization cross section.

5.4. *Chaotic scattering and resonance formation in electron–hydrogen collisions*

The connection between ionization and two-electron resonances has been the subject of theoretical interest for some time. A long standing conjecture (see, for example, Ref. [132]) has interpreted the symmetrically excited two-electron resonances as being formed from standing waves along the potential ridge (solid wave fronts in Fig. 16). These standing waves have been thought of as a continuation of the escaping wavepackets along the ridge above threshold, in analogy to

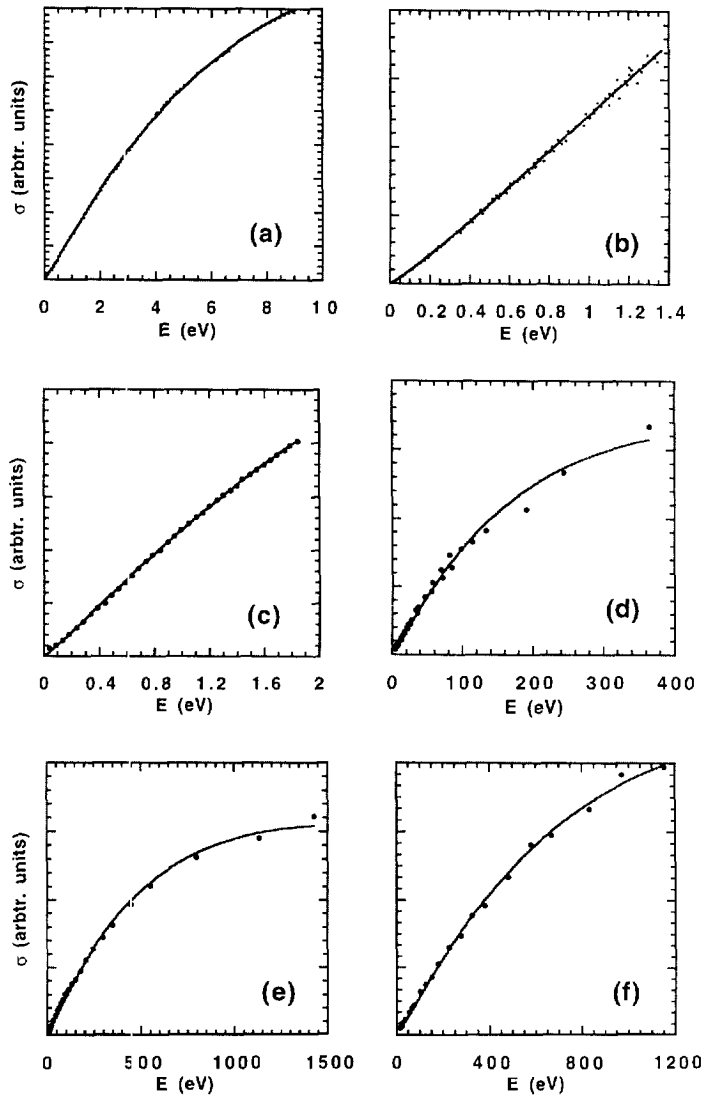

Fig. 14. Total ionization cross sections in arbitrary units. The solid line is the hydrogen cross section with adapted scaling parameters according to Eq. (158). The ionization cross sections (a)–(c) are for the valence shell electrons (a) H(1s) [97], (b) He(1s) [128] and (c) Na(3s) [129]. In (d)–(f) innershell ionization is shown for (d) Ne(1s) [130], (e) Ar(1s) and (f) Xe(2p) (both Ref. [131]).

the two-body problem. However, due to its instability the quasi-standing waves of resonant states never ride on the ridge $r_1 = r_2$ but rather cross it a number of times during their lifetime (see Fig. 16). This conclusion is suggested by the adiabatic hyperspherical [133, 134] and molecular [135] work on resonances, if correctly interpreted, as well as by the semiclassical work using periodic orbits [106, 20]. It also follows from the nodal patterns of 'exact' numerical resonance wave functions [136].

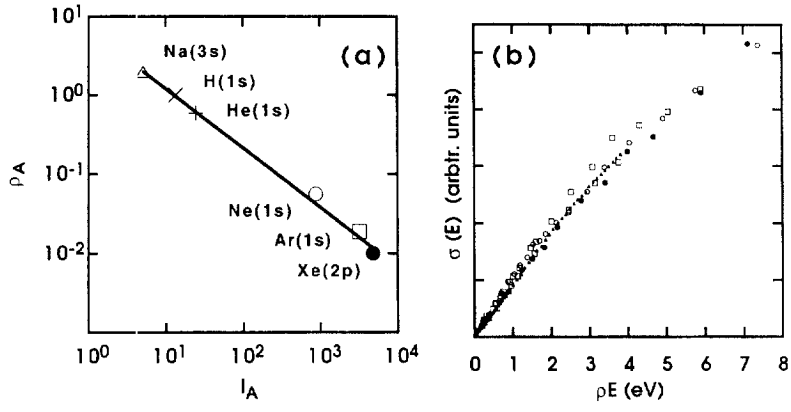

Fig. 15. (a) The energy scaling parameter ρ plotted versus the ionization potential I for the cross sections from Fig. 14. The slope of the line in the log–log plot is $-\frac{3}{4}$. (b) The experimental cross sections from Fig. 14 scaled according to $\rho(I)$ from Eq. (159) to the energy scale of hydrogen, (×) H(1s), (△) Na(3s), (○) Ne(1s), (□) Ar(1s), and (●) Xe(2p).

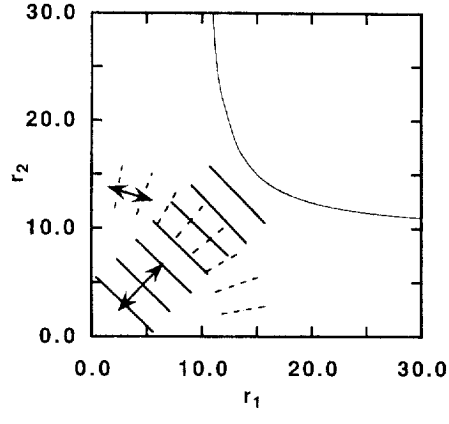

Fig. 16. Schematic illustration of wave fronts for a possible quasi-stationary state along (solid) and across (dashed) the potential ridge at $r_1 = r_2$ and $\theta_{12} = \pi$. The arrows point to the periodic motion of the wave fronts. The light solid line indicates the potential boundary for an energy of $E = -0.1$ a.u.

If the symmetrically excited two-electron resonances have their wave fronts dominantly across the ridge it is less clear how ionizing waves should evolve from these resonant states tuning the energy through the ionization threshold. So far there has been no method which could be used to describe resonances as well as the ionization within one framework, e.g. a simulated scattering experiment. The semiclassical S-matrix provides such a framework and we can study the structure of relevant classical trajectories to understand the evolution from resonances to ionization and the connection between these two processes. We calculate the scattering amplitude for a simulated scattering experiment with hydrogen as a target and an electron as the projectile on the collinear manifold, exactly like in Eq. (139) for ionization. We only have to lower the energy of the projectile so that the total energy becomes negative [107].

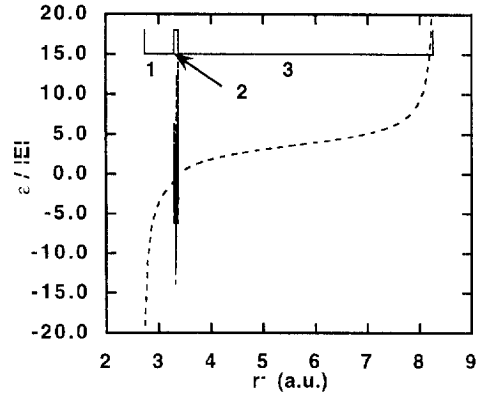

Fig. 17. Same as Fig. 4 but for a total energy $E = -0.1$ a.u. below threshold.

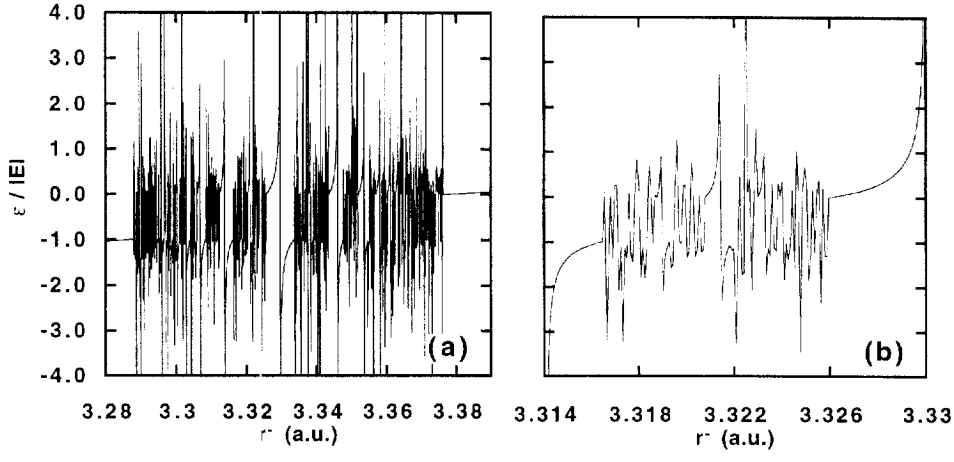

Fig. 18. Details of Fig. 17 illustrating interval 2. Note the self-similar structure of the fractal comparing Figs. 17, 18a and 18b.

5.4.1. *Qualitative analysis*

The deflection function is, as before, the important object for the (semi-)classical analysis. It is shown in Fig. 17 for an energy of $E = -0.1$ a.u. There is still the interval 1 representing classical exchange processes which looks very similar to the corresponding interval 1 for energies above threshold (Fig. 4). This is also true for the interval 3 representing excitation. However, the interval 2, which stands for ionization, has been replaced by a fractal object with self similar structure (interval 2, see Fig. 18) that represents chaotic scattering.[5] A similar fractal structure was observed in an electron–He^+ scattering simulation with classical trajectories [138]. Apparently, what had been ionization above threshold turns into chaotic scattering below threshold. In the early studies of reactive scattering chaotic scattering was already observed although the apparatus of nonlinear dynamics to deal with this phenomenon was not at hand back then [139].

[5] For a mathematical description of chaotic scattering see Ref. [137].

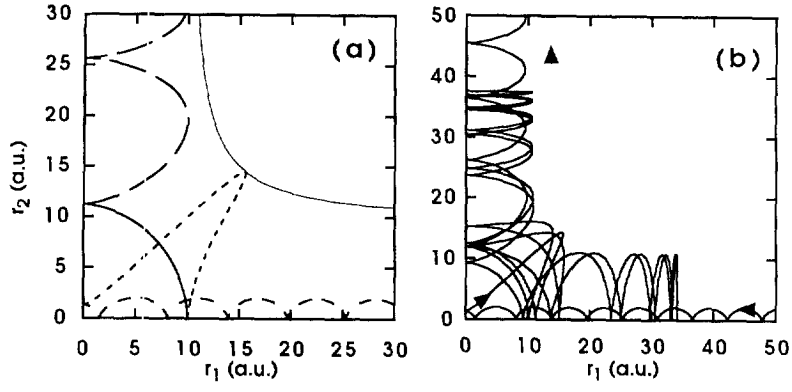

Fig. 19. Delayed trajectories with initial conditions r^- from interval 2, for the coding of the segments in (a), see text.

Chaotic trajectories are responsible for the fractal structure of the deflection function and they are the key to the connection between chaotic scattering and ionization. Following a trajectory from the interval 2 in time (Fig. 19a), the first element is the incoming part (dashed line). The second element (dotted line) shows that the trajectory indeed has ionizing character, reminiscent of its initial condition that falls into the interval 2 leading to ionization above threshold. However, we are now below threshold and the electrons do not have sufficient energy to escape. Eventually, they must hit the potential boundary (light solid line) and the trajectory must turn around. What follows now is a *new* element of the scattering orbit (dark solid line), only present for orbits that belong to the interval 2 below threshold. The two electrons bounce in some sequence (that is characteristic for the specific orbit and can be used to classify the orbit rigorously with a binary code) into the nucleus before the trajectory eventually exits using the usual outgoing element (long dashed line) to become an exchange or an excitation event. The binary code is that of a periodic orbit which the scattering trajectory approaches for some time. In the case of Fig. 19a the relevant periodic orbit is the shortest one of the two-electron system. It can be characterized by the code '01' where '0' and '1' stand for a collision of electrons 1 and 2 with the nucleus, respectively. The periodic orbits can be organized into families according to the bouncing sequence of the electrons reflected by the codes [141]. Certain periodic orbits have infinitely long codes and correspondingly a period which tends to infinity. They constitute chaotic dynamics for the two-electron system. Following one of these periodic orbits and eventually bouncing many times into the nucleus creates a time delay compared to the direct trajectories from the intervals 1 and 3. This time delay is the signature of resonance scattering and it is this element of the scattering orbit that has been identified recently with the dynamics of quasi-stationary resonant states [140].

To summarize briefly, a chaotic scattering trajectory as in Fig. 19 has four elements, the incoming part (dashed) the ionizing part (dotted), the resonance part (solid) and the outgoing part (long dashed). It thus combines the ionizing part through which it is related to the real ionizing trajectory above threshold with the resonant part that is responsible for a characteristic time delay.

Memory loss: From the structure of the classical deflection function $\varepsilon(r^-)$ above (Fig. 4) and below (Fig. 17) threshold and the structure of the orbits belonging to the respective interval 2 it is clear that resonance scattering and ionization are related. However, there is a subtle feature induced by the chaotic motion that reaches into the seemingly regular regime of ionization. The extreme

sensitivity to initial conditions characteristic for the chaotic trajectories below threshold and visible in the fractal structure of the deflection function $\varepsilon(r^-)$ appears above threshold as a remarkable *insensitivity* to the initial state from which the atom was ionized. This effect can be understood by interpreting the chaotic scattering trajectories as orbits that neither lead to direct excitation nor to exchange but to 'ionization'. However, since this is energetically not possible, the electrons along these orbits bounce many times into the nucleus until the orbit has sufficiently forgotten its initial 'ionizing' character and eventually finds a conventional exchange or excitation exit channel. Thus, the effect of *loss of memory* of initial conditions *above* threshold, attributed by Wannier to the (assumed) ergodic character of the dynamics [82] is much more obvious in the chaotic regime *below* threshold and one might loosely say that the necessity for the electrons to forget the initial conditions in order to leave the nucleus create the chaotic behavior of the trajectories. A consequence of the *memory loss* above threshold is the independence of the energy sharing Eq. (140) from the initial state (see Section 5.2.3).

5.4.2. *Quantitative analysis and comparison with experiment*

At a first glance it might seem hopeless to deal with a fractal object like the interval 2 in Fig. 18. Nevertheless, we can form the analogy to the total ionization cross section. Instead of integrating all contributions from interval 2 over all electron energies ε as in Eq. (139) for ionization, we integrate now over all contributions from the interval 2. The quantity we will obtain is the probability for resonance scattering, i.e. the probability that the electron suffered a time delay in the scattering event and, for a short time, an (excited) three-body complex had been formed. For each ε there is not only one but an infinite set of trajectories $\{i\}$ contributing to the sum of Eq. (125). However, to each index i belongs a continuous branch of trajectories with all energies ε. This branch yields upon integration over ε a small subinterval δ_i. The sum over i recovers then the entire interval $\Delta r^-(2) = \sum_i \delta_i$ of chaotic scattering, which replaces $\Delta r^-(2)$ in Eq. (139),

$$P_{\text{frac}}(E) = \frac{1}{R}\sum_i \int_{-\infty}^{\infty} \mathrm{d}\varepsilon \left| \frac{\partial \varepsilon}{\partial r_i^-} \right|_{\varepsilon^-}^{-1} = \sum_i \frac{\delta_i}{R} = \frac{\Delta r^-(2)}{R} . \tag{160}$$

Thus, the probability for resonance formation below threshold is in exact analogy to the total ionization cross section (Eq. (139)) above threshold. Together the probabilities represent three-body events where both electrons have to participate in the scattering process simultaneously.

Experimentally, such events have been detected by measuring extremely slow ('zero kinetic energy', $\varepsilon \approx 0$) electrons produced in electron–atom collisions [128] or in photoionization [142]. Assuming that the energy distribution of the electron $\mathrm{d}\sigma/\mathrm{d}\varepsilon$ is almost flat for energies $E \approx 0$ (see Section 5.2.3 and Refs. [128, 76]) the probability P_{frac} for three-body events, Eq. (160), is related to the slow electron spectrum through

$$\sigma_{\varepsilon=0}(E) \approx \sigma_{\pm} P(E)/E . \tag{161}$$

The constant of proportionality $\sigma_{\pm}$ is expected to be different for negative and positive energies E. The actual ratio σ_-/σ_+ depends on experimental parameters (such as pressure in the gas cell) and is not yet fully understood [142]. Nevertheless, the *energy dependence* can be checked against $P(E)$. The cross section Eq. (161) calculated with $P(E)$ from Eq. (160) is shown in Fig. 20 with black points. The spectrum has been normalized to the experimental data from Ref. [128] (open squares)

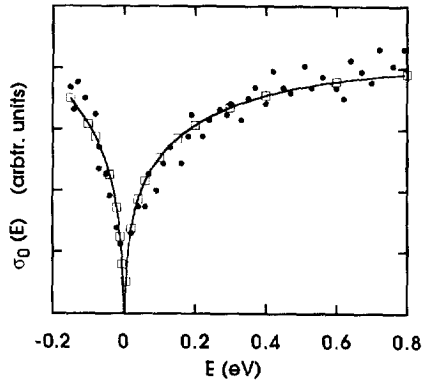

Fig. 20. Cross section for the production of slow electrons following electron impact on atoms close to the fragmentation threshold. The open squares are experimental data for a He($1s^2$) target [128]. The black circles are the theory for a hydrogen target H(1s). The solid line is a fit of the theory according to Eq. (162).

separately for $E > 0$ (σ_+) and $E < 0$ (σ_-). The solid line is a parametrization of the theoretical cross section with the function

$$\sigma_0(E) = \sigma_\pm |E|^{\zeta-1}(1 + a|E|^{1/2} + bE), \tag{162}$$

where $\zeta = 1.127$. For $E > 0$, Eq. (162) reflects the 'classical' result (Section 5.2 and Refs. [82,76]) that the total ionization cross section close to threshold is proportional to the 1.127th power of E. Noting from Fig. 20 and Eq. (162) that this holds also below threshold we can conclude that $|E|^{1.127}$ originates in the three-body amplitude of the S-matrix and should be independent of the process through which it was activated. The residual dynamics, essentially the density of states, depend on the initial state and the excitation as a whole (by photon or particle impact, etc.) and varies slowly with energy. This includes slow electrons from direct excitation. Hence, we can take these contributions into account with a Taylor expansion about $E = 0$ in Eq. (162) represented by the energy-independent parameters a and b. Since a and b depend on the actual threshold process they are not universal like the threshold exponent ζ.

Through comparison with the experiment we have established so far that the classical three-body cross section Eq. (160) is a meaningful quantity close to the fragmentation threshold. However, one might suspect that the good agreement between experiment and theory below threshold is misleading: The absence of structure in the cross section could be a consequence of the finite-energy resolution on the experimental side and an artifact of the classical treatment on the theoretical side.

More light can be shed on this problem with a quantum mechanical calculation of the two-electron resonances just below threshold. Of particular interest is the trend of the widths Γ as a function of energy E. The widths, formulated as transition matrix elements with an S-matrix [143, Ch. 14], contain the same three-body amplitude as the cross section for ionization/resonant scattering. Hence, we expect an energy dependence $|E|^\zeta$ for widths of states which approach in the limit $E \to 0^-$ a similar geometrical configuration as it is given by the collinear manifold through the classical fixed point with $\theta = \pi$. These states are exactly the resonances which were for some times interpreted as standing waves on the ridge of the potential $r_1 = r_2$. In the literature they are often referred to as *ridge states*, *Wannier* resonances, *saddle* resonances or *intrashell* resonances. The last name

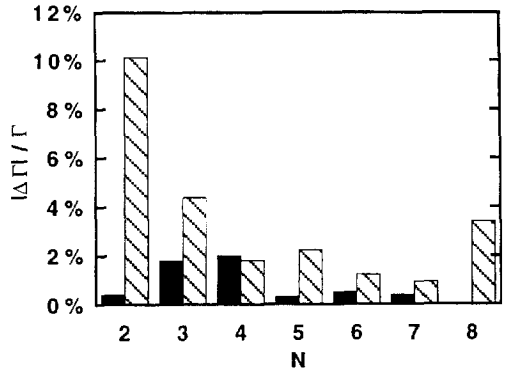

Fig. 21. Relative error of the fit Eq. (162) for $^1S^e$ saddle resonances in H^- shown with black columns. For comparison the error for a fit with a linear exponent $\zeta = 1$ is shown with white columns.

indicates that these resonances are characterized by approximately equal principal quantum numbers $n_1 = n_2 \equiv N$ of both electrons. Widths Γ_N and positions E_N for the saddle resonances $2 \leq N \leq 8$ in H^- have been calculated quantum mechanically with a complex scaling algorithm [144]. Fig. 21 shows the relative error for the fit of Γ_N/E_N with Eq. (162). To demonstrate the sensitivity on the exponent $\zeta = 1.127$ we also give the fit with a linear exponent $\zeta = 1$ which reproduces the quantum mechanical widths not very well.

Thus, the picture of the threshold dynamics for $E \to 0^-$ obtained classically is quantum mechanically confirmed. In particular, the energy dependence of the widths $\Gamma \propto |E|^{1.127}$ implies that these resonances will strongly overlap because their spacing $\Delta E_N - E_{N-1} \propto N^{-3} \propto |E|^{1.5}$ decreases faster towards $E = 0$ than their widths. Indeed, the $N = 8$ resonance was the highest saddle resonance isolated enough so that a converged complex energy could be obtained. The experimental spectrum in Fig. 20 does not exhibit isolated resonances for the displayed energy range of $E \geq -0.15\,\text{eV}$. Although not conclusive due to the experimental energy resolution this observation is nevertheless consistent with our quantum calculation because the $N = 8$ resonance lies at $E = -0.28\,\text{eV}$.

On the other side, a quasiregular part of the spectrum will prevail towards threshold although the energy intervals it occupies become smaller and smaller compared to the intervals the irregular spectrum covers. The surviving regular spectrum consists of configurations where $n_1 \gg n_2 \gg 1$, that is where electron one is very far outside the already highly excited core with the second electron. Such a configuration also implies little interaction between the two electrons and leads consequently to a very long lifetime of these asymmetric resonances making them difficult to observe in the experiment.

Nevertheless, one interesting conclusion for the high precision experiments currently being prepared in the limit $E \to 0^-$ can be drawn from the present discussion: the spectrum of isolated resonances that can be related to approximate constants of motion [135] should disappear for $E \to 0^-$. Furthermore, the energy dependence of the widths for saddle resonances, which have been related to the Wannier ionization mechanism for a long time, is given by the Wannier power law for $|E| \to 0$. Different power laws $|E|^\zeta$ have been predicted [79, 145–147] for the widths which neither agree among themselves nor with our result apart from a recent prediction of an approximately linear behavior $\zeta \approx 1$ for helium [148]. A direct comparison is complicated by the fact that the quantities

which have been discussed (partial cross section for excitation, intensity at resonance, total width, etc.) are slightly different. However, it should be stressed that our $\Gamma \propto |E|^{1.127}$ is the result of a fit to data from very accurate quantum mechanical calculations. This is important since the exponent ζ is surprisingly sensitive to the accuracy of the resonance parameters. Hence, the energy dependence of widths obtained within some approximation or extracted from numerical data of lower accuracy should be interpreted with care.

Overall, we can conclude that the fragmentation threshold connects smoothly the intimately related processes of resonance formation and ionization through the energy dependence $|E|^{1.127}$. There are still a number of open questions. For instance, it is necessary to understand *how* the complicated spectrum of multiple Rydberg and dipole-like series of resonances disappears with $E \to 0^-$. It is conceivable [148] that in a small energy range a global fluctuation pattern like that of Ericson fluctuations known from nuclear physics [149] replaces the resonance structure before the cross section becomes smooth very close to $E = 0$.

6. Photoionization of atoms

In this section we will describe a combined quantum (semi-)classical approach to photo processes. We will begin with the total photo cross section. For smooth potentials, the total photo cross section is essentially an initial-state property since over all final states that are energetically allowed has been summed. This is most obvious in the time-dependent representation where the absorption cross section is formulated as a time-dependent dipole polarizability [150, 151]. In this formulation one can approximate the dynamics, i.e. the propagator, leaving the initial state exact (quantum mechanical). The probably best-known approximation in this context is the *reflection principle* in molecular physics. It is a quasiclassical approximation because commutators (i.e. the order of $\hbar$ and higher) are neglected in the propagator. After a short description of the traditional molecular application we will demonstrate how this concept can be applied to our problem of electronic motion in Coulomb problems instead of nuclear motion in molecules.

Hereafter, we will use the semiclassical concepts of propagation in reduced phase space as already described in the previous sections to estimate with little effort the ratio of double to single photoionization in helium. The idea here is to identify projectors in connection with partial fixed points which can be related to physical observables. The energy sharing between the electrons, already discussed in the last section, is a suitable variable to determine the projectors for single and double ionization.

The first step consists of a theoretical approach for the total cross section of atoms which is such a global quantity that the interaction and correlation of the electrons must only be probed on a short time scale. The ratio of single to double ionization is the next, least differential observable. The projectors onto these spaces can be understood as the long time limit of the propagation only performed in those parts of phase space which are most relevant to decide two or three particle fragmentation. The combination of both steps allows to predict the *absolute* cross section for double photoionization.

The (semi-)classical formulation of photoionization as presented here has also a very interesting (and not yet solved) aspect concerning the two-electron ground state of helium. How does one represent this state classically where all trajectories but the periodic orbits autoionize after a finite

time? This is due to the electron–electron interaction and the missing lower limit for classical electron energies which always allows one electron to fall into the nucleus while the other one escapes.

Since this is not a review about photoionization primarily we do not even attempt to present an overview over the huge body of work which has been accumulated in the literature. A good overview until 1988 is provided in Ref. [152].

6.1. The total photo-cross section: an analytical approximation

6.1.1. The reflection principle for molecules

The general time-dependent expression for photoabsorption reads [150]

$$\sigma(\omega) = \frac{2\pi\alpha_F}{\omega} \int_{-\infty}^{\infty} dt \, \langle \Psi | D(0)^{\dagger} D(t) | \Psi \rangle \, e^{i\omega t} \tag{163}$$

with the time-dependent dipole operator

$$D(t) = e^{-iHt} D_0 e^{iHt} . \tag{164}$$

In the argument of the exponential in Eq. (164) we have suppressed $1/\hbar$ which is unity in atomic units. The frequency of the photon determines the final energy E_f through $\omega = E_f - E_i$, where Ψ is the initial wave function with eigenenergy E_i and α_F is the fine structure constant. Photoabsorption in a molecule under the Born–Oppenheimer and Condon approximation (vertical transitions) means that the photon is absorbed by an electron whereby the nuclear dynamics is shifted from a lower potential curve described by the Hamiltonian H_0 to a higher potential curve with Hamiltonian H_1 for the nuclear motion. The dipole moment D_0 does not depend on nuclear degrees of freedom in the Condon approximation. Hence, we can simplify Eq. (163), which refers to the nuclear motion, as

$$\sigma(\omega) = \frac{2\pi\alpha_F \mu^2}{\omega} \int_{-\infty}^{\infty} dt \, \langle \Psi | e^{-iH_1 t} e^{iH_0 t} | \Psi \rangle \, e^{i\omega t} , \tag{165}$$

where Ψ now represents the initial nuclear wave function and μ^2 is the squared electronic dipole matrix element. The dynamical problem to be solved involves forward propagation of the state Ψ until time t on the 'lower' potential surface which is characterized by H_0, followed by a backward propagation on the 'upper' surface with H_1. If we use for both propagations the same approximation we can hope that errors will partially cancel. Writing $H_1 - H_0 = \Delta$ the obvious approximation is the zeroth-order term of the Baker–Hausdorff expansion

$$e^{-i(H_0-\Delta)t} e^{iH_0 t} \approx e^{-i\Delta t} . \tag{166}$$

This amounts to neglecting all commutators between H_0 and H_1 and is therefore essentially a (semi-)classical approximation which can also be derived in a slightly different spirit from an expansion in $\hbar$. The result is known in molecular physics as the reflection principle [150]. One can include the second-order term in the commutator which is proportional to $i\boldsymbol{p}t^2$ in the exponential. However, the action of the $\boldsymbol{p}$ operator onto the wave function is not readily calculated and one usually replaces the operator by its expectation value, $\boldsymbol{p} \approx \langle \boldsymbol{p} \rangle$. Since for stationary states Ψ the expectation value of the momentum is zero there is no additional contribution. However, this term is important if Ψ represents a moving object, e.g. a wavepacket [153].

In the molecular context $\Delta = V_1 - V_0$ is usually the difference between the lower and the upper potential surface. In coordinate representation $\exp[i\Delta(r)t]$ reduces to a phase and the time integral can be performed analytically leading to a δ-function which relates the position r in the wave function to the photon frequency ω. Hence, the photo cross section $\sigma(\omega) \propto |\Psi(r(\omega))|^2$ 'reflects' quite directly the wave function, more precisely the probability density.

6.1.2. A reflection principle for photoabsorption in atoms

On a first glance it is not possible to use the ideas of the molecular reflection principle for atoms. First, the dipole operator depends now on the dynamically relevant coordinates of the electrons. Second, in atoms dynamics does not take place on different potential surfaces leading to a difference Δ of the respective Hamiltonians. However, as we will show, both obstacles can be overcome.

One electron: For transparency, we will discuss the case of one electron first. In the atomic case the only difference before and after the absorption is the angular momentum. This difference may be used to create different 'radial' Hamiltonians before and after the absorption. We separate the angular degrees of freedom in Eq. (163) algebraically by inserting a complete set $\sum |lm\rangle\langle lm|$ of spherical harmonics at the appropriate places. Recalling that the dipole moment is a vector operator and assuming, for simplicity, linear polarization along the z-axis all sums collapse to one term and we get

$$\langle \Psi | D(0)^\dagger D(t) | \Psi \rangle = \int_0^\infty \mathrm{d}r\, \psi^* d_0^\dagger \mathrm{e}^{-\mathrm{i}H_1 t} d_0 \mathrm{e}^{\mathrm{i}H_0 t} \psi \,, \tag{167}$$

where

$$\psi = \langle 00 | r\Psi \rangle = 2\beta^{3/2} r \mathrm{e}^{-\beta r} \,, \tag{168}$$

and $\mathrm{e}^{-\mathrm{i}H_l t} = \langle l0 | \mathrm{e}^{-\mathrm{i}Ht} | l0 \rangle$ with

$$H_l = -\frac{1}{2}\frac{\mathrm{d}^2}{\mathrm{d}r^2} - \frac{Z}{r} + \frac{l(l+1)}{2r^2} \,. \tag{169}$$

To be slightly more general we have used a screened hydrogenic wave function with effective charge β. The pure hydrogenic case is obtained by setting $\beta = Z$. For reasons that will become clear in a moment we will use the acceleration form for the dipole moment

$$D_0 = \frac{Z}{\mathrm{i}\omega}\frac{1}{r^2}\cos\Theta \tag{170}$$

and therefore

$$d_0 = \langle 10 | D_0 | 00 \rangle = \frac{1}{\sqrt{3}}\frac{Z}{\mathrm{i}\omega}\frac{1}{r^2} \,. \tag{171}$$

Having defined two effective Hamiltonians we still have to solve the problem that the dipole operator Eq. (171) depends on r which leads to complicated commutators with the propagators in Eq. (167). However, in the form of Eq. (171) the dipole operator is proportional to the centrifugal potential in

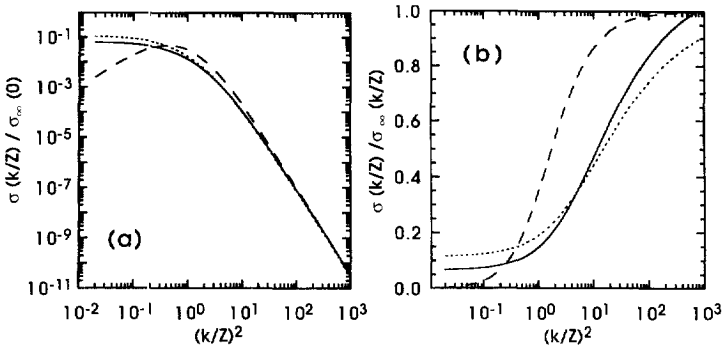

Fig. 22. Total photoabsorption cross section for hydrogen, full line: from Eq. (174), dotted line: exact result, dashed line: high-energy approximation, the scaling function is $\sigma_\infty(y) = (\alpha\pi 2^8)/(3Z^2(y^2+1)^{3.5})$. Part (a) in logarithmic representation, part (b) with the major energy dependence $\sigma_\infty(y)$ factored out.

H_I and we can write [154]

$$\sigma(\omega) \equiv \frac{2\pi\alpha Z^2}{3\omega^3} \int_{-\infty}^{\infty} \mathrm{d}t \, \langle\psi|(H_1 - H_0)\mathrm{e}^{-\mathrm{i}H_1 t}(H_1 - H_0)\mathrm{e}^{\mathrm{i}H_0 t}|\psi\rangle \, \mathrm{e}^{\mathrm{i}\omega t}$$
$$= \frac{2\pi\alpha Z^2}{3\omega} \int_{-\infty}^{\infty} \mathrm{d}t \, \langle\psi|\mathrm{e}^{-\mathrm{i}H_1 t}\mathrm{e}^{\mathrm{i}H_0 t}|\psi\rangle \, \mathrm{e}^{\mathrm{i}\omega t} \, . \tag{172}$$

This identity can easily be verified by differentiating the integrand of Eq. (172) twice with respect to time and using the fact that ψ is an eigenfunction of H_0.

Now, the form of Eq. (172) is identical to the nuclear dynamics of photoabsorption in molecules under the Born–Oppenheimer and Condon approximation of Eqs. (165) and (166).

With Eqs. (172) and (166) we can finally write the total cross section as

$$\sigma(\omega) \approx \frac{2\pi\alpha Z^2}{3\omega} \int_{-\infty}^{-\infty} \mathrm{d}t \langle\psi|\mathrm{e}^{-\mathrm{i}\Delta_1 t}|\psi\rangle \mathrm{e}^{\mathrm{i}\omega t} \, . \tag{173}$$

We will call Eq. (173) the hybrid approximation. It is quantum mechanical as far as the initial state and the exactly calculated commutators between the dipole moment and the propagator are concerned. Only the 'difference' of the propagation with H_0 and H_1 is approximated classically (see Eq. (166)).

The time integration in Eq. (173) leads now to a δ-function fixing the radial variable to $r = \omega^{-1/2}$. The final result with the wave function Eq. (168) is

$$\sigma_\beta(\omega) = \frac{Z^2}{\beta^4} \frac{2^7\pi^2\alpha}{3\sqrt{2}} \frac{1}{x^{7/2}} \mathrm{e}^{-\sqrt{8/x}} \, , \tag{174}$$

where $x = 2\omega/\beta^2$. Note that the quantum-classical hybrid formulae, Eqs. (173) and (174), fulfill the sum rule for the oscillator strength. This is clear since the sum rule is the short-time limit and the only approximation was made in the time propagation.

In Fig. 22 the present result for hydrogen is compared to the exact cross section [155, pp. 299–304] and the usual high-energy approximation where the final state is replaced by a plane wave [155]. Eq. (174) is a reasonable approximation from threshold to several hundred eV and its superiority

over the high-energy approximation is clearly seen. The hybrid formula has the correct high-energy dependence of $\omega^{-7/2}$ with a prefactor that is by 11% too large compared to the exact cross section. However, this will only have an effect well beyond 10^3 eV where Compton scattering will play an increasing role.

Many electrons: The described hybrid approach can be applied to calculate total photo-cross sections for many-electron systems with the Hamiltonian $H = H_0 + h$ where $H_0 = \sum_j H^{(j)}$ and $h = \sum_{j,k>j} V^{(jk)}$ with

$$\begin{aligned} H^{(j)} &= -\frac{1}{2}\nabla_j^2 - \frac{Z}{r_j}\,, \\ V^{(jk)} &= 1/|\boldsymbol{r}_j - \boldsymbol{r}_k|\,. \end{aligned} \tag{175}$$

In the spirit of the reflection principle the additional approximation of a classical propagation of the electron–electron interactions h is introduced. This is accomplished by using the first term of the Baker–Hausdorff formula in

$$\mathrm{e}^{\mathrm{i}(H_0+h)t} \approx \mathrm{e}^{\mathrm{i}H_0 t}\mathrm{e}^{\mathrm{i}ht} = \prod_j \mathrm{e}^{\mathrm{i}H^{(j)}t} \prod_{j,k>j} \mathrm{e}^{\mathrm{i}V^{(jk)}t}\,. \tag{176}$$

Under the approximation Eq. (176) we can write

$$\sigma(\omega) = \frac{2\pi\alpha}{\omega}\int_{-\infty}^{+\infty} \mathrm{d}t\,\langle\Psi|\mathscr{D}^{\dagger}(0)\mathscr{D}(t)|\Psi\rangle\,\mathrm{e}^{\mathrm{i}\omega t}\,, \tag{177}$$

where the time-dependent dipole operator has now the form

$$\mathscr{D}(t) = \sum_j D^{(j)}(t) = \sum_j \mathrm{e}^{-\mathrm{i}H^{(j)}t} D_0^{(j)} \mathrm{e}^{\mathrm{i}H^{(j)}t}\,. \tag{178}$$

The interpretation of Eq. (177) is simple: The dipole operator for each electron j is propagated by the isolated dynamics of this electron only. However, electron–electron correlation has not been completely neglected in Eq. (177). First, the interelectronic potentials are included classically and appear indirectly through the energy difference $\omega = E_{\mathrm{f}} - E_{\mathrm{i}}$. Second, there are 'cross'-terms between dipole operators of different electrons, $\langle\Psi|D^{(j)\dagger}(0)D^{(k)}(t)|\Psi\rangle$. These terms probe the electron correlation inherent in the initial-state wave function Ψ. The effect becomes already visible for a two-electron atom.

Two electrons: helium: With a properly symmetrized ground-state wave function Ψ we may write

$$\sigma(\omega) = \frac{4\pi\alpha}{\omega}\int_{-\infty}^{+\infty} \mathrm{d}t(\langle\Psi|D^{(1)\dagger}(0)D^{(1)}(t)|\Psi\rangle + \langle\Psi|D^{(2)\dagger}(0)D^{(1)}(t)|\Psi\rangle)\mathrm{e}^{\mathrm{i}\omega t}\,. \tag{179}$$

The first term in Eq. (179) describes the one-electron contribution and the second term represents the correlation effect. It is absent for an uncorrelated initial state of the two electrons,

$$\Psi = \frac{\beta^3}{\pi}\mathrm{e}^{-\beta(r_1+r_2)}\,, \tag{180}$$

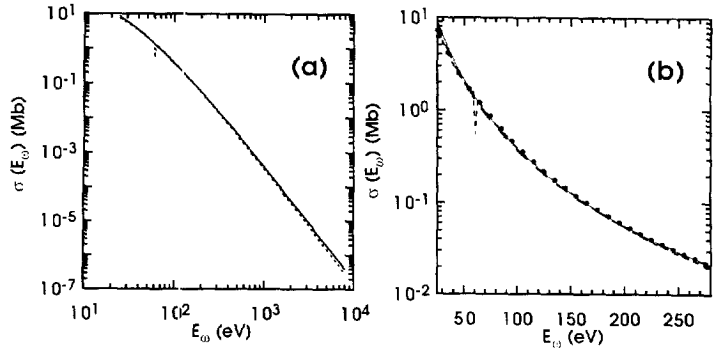

Fig. 23. Total photoabsorption cross section for helium, full line: from Eq. (181) with initial energy $E_i = 2.848$ a.u. (see text), dashed line: with experimental energy (indistinguishable from full line), black points (only in (b)): data from a calculation by Pont and Shakeshaft [156], dotted line: experiment [157].

under which the cross section simplifies so far that it can be even evaluated analytically with the reflection approximation, Eq. (166), leading to the essentially hydrogenic result

$$\sigma(\omega) = 2\sigma_\beta(\omega) = \frac{Z^2}{\beta^4}\frac{2^8\pi^2\alpha}{3\sqrt{2}}\frac{1}{x^{7/2}}e^{-\sqrt{8/x}}, \tag{181}$$

where again $x = 2\omega/\beta^2$. For helium ($\beta = Z - 5/16$, $Z = 2$) we compare in Fig. 23 the approximation Eq. (181) with the experiment by Samson et al. [157] and with numerically converged data from Pont and Shakeshaft [156]. One sees immediately that the high-energy behavior $\sigma \propto \omega^{-7/2}$, as derived by Byron and Joachain [158], is correctly reproduced. Below the double-ionization threshold (79 eV) resonances are interpolated smoothly by the hybrid formula (Fig. 23). The values from Eq. (181) are slightly too low for moderate energies compared to the numerical and the experimental data. This finding is consistent with the one-electron case (Fig. 22) and is therefore not due to the more complicated two-electron dynamics. A slightly better agreement of the hybrid-formula with the experiment and the numerical calculation is obtained if in the photon frequency $\omega = E - E_i$ the initial state energy is used which is produced by the approximated wave function Eq. (180), namely $E_i = 2.848$ a.u. (Fig. 23).

The fact that photoabsorption in the two-electron system is well represented by the hybrid formula permits the conclusion that the physical picture behind the present approach is reasonable: initially, *one* electron absorbs the photon and takes all its angular momentum and energy. This is reflected in the total photo-cross section which is sensitive mainly to short time dynamics. Correlated many-electron dynamics develops subsequently and will lead to an exchange of energy and angular momentum between the electrons and in the case of helium eventually to some double-ionization events [159]. These long-time effects can of course not be described by the crude approximations, Eqs. (166) and (176), to the propagator.

6.2. *Double photoionization of helium*

Double photoionization is one of the most studied problems of correlated electron motion, theoretically as well as experimentally. The difficult problem of multidifferential cross sections has been

advanced considerably over the last years and theoretical [160, 161] and experimental [162, 163] results are in good agreement. A seemingly simpler observable, the ratio between double and single ionization, $\rho = \sigma^{++}/\sigma^{+}$, is still under dispute. Even the most recent and advanced full numerical results do not agree very well among each other [156, 164, 165]. The experimental data [170–178], even recent ones [167, 168], do neither agree among each other nor with the theoretical values.

The ratio $\rho = \sigma^{-+}/\sigma^{+}$ is ideally suited for the application of the concept of projectors in reduced phase space as introduced in Section 2.3. Essentially, we will calculate the single- and double-ionization probability at the stable partial fixed point, i.e. the collinear manifold. The final state is the same as for electron-impact ionization. The initial state, however, needs a careful definition.

6.2.1. The problem of a classical two-electron bound state: The initial state

Classically, a stable bound state with two electrons does not exist. While in quantum mechanics the uncertainty principle prevents an electron from falling into the nucleus, this can and will happen for almost all initial conditions of two-electron trajectories. Consequently, the other electron takes the energy and leaves the atom which is ionized. Only for periodic orbits (most of them are, however, unstable) this does not happen. Presently, it is not clear how to represent the two-electron ground state fully dynamically in a semiclassical theory. An interesting approach to semiclassical ground states of non-separable systems using semiclassical path integrals in imaginary time has been proposed recently [169]. Fortunately, for the photoabsorption process this is not necessary since the stationary motion of the two electrons in the ground state does not have to be followed in time. Rather, we can take a snapshot in the very moment the photon is absorbed and follow from that time on the correlated two-electron dynamics which is non-stationary on the final energy surface. We model the two electrons in the ground state before the photon is absorbed on the collinear collision manifold with an analytical phase-space distribution which is close to the various planar periodic orbits presently discussed for the helium atom [182]. We put the two electrons in a completely out of phase motion on a quarter circle of fixed hyperradius $\mathscr{R}_0 \equiv (r_1^2 + r_2^2)^{1/2} = 1.4$ a.u. This value comes from the average hyperradius (4.15 in energy scaled atomic units, see Ref. [182]) divided by the appropriate energy for the ground state (which is for the corresponding classical orbit roughly -2.97 a.u. in WKB quantization [182]). With the interelectronic angle $\theta = \pi$, the resulting phase-space distribution is a one-parameter manifold dependent on the phase $0 \leq \eta \leq \pi/2$ of the orbit on the circle of radius $\mathscr{R}_0$. This phase-space distribution is close to the periodic orbit of least action (i.e. the shortest periodic orbit) which is known to contribute dominantly to the ground-state energy in a semiclassical representation of the Greens function with periodic orbits [20].

6.2.2. The absorption of the photon and the final state

As a next step we have to formulate the absorption of the photon. We assume that initially one electron absorbs the photon, i.e. takes all its energy and momentum,

$$(p_1^-)^2 = (p_1')^2 + 2\omega\,, \qquad (p_2^-)^2 = (p_2')^2\,, \tag{182}$$

where $\omega = E - E'$. We use unmarked variables for the final state after propagation, variables with the superscript minus for quantities referring to the initial state after the photoabsorption on the new energy shell $E = E^- + \omega$, and primed variables for the initial state before the photon has been absorbed.

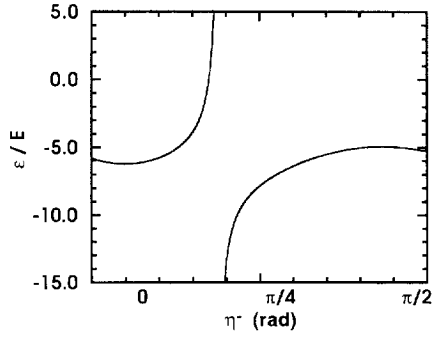

Fig. 24. Classical deflection function (see text) for the helium electron pair after absorption of a photon.

Propagation of the electron pair: After the photoabsorption the two electrons are propagated under the full Hamiltonian on the collinear manifold and can exchange energy due to the electron–electron interaction. The initial variable is the phase η^- on the hypercircle $\mathscr{R}_0$ and the final observable is, as before, the energy ε of one electron. Hence, the deflection function $\varepsilon(\eta^-)$, shown in Fig. 24, is the crucial dynamical function. The dipole amplitude is constructed according to Eq. (43) and reads

$$d(\varepsilon,E',E)=\sum_j\sqrt{\mathscr{D}_j(\varepsilon,E',E)}\exp[\mathrm{i}\Phi_j-\mathrm{i}\nu_j\pi/2] \tag{183}$$

with

$$\mathscr{D}_j(\varepsilon,E',E)=\frac{2}{\pi}\left|\frac{\mathrm{d}\eta^-}{\mathrm{d}\varepsilon}\right|_j(r_1^-(\varepsilon)+r_2^-(\varepsilon))^2\,, \tag{184}$$

the classical probability for the jth orbit leading to a final energy ε of one electron following photon impact. Φ_j is the classical action and ν_j the Maslov index of the jth orbit, while $r_1^-(\varepsilon)=\mathscr{R}_0\cos\eta^-(\varepsilon)$ and $r_2^-=\mathscr{R}_0\sin\eta^-$ are the positions of the electrons before, or identically, immediately after the absorption. The deflection function (Fig. 24) is monotonic apart from two small intervals $\Delta\eta^-$ where extrema are formed which lead to caustics. We will circumvent the problem which results from the caustics by approximating the total ionization probability in the restricted phase space classically,

$$P_{\mathrm{D}}(E',E)=\int_{-\infty}^{\infty}\sum_j\mathscr{D}_j(\varepsilon,E',E)\,\mathrm{d}\varepsilon=\mathscr{R}_0^2\left(1+\frac{2}{\pi}\right). \tag{185}$$

6.2.3. Single- and double-ionization cross sections

The ratio of single-to-double photoionization: For the double-ionizing events ($0\le\varepsilon\le E$) only *one* trajectory contributes to the sum in Eq. (184) (see Fig. 24). However, we must take into account the Pauli principle for the identical electrons and add to the contribution from the trajectory with final energy ε the amplitude from the trajectory where the other electron has energy ε. The action is invariant under electron exchange, $\Phi(\varepsilon,E',E)=\Phi(E-\varepsilon,E',E)$. Hence, the differential probability for finding one electron with energy ε in a double-ionized state after photon impact reads

$$P_{\mathrm{D}}(\varepsilon,E',E)=|\mathscr{D}(\varepsilon,E',E)^{1/2}+\mathscr{D}(E-\varepsilon,E',E)^{1/2}|^2\,. \tag{186}$$

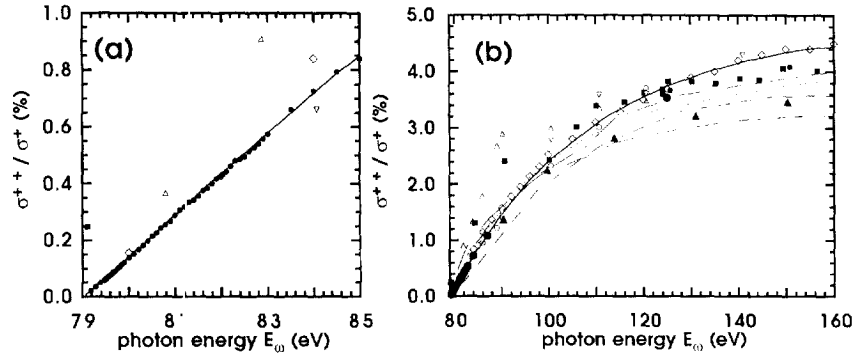

Fig. 25. Ratio of double-to-single photoionization, solid line: theory according to Eq. (187), other theories (curves have been graphically extracted from the respective publications): dashed line [164]; dotted line [165] (acceleration gauge); dotted-dashed line [180] (velocity gauge, smoothed); long dashes [179] (velocity gauge), data from Ref. [181] are similar to Ref. [164] and are not shown; experiments: (●) [173]; filled triangles [167]; filled squares [168]; [178]; (△) [177]; (▽) [172]; (+) [170]; (○) [176].

From Eq. (186) we obtain easily the probability P_D^{++} for photo-double ionization

$$P_D^{++}(E',E) = \int_0^{E/2} P_D(\varepsilon, E', E)\, d\varepsilon\,. \tag{187}$$

The desired ratio of σ^{++}/σ^{+} is now given by $P_D^{++}/(P_D - P_D^{++})$ and is shown in Fig. 25 along with experimental and other theoretical results. Excellent agreement is achieved in the threshold region (Fig. 25a) with the best available experimental data by Kossmann et al. [173, 174]. Here, the theoretical and experimental data reproduce the classical result by Wannier in the limit $E \to 0$, namely, $\sigma^{++} \propto E^{1.056}$. The semiclassical ratio lies higher than most of the experimental data in the intermediate energy region (Fig. 25b).

Absolute double-photoionization cross section: Having the total photo-cross section from Section 6.1 at hand together with the probabilities for two-body and three-body fragmentation from Eqs. (185) and (187) we can apply Eq. (41) for the double-ionization cross section:

$$\sigma^{++} = (P_D^{++}/P_D)\,\sigma_D\,. \tag{188}$$

The result is shown in Fig. 26. While the agreement is remarkably good in the threshold region one sees (as in Fig. 25) an increasing deviation towards higher energies. As mentioned above, this is to be expected since the calculation of process (B), the propagation of the correlated two-electron dynamics after the absorption of the photon has been carried out in a restricted phase space only.

A full semiclassical propagation of the electron pair would certainly improve the asymptotic behavior for $E \to \infty$. Another problem which must be solved in this context is the representation of the initial state. Here, it has been modeled by a phase-space distribution on a fixed hyperradius $\mathcal{R}_0$. Conceptual improvement of the present approach will depend mainly upon future ideas how to model a two-electron ground state classically. Interestingly, the discrepancy among full numerical treatments of the double-photoionization process has been also attributed to the approximate representation of the helium ground state [165].

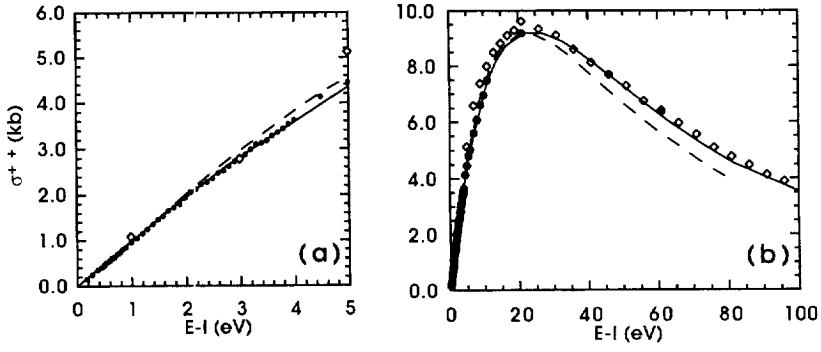

Fig. 26. The absolute photo-double ionization cross section as a function of the energy above the double-ionization threshold. The present theory and data by Pont and Shakeshaft [156] are shown as solid and broken lines, respectively. Experimental data are from Ref. [178] (◇) and from Kossmann et al. [173,174] (●).

One might find it surprising that the cross sections for atomic photo-double ionization far from threshold can be described by an electron motion restricted to the collinear phase space. However, again, this can be understood from a similar behavior below threshold which is reflected by the propensity rules for photoabsorption from the ground state into doubly excited states of helium [134, 135, 166]: There, it is found that predominantly two-electron resonant states are populated whose geometry in a body-fixed frame approaches for high excitation energies a collinear configuration. More importantly, from a general perspective, the seemingly oversimplified picture of atomic photo-double ionization as a two-step process is confirmed by the quantitative comparison with the experiment. Recently, this two-step process has been independently suggested to understand the distribution of the recoil momentum of the He^{++}-ion after photo-double ionization which is directly observable in experiments performed by cold target recoil ion momentum spectroscopy [167].

To summarize, with a quantum-classical hybrid approach it has been possible to calculate the *absolute* single and double ionization cross sections following photon impact on helium. The ratio σ^{++}/σ^{+} has been calculated *semiclassically* by propagation of the two-electron dynamics starting from a classical initial-phase-space distribution, and the absolute total cross section has been calculated analytically with a standard quantum wavefunction for the Helium ground state and a classical reflection approximation for the dynamics.

7. Outlook

Semiclassical methods have been advanced remarkably over the last ten years. Considering the fact that they will always be an approximation this might seem to be very astonishing, moreover in an environment of computing power which also has exploded over the last decade, and which allows for more and more problems to be solved fully quantum mechanically. There are (at least) four reasons for this development which will also determine the future perspective of semiclassical methods.

1. The increasing computing power and the related visualization techniques have given a push to modern semiclassical methods as well: It is no longer a problem to compute billions of classical trajectories and it is also relatively easy to visualize individual trajectories, bundles, or wavefronts. In particular, the recent success of time-dependent semiclassical studies of molecular problems relies on this computing power.
2. The numerical results of increasingly sophisticated quantum treatments must be understood and interpreted. This is another source of renewed demand for semiclassical approximations. In particular, the connection between classical chaos and corresponding quantum behavior has driven the interest in semiclassical methods.
3. For problems which are easier to handle in a semiclassical approximation such an approach will always be ahead of a full quantum treatment in the sense that with given numerical capacities one can tackle, e.g., a few degrees of freedom more semiclassically than quantum mechanically.
4. Finally, there might be a few problems which are almost impossible to solve fully quantum mechanically since they are intrinsically semiclassical.

Certainly to the last category belongs the threshold problem of particles which interact through Coulomb forces. This has been a major motivation to study Coulombic problems semiclassically, as reported here. However, in addition a number of characteristic features of the *classical* system have emerged, from the stability properties of a Coulombic few-body system in a plane, or in even more drastically reduced configuration spaces, to the single minimum for the hyperradius of a Coulomb trajectory at positive energies. It could be shown that the last property has dramatic effects on the entire spectrum of a system of Coulombic particles (absence of resonances for $E > 0$, threshold behavior for $E \approx 0$, etc.). These results are an example of category 2 from above.

With new semiclassical techniques still in development it is perfectly reasonable to investigate test cases for which quantum results are available for comparison. For the future and in reference to point 3, however, it is desirable to have an error estimate of a semiclassical approach, or, put it positively, to know the range of applicability in a suitable parameter space. Clearly, any asymptotic theory has difficulties with this question. However, progress in this respect is necessary for semiclassical results to be taken seriously where no quantum results are available for comparison.

Acknowledgements

It is a pleasure to thank G. Alber, J.S. Briggs, and F. Großmann for many helpful discussions and T. Pattard and G. van de Sand for carefully reading the manuscript. Financial support by the DFG under the Gerhard Hess-Programm and within the Sonderforschungsbereich 276 is gratefully acknowledged.

References

[1] M. Born, Vorlesungen über Atommechanik, Springer, Berlin, 1925 (English translation: The Mechanics of the Atom, Ungar, New York, 1927).
[2] A. Unsoeld, Ann. Phys. 82 (1927) 355.
[3] G.W. Kellner, Z. Phys. 44 (1927) 91.
[4] J.C. Slater, Proc. Natl. Acad. Am. 13 (1927) 423.

[5] K.W. Ford, J.A. Wheeler, Ann. Phys. NY 7 (1959) 259.
[6] M.C. Gutzwiller, J. Math. Phys. 8 (1967) 1979.
[7] M.C. Gutzwiller, J. Math. Phys. 10 (1969) 1004.
[8] M.C. Gutzwiller, J. Math. Phys. 11 (1970) 1791.
[9] M.C. Gutzwiller, J. Math. Phys. 12 (1971) 343.
[10] P. Pechukas, Phys. Rev. 181 (1969) 166.
[11] J.H. Van Vleck, Phil. Mag. 22 (1922) 842.
[12] W.H. Miller, J. Chem. Phys. 53 (1970) 1949.
[13] W.H. Miller, J. Chem. Phys. 53 (1970) 3578.
[14] W.H. Miller, Chem. Phys. Lett. 7 (1970) 431.
[15] R.A. Marcus, Chem. Phys. Lett. 7 (1970) 525.
[16] R.A. Marcus, J. Chem. Phys. 54 (1971) 3965.
[17] R. Abrines, I. Percival, Proc. Roy. Soc. 88 (1966) 861.
[18] R. Abrines, I. Percival, Proc. Roy. Soc. 88 (1966) 873.
[19] R.E. Olson, Phys. Rev. A 36 (1987) 1519.
[20] G.S. Ezra, K. Richter, G. Tanner, D. Wintgen, J. Phys. B 24 (1991) L413.
[21] G. Tanner, K.T. Hansen, J. Main, Nonlinearity 9 (1996) 1641.
[22] H. Friedrich, D. Wintgen, Phys. Rep. 183 (1989) 37.
[23] K. Richter, D. Ulmo, R.A. Jalabert, Phys. Rep. 276 (1996) 1.
[24] M.C. Gutzwiller, Chaos in Classical and Quantum Mechanics, Springer, New York, 1990.
[25] G. Tanner, D. Wintgen, Phys. Rev. Lett. 75 (1995) 2928.
[26] A. Walton, D. Manolopoulos, Molec. Phys. 87 (1996) 961.
[27] F. Grossmann, Chem. Phys. Lett. 262 (1996) 470.
[28] B.W. Spath, W.H. Miller, Chem. Phys. Lett. 262 (1996) 486.
[29] S. Garashchuk, D. Tannor, Chem. Phys. Lett. 262 (1996) 477.
[30] M.V. Berry, K.E. Mount, Rep. Prog. Phys. 35 (1974) 315.
[31] W.H. Miller, Adv. Chem. Phys. 25 (1974) 69.
[32] W.H. Miller, Adv. Chem. Phys. 30 (1975) 77.
[33] M.A. Sepulveda, F. Großmann, Adv. Chem. Phys. 96 (1996) 191.
[34] C. Cohen–Tannoudji, B. Diu, F. Laloë, Quantum Mechanics I+II, Wiley, New York, 1977.
[35] C.J. Joachain, Quantum Collision Theory I+II, North-Holland, Amsterdam, 1975.
[36] H. Goldstein, Classical Mechanics, Addison-Weseley, Reading, MA, 1980.
[37] M.S. Child, Molecular Collision Theory, Academic Press, London, 1974.
[38] A.J. Lichtenberg, M.A. Lieberman, Regular and Stochastic Motion, Springer, New York, 1983.
[39] A.M. Ozorio de Almeida, Hamiltonian Systems: Chaos and Quantization, Cambridge University Press, New York, 1988.
[40] K. Richter, J.S. Briggs, D. Wintgen, E.A. Solovev, J. Phys. B 25 (1992) 3929.
[41] B. Eckhardt, Habilitationsschrift, Universität Marburg, 1991.
[42] W.H. Miller, E.J. Heller, J. Chem. Phys. 95 (1991) 9428.
[43] G. van de Sand, A. Isele, J.M. Rost, to be published.
[44] J.R. Taylor, Scattering Theory, Wiley, New York, 1972.
[45] J.M. Rost, E.J. Heller, J. Phys. B 27 (1994) 1387.
[46] L.D. Landau, E.M. Lifshitz, Mechanics, Pergamon Press, Oxford, 1978.
[47] J.D. Louck, J. Mol. Spec. 4 (1960) 298.
[48] A.O. Barut, R. Raczka, Theory of Group Representations and Applications, World Scientific, Singapore, 1986.
[49] J.C. Slater, Quantum Theory of Matter, Krieger, Huntington, 1977.
[50] E.J. Heller, Phys. Rev. Lett. 53 (1984) 1515.
[51] J. Phys. Chem. 97 (special issue), 1993.
[52] D.R. Herschbach, J. Chem. Phys. 84 (1986) 838.
[53] S. Kais, D.R. Herschbach, J. Chem. Phys. 98 (1993) 3990.
[54] B. Simon, Int. J. Quantum Chem. 14 (1978) 529.
[55] P. Kustaanheimo, E. Stiefel, J. Reine Angew. Math. 218 (1965) 204P.

[56] H. Kleinert, Pfadintegrale, BI Wissenschaftsverlag, Leipzig, 1993.
[57] H.A. Kramers, Z. Phys. 39 (1926) 829.
[58] R. Langer, Phys. Rev. 51 (1937) 669.
[59] R.S. Manning, G.S. Ezra, Phys. Rev. A 50 (1994) 954.
[60] H. Friedrich, J. Trost, Phys. Rev. Lett. 76 (1996) 4869.
[61] D.E. Herrick, Adv. Chem. Phys. 52 (1983) 1.
[62] A. Norcliffe, I.C. Percival, J Phys. B 1 (1968) 774.
[63] A. Norcliffe, I.C. Percival, J Phys. B 1 (1968) 784.
[64] A. Norcliffe, I.C. Percival, M.J. Roberts, J. Phys. B 2 (1969) 578.
[65] A. Norcliffe, I.C. Percival, M.J. Roberts, J. Phys. B 2 (1969) 590.
[66] J. Chadwick, Proc. Roy. Soc. A 128 (1930) 114.
[67] F.T. Smith, J. Chem. Phys. 42 (1965) 2419.
[68] W. Pauli, Ann. Phys. IV 68 (1922) 177.
[69] D. Wintgen, A. Bürgers, K. Richter, G. Tanner, Prog. Theor. Phys. 116 (Suppl.) (1994) 121.
[70] J. Müller, J. Burgdörfer, Phys. Rev. Lett. 70 (1993) 2375.
[71] L.I. Schiff, Quantum Mechanics, McGraw-Hill, Singapore, 1968.
[72] J. Berakdar, J.S. Briggs, Phys. Rev. Lett. 72 (1994) 3799.
[73] D.R. Schultz, R.E. Olson, C.O. Reinhold, J. Phys. B 24 (1991) 521.
[74] M. Draeger, G. Handke, W. Ihra, H. Friedrich, Phys. Rev. A 50 (1994) 3793.
[75] W. Ihra, M. Draeger, G. Handke, H. Friedrich, Phys. Rev. A 52 (1995) 3752.
[76] J.M. Rost, Phys. Rev. Lett. 72 (1994) 1998.
[77] J.M. Rost, J. Phys. B 28 (1995) 3003.
[78] A.K. Kazansky, V.N. Ostrovsky, Phys. Rev. A 48 (1993) R871.
[79] A.K. Kazansky, V.N. Ostrovsky, J. Phys. B 27 (1994) 5197.
[80] I. Bray, A.T. Stelbovics, Phys. Rev. Lett. 70 (1993) 744.
[81] D. Kato, S. Watanabe, Phys. Rev. Lett. 74 (1995) 2443.
[82] G.H. Wannier, Phys. Rev. 90 (1953) 817.
[83] A.E. Wetmore, R.E. Olson, Phys. Rev. A 34 (1986) 2822.
[84] R.K. Peterkop, J. Phys. B 4 (1971) 513.
[85] A.R.P. Rau, Phys. Rev. A 4 (1971) 207.
[86] A.R.P. Rau, Phys. Rep. 110 (1984) 369.
[87] H. Klar, J. Phys. B 14 (1981) 3255.
[88] H. Klar, J. Phys. B 14 (1981) 4165.
[89] J.M. Feagin, J. Phys. B 17 (1984) 2433.
[90] J.F. McCann, D.S.F. Crothers, J. Phys. B 19 (1986) L399.
[91] X.Q. Guo, D.M. Crowe, M.S. Lubell, F.C. Tang, A. Vasilakis, J. Slevin, M. Eminyan, Phys. Rev. Lett. 65 (1990) 1857.
[92] J.R. Friedman, X.Q. Guo, M.S. Lubell, Phys. Rev. A 46 (1992) 652.
[93] M.S. Lubell, Phys. Rev. A 47 (1993) R2450.
[94] A. Temkin, J. Phys. B 7 (1974) L450.
[95] A. Temkin, Phys. Rev. Lett. 49 (1982) 365.
[96] A. Temkin, A.K. Bhatia, Phys. Rev. A 38 (1988) 494.
[97] J.W. McGowan, E.M. Clarke, Phys. Rev. 167 (1968) 43.
[98] J.M. Feagin, J. Phys. B 28 (1995) 1495.
[99] J.H. Macek, S.Yu. Ovchinnikov, Phys. Rev. A 49 (1994) R4273.
[100] J.H. Macek, S.Yu. Ovchinnikov, Phys. Rev. Lett. 74 (1995) 4631.
[101] J.H. Macek, S.Yu. Ovchinnikov, Phys. Rev. A 54 (1996) 544.
[102] W. Ihra, F. Mota-Furtado, P.F. O'Mahony, Phys. Rev. A 55 (1997) 4263.
[103] R. Möhlenkamp, H.J. Korsch, Phys. Rev. A 34 (1986) 4716.
[104] E.A. Solovev, Sov. Phys.-JETP 63 (1986) 538.
[105] E.A. Solovev, Sov. Phys. Usp. 32 (1989) 228.
[106] K. Richter, D. Wintgen, J. Phys. B 23 (1990) L197.

[107] J.M. Rost, J. Phys. B 27 (1994) 5923.
[108] F.H. Read, J. Phys. B 17 (1984) 3965.
[109] M. Gailitis, J. Phys. B 19 (1986) L697.
[110] J.J. Thomson, Phil. Mag. 23 (1912) 449.
[111] J. Franco, E. Daltabuit, Rev. Mex. Astron. Astrof. 2 (1978) 325.
[112] W. Lotz, Z. Phys. D 206 (1967) 205.
[113] W. Lotz, Z. Phys. D 216 (1967) 241.
[114] W. Lotz, Z. Phys. D 232 (1970) 101.
[115] S.M. Younger, T.D. Märk, in: T.D. Märk, G.H. Dunn (Eds.), Electron Impact Ionization, Springer, Wien, 1985.
[116] H. Deutsch, K. Becker, T.D. Märk, Int. J. Mass. Spec. 151 (1995) 207.
[117] J.M. Rost, T. Pattard, Phys. Rev. A 55 (1997) R5.
[118] M.B. Shah, D.S. Elliot, H.B. Gilbody, J. Phys. B 20 (1987) 2481.
[119] G.O. Jones, M. Charlton, J. Slevin, G. Laricchia, Á. Kövér, M.R. Poulsen, S. Nic Chormaic, J. Phys. B 26 (1993) L483.
[120] P. Hvelplund, H. Knudsen, U. Mikkelsen, E. Morenzoni, S.P. Møller, E. Uggerhøj, T. Worm, J. Phys. B 27 (1994) 925.
[121] P. Ashley, J. Moxom, G. Laricchia, Phys. Rev. Lett. 77 (1996) 1250.
[122] T. Pattard, B. Eckhardt, J.M. Rost, unpublished.
[123] W. Wu, C.L. Cocke, J.P. Giese, F. Melchert, M.L.A. Raphaelian, M. Stöckli, Phys. Rev. Lett. 75 (1995) 1054.
[124] H. Knudsen, L.H. Andersen, P. Hvelplund, G. Astner, H. Cederquist, H. Danared, K. Liljeby, K.-G. Resnfelt, J. Phys. B 17 (1984) 3545.
[125] E. Brook, M.F.A. Harrison, A.C.H. Smith, J. Phys. B 11 (1978) 3115.
[126] M.B. Shah, D.S. Elliot, H.B. Gilbody, J. Phys. B 20 (1987) 3501.
[127] H. Knudsen, L. Brun–Nielsen, M. Charlton, M.R. Poulsen, J. Phys. B 23 (1990) 3955.
[128] S. Cvejanović, F.H. Read, J. Phys. B 7 (1974) 1841.
[129] M.H. Kelley, W.T. Rogers, R.J. Celotta, S.R. Mielczarek, Phys. Rev. Lett. 51 (1983) 2192.
[130] M. Kamm, W. Weber, W. Mehlhorn, J. Phys. B 27 (1994) 2585.
[131] R. Hippler, H. Klar, K. Saeed, I. McGregor, A.J. Duncan, H. Kleinpoppen, J. Phys. B 16 (1983) L617.
[132] U. Fano, A.R.P. Rau, Atomic Collisions and Spectra, Academic Press, London, 1986.
[133] H.R. Sadeghpour, C.H. Greene, Phys. Rev. Lett. 65 (1990) 313.
[134] H.R. Sadeghpour, Phys. Rev. A 43 (1991) 5821.
[135] J.M. Rost, J.S. Briggs, J. Phys. B 24 (1991) 4293.
[136] J.M. Rost, R. Gersbacher, K. Richter, J.S. Briggs, D. Wintgen, J. Phys. B 24 (1991) 2455.
[137] Ch. Jung, J. Phys. A 19 (1986) 1345.
[138] Y. Gu, J.M. Yuan, Phys. Rev. A 47 (1993) R2442.
[139] C.C. Rankin, W.H. Miller, J. Chem. Phys. 55 (1971) 3150.
[140] D. Wintgen, K. Richter, G. Tanner, CHAOS 2 (1992) 19.
[141] J.M. Rost, G. Tanner, in: H. Friedrich, B. Eckhardt (Eds.), Classical, Semiclassical and Quantum Dynamics in Atoms, Lecture Notes in Physics, vol. 485, Springer, Berlin, 1997, p. 274.
[142] S. Cvejanović, R.C. Shiell, T.J. Reddish, J. Phys. B 28 (1995) L707.
[143] A.S. Davydov, Quantenmechanik, VEB, Leipzig, 1978.
[144] A. Bürgers, D. Wintgen, J.M. Rost, J. Phys. B 28 (1995) 3163.
[145] J.M. Feagin, J. Macek, J. Phys. B 17 (1984) L245.
[146] S. Cvejanović, Z. Dohecevic, P. Grujic, J. Phys. B 23 (1990) L167.
[147] T.A. Heim, A.R.P. Rau, J. Phys. B 28 (1995) 5309.
[148] J. Burgdörfer, X. Yang, J. Müller, Chaos, Sol. Fractals 5 (1995) 1235.
[149] T. Ericson, Phys. Rev. Lett. 5 (1960) 430.
[150] E.J. Heller, J. Chem. Phys. 68 (1978) 2066.
[151] R. Schinke, Photodissociation Dynamics, Cambridge University Press, Cambridge, 1993.
[152] V. Schmidt, Rep. Prog. Phys. 55 (1992) 1483.
[153] M. Braun, Ch. Meier, V. Engel, J. Chem. Phys. 103 (1995) 7907.
[154] J.M. Rost, J. Phys. B 28 (1995) L601.

[155] H.A. Bethe, E.E. Salpeter, Quantum Mechanics of One- and Two-Electron Atoms, Plenum, New York, 1977.
[156] M. Pont, R. Shakeshaft, J. Phys. B 28 (1995) L571.
[157] J.A.R. Samson, Z.X. He, L. Yin, G.N. Haddad, J. Phys. B 27 (1994) 88.
[158] F.W. Bryon, C.J. Joachain, Phys. Rev. 164 (1967) 1.
[159] J.M. Rost, Phys. Rev. A 53 (1996) R640.
[160] F. Maulbetsch, J.S. Briggs, J. Phys. B 26 (1993) L647.
[161] F. Maulbetsch, M. Pont, J.S. Briggs, R. Shakeshaft, J. Phys. B 28 (1995) L341.
[162] O. Schwarzkopf, B. Krässig, J. Elmiger, V. Schmidt, Phys. Rev. Lett. 70 (1993) 3008.
[163] G. Dawber, L. Avaldi, A.G McConkey, H. Rojas, M.A. McDonald, G.C. King, J. Phys. B 28 (1995) L271.
[164] J.Z. Tang, I. Shimamura, Phys. Rev. A 52 (1995) R3413.
[165] A.S. Kheifets, I. Bray, Phys. Rev. A 54 (1996) R997.
[166] J.M. Rost, K. Schulz, G. Kaindl, M. Domke, J. Phys. B 30 (1997) 4663.
[167] R. Dörner et al., Phys. Rev. Lett. 76 (1996) 2654.
[168] J.C. Levin, G.B. Armen, I.A. Sellin, Phys. Rev. Lett. 76 (1996) 1220.
[169] F.J. Weiper, J. Ankerhold, H. Grabert, E. Pollak, Phys. Rev. Lett. 77 (1996) 2662.
[170] V. Schmidt, N. Sander, H. Kutzmüller, P. Dhez, F. Wuilleumier, E. Källne, Phys. Rev. A 13 (1976) 1748.
[171] G.R. Wight, M.J. Van der Wiel, J. Phys. B 9 (1976) 1319.
[172] D.M.P. Holand, K. Codling. J.B. West, G.V. Marr, J. Phys. B 12 (1979) 2465.
[173] H. Kossmann, V. Schmidt, T. Andersen, Phys. Rev. Lett. 60 (1988) 1266.
[174] H. Kossmann, Ph.D. Thesis. Univ. of Freiburg, 1989.
[175] P. Lablanquie, K. Ito, P. Morin, I. Nenner, J.H.D. Eland, Z. Phys. D 16 (1990) 77.
[176] R. Wehlitz, F. Heiser, O. Hemmers, B. Langer, A. Menzel, U. Becker, Phys. Rev. Lett. 67 (1991) 3764.
[177] R.J. Bartlett, P.J. Walsh, Z.X. He, Y. Chung, E.M. Lee, J.A.R. Samson, Phys. Rev. A 46 (1992) 5574.
[178] J.M. Bizau, F.J. Wuilleumier, J. Electron Spectrosc. Relat. Phenom. 71 (1995) 205.
[179] K. Hino, T. Ishihara, F. Shimizu, N. Toshima, J.H. McGuire, Phys. Rev. A 48 (1993) 1271.
[180] K.W. Meyer, C.H. Greene, Phys. Rev. A 50 (1994) R3573.
[181] M. Pont, R. Shakeshaft, Phys. Rev. A 48 (1995) 875.
[182] P.V. Grujic, N.S. Simonovic, J. Phys. B 28 (1995) 1159.